Micro-mechanical Characterization of Ductile Damage in Sheet Metal

This research was carried out as part of the innovation program of the Materials Innovation Institute (M2i) (formerly, the Netherlands Institute for Metals Research) on "Forming the Limits of Damage Predictions WP 1", project number MC2.05205-1.

CIP-DATA LIBRARY TECHNISCHE UNIVERSITEIT EINDHOVEN

Taşan C. C.

Micro-mechanical Characterization of Ductile Damage in Sheet Metal.
Eindhoven University of Technology, 2010.
Proefschrift.

A catalogue record is available at the Eindhoven University of Technology Library.
ISBN: 978-90-77172-54-4

This thesis is prepared with LaTeX2$_\epsilon$
Cover design: Sjoerd Cloos
Printed by the Universiteitsdrukkerij TU Eindhoven, Eindhoven, The Netherlands.

Micro-mechanical Characterization of Ductile Damage in Sheet Metal

PROEFSCHRIFT

ter verkrijging van de graad van doctor aan de Technische Universiteit Eindhoven, op gezag van de rector magnificus, prof.dr.ir. C.J. van Duijn, voor een commissie aangewezen door het College voor Promoties in het openbaar te verdedigen op woensdag 21 april 2010 om 16.00 uur

door

Cemal Cem Taşan

geboren te Ankara, Turkije

Dit proefschrift is goedgekeurd door de promotor:

prof.dr.ir. M.G.D. Geers

Copromotor:
dr.ir. J.P.M. Hoefnagels

Contents

Micro-mechanical Characterization of Ductile Damage in Sheet Metal

Summary

Triggered by the recent popularity of advanced high strength steels (AHSS) and aluminium alloys for weight-reduction in automotive components, industrial interest in deformation-induced ductile damage in sheet metal is increasing in the last decades. Severe deformation during forming or service triggers different damage micro-mechanisms in the multi-phase microstructures of these materials, leading often to unpredicted failures. These failures can be avoided by (a) the optimization of metal microstructures to be less susceptible to damage-induced failures, which requires experimental characterization of damage micro-mechanisms or (b) the incorporation of continuum damage models in forming simulations to design forming operations within safe deformation limits, which requires experimental quantification of damage accumulation. However, both strategies are hampered by the limitations of the currently available experimental diagnostics. Therefore, the aim of this work is to develop new experimental methodologies that allow for (i) characterization of damage micro-mechanisms and (ii) accurate quantification of damage accumulation, with a focus on industry-relevant sheet metal.

As a starting point, the influence of damage evolution on localization and fracture is investigated by deforming two steels of different microstructure in different strain paths. The results revealed that for microstructures with many damage mechanisms (e.g. AHSS), damage accumulation significantly affects both necking and fracture limits, verifying the strong need for thorough characterization of damage micro-mechanisms in different strain-paths. The analysis of these mechanisms requires the development of a miniaturized testing setup that could fit within a scanning electron microscope (SEM) to track deformation-induced microstructure evolution in real time. To this end, a miniaturized Marciniak test setup is designed, built and tested, which allows the real-time, multi-axial testing of industrial sheet metal to the point of fracture within a SEM. A major benefit of the in-situ analysis with miniaturized equipment is the possibility of obtaining evolution of local strain distribution at the microstructure level, as demonstrated in a case study that clarifies the mechanical influence of the morphology and properties of microstructural banding in steels. The effect of band continuity and hardness are elucidated, yielding a clear detrimental influence especially for hard bands with a continuous morphology. Finally, an improved experimental methodology is developed to analyse 3D features of ductile deformation, with minimum specimen preparation artifacts.

For the damage quantification problem a wide variety of experimental methodologies have been proposed in the literature, without a thorough evaluation with respect to measurement accuracy, precision, practicality, etc. To determine the most suitable damage quantification strategy for continuum damage models, damage morphology-based damage quantification methodologies (the volume fraction methodology, area fraction methodology, or density measurement methodology) and material property-based damage quantification methodologies (the indentation-based methodology, modified indentation methodology and micropillar compression methodology) are comparatively analyzed. The obtained results clearly indicated that methodologies that quantify ductile damage through its morphology have limited accuracy and probe a narrow damage spectrum, revealing the need for accurate material-property based damage quantification techniques. The indentation based methodology is a widely used example of such methodologies, however, a numerical-experimental analysis revealed that it cannot be used for this purpose, as the damage-induced degradation of both hardness and modulus is masked by other deformation-induced microstructural mechanisms (e.g. grain shape change, texture development, etc.). To this end, two original mechanical property-based damage quantification methodologies are proposed in this work. A new indentation-based methodology is developed and evaluated, that eliminates the influence of the microstructural heterogeneity to properly capture the damage-induced degradation of indentation hardness and modulus. And finally, an elastic compression-based methodology is developed where the elastic damage parameter is obtained through the deformation-induced degradation of the compression modulus of electro-discharge machined micropillars. The results from these two methodologies clearly indicate that methodologies that quantify ductile damage through its influence on a mechanical property (e.g. hardness, modulus) have significantly higher accuracy, and therefore more suitable for identifying damage parameters for continuum damage models.

CHAPTER ONE

Introduction

The human curiosity to understand failure of materials goes back to the early days of the struggle between mankind and nature; a hunter trying to sharpen his arrow or a caveman trying to carve an image of his daily life on the walls of his cave must have wondered if there would be possible ways to make their tools more durable (figure 1.1). Undoubtedly, we have come a long way since those days in terms of the understanding of material behavior, which we now apply to the development of much more sophisticated tools and technologies than the arrows and chisels of our ancestors. In fact, material failure is in the heart of the technical revolution throughout the decades (e.g. in the aerospace industry).

Figure 1.1: Ancient chisel with a hairline crack [1].

Despite this progress, technological demands and requirements are ever-increasing to improve human comfort and safety. A clear example of the progress driven by such motivations can be seen upon close inspection of the complex design of today's automotives, in which a wide range of new multi-functional materials (e.g. advanced high strength steels, composites, shape memory alloys, etc.) are used to boost speed, acceleration, traction, driving comfort and crash-safety. Of course, the use of such complex materials is not limited to the automotive industry but wide-spread to many

products (from soda cans to laptop computers) where superior performance, multi-functionality and durability are required.

1.1 New Materials, New Failure Mechanisms

While new materials are being developed to provide such superior properties (often by manipulating the material at the micron-scale), it becomes more and more difficult to analyze, understand and predict their behavior with existing techniques. This is especially challenging for metals, where the industrial drive towards an enhanced performance is strongest. A transformation-induced plasticity (TRIP) steel, for example, allows enhanced ductility and strength that is typically required in the forming operations of automotive bodies (figure 1.2). It is known that the improvement in the mechanical behavior (e.g. with respect to more conventional high-strength low alloy (HSLA) steels) is achieved due to the microstructural transformation of the existing metastable austenite phase to martensite during deformation. However, a detailed understanding of the resulting failure mechanisms (to enable prediction of safe deformation limits in different forming operations) remains to be achieved. Similar challenges have arisen for many other new metals (dual-phase steels, nanostructured metals, thin metal films, etc.) making fracture-sensitivity a major concern for the industry and a challenging topic for research.

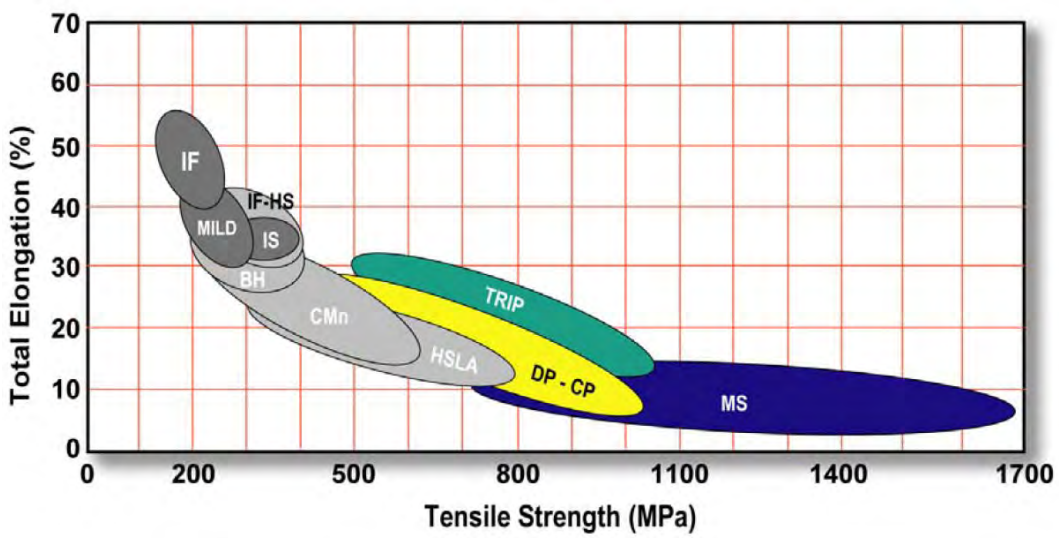

Figure 1.2: New steels (e.g. transformation-induced plasticity (TRIP) steel, dual phase (DP) steel, martensitic (MS) steel, etc.) provide enhanced combination of ductility and strength compared to traditional steels [2].

In ductile metals failure usually occurs through a number of characteristic steps (i.e. severe deformation, diffuse necking, localized necking) avoiding instantaneous loss of integrity. In fact, in most industrial cases (e.g. sheet metal forming operations) the

failure criterion is identified with the point of necking (strain localization). However, both in forming operations (e.g. the hemming process of new aluminium alloys for car door panels (figure 1.3a), or in service (e.g. crash performance of advanced high strength steel crash box structures in cars bodies (figure 1.3b) failure without prior strain localization has been reported by the industry, which cannot be predicted with the available simulation tools.

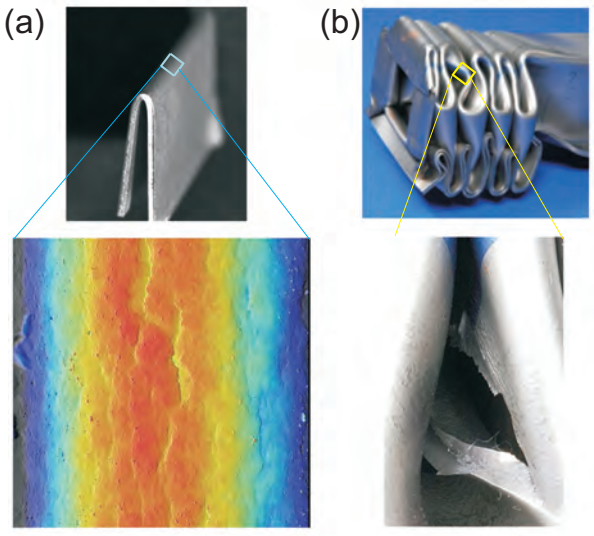

Figure 1.3: Severe roughening and failure as observed in (a) the hemming process of aluminium 6016 alloys, and (b) crash box structures of dual phase 600 steel.

1.2 The Important Role of Damage Evolution

What triggers the fracture in the absence of localization is the deformation-induced damage evolution (i.e. accumulation of microvoids, microcracks, and other similar defects causing the softening of the material upon severe deformation). These damage mechanisms do not only depend on the composition and microstructure of the material, but also on the sample and loading conditions (e.g. geometry, stress state, strain path, etc.). For example, it is known that microvoid nucleation occurs primarily through martensite cracking and martensite-ferrite decohesion in dual phase steels. However, the activity of these mechanisms depends strongly on the martensite fraction, martensite carbide content and martensite morphology, as well as the applied strain path (as shown, e.g., in chapter 2 of this thesis). Accordingly, the remedy for undesirable damage-induced fracture from a metallurgical perspective would be optimizing the metal microstructures to be less sensitive to damage micromechanisms. This strategy, however, calls for an in-depth understanding of the influence of each of the above mentioned microstructural and operational parameters

on the occurring microstructural damage mechanisms through detailed experimental characterization (figure 1.4a). On the other hand, fracture should be predictable through a mechanics approach, by enhancing the predictive capabilities of the simulations in order to design forming operations that subject the material to less severe loading paths. This can be achieved by incorporating continuum damage models in forming simulations to take damage evolution (and hence damage-induced failures) into account (figure 1.4b). Interestingly, this strategy also calls for adequate experimental input, since the predictive strength of continuum damage models relies on the accuracy of the experimentally obtained and material-specific damage evolution parameters.

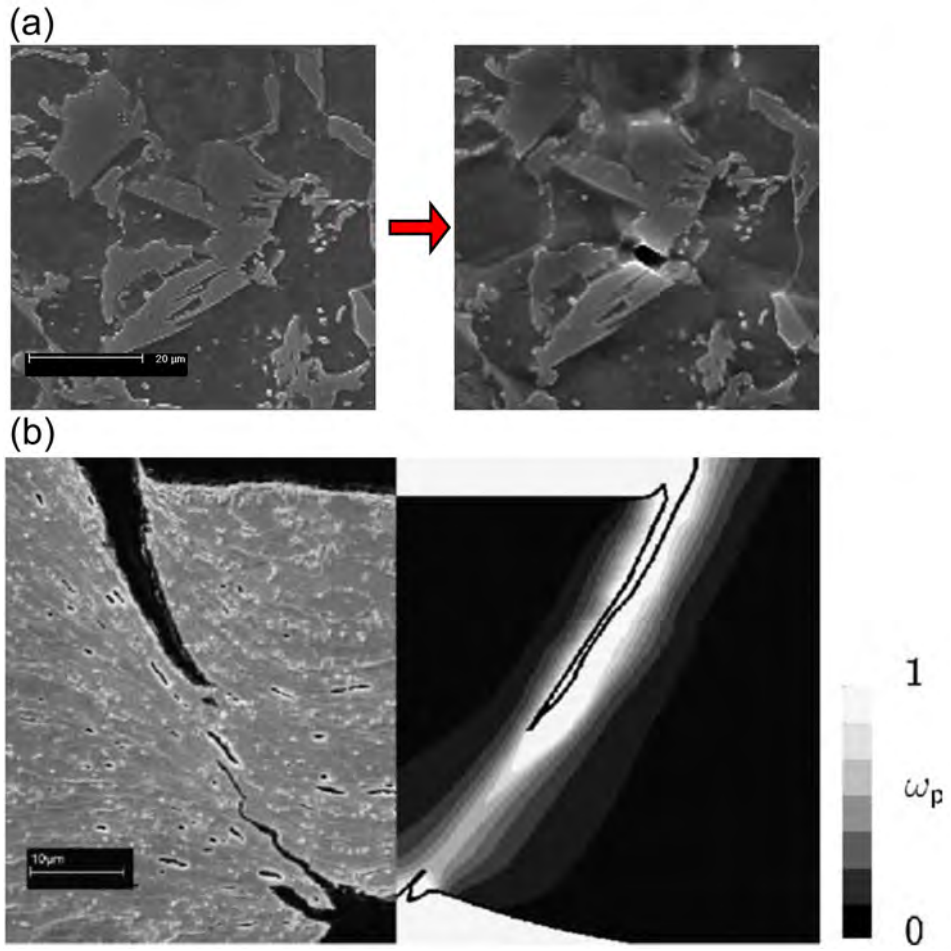

Figure 1.4: (a) Experimental observation of damage nucleation through martensite cracking in DP steel. (b) Damage prediction through simulations can realistically predict damage evolution in score forming operations [3].

Evidently, there is a clear need for detailed experimental analyses of damage phenomena in these advanced materials, (i) to characterize active microstructural damage mechanisms in order to qualify their initiation, evolution and interaction and (ii) to measure the damage evolution in a quantitative manner. Presently available ex-

perimental techniques do not suffice the requirements for these goals. For example, macro-scale deformation tests and post-mortem fractography analyses have been traditionally used to characterize metal deformation, but the identification of the damage mechanisms in complex microstructures requires in-situ testing methodologies, providing real time analysis of microstructural deformation mechanisms. Similarly, it is questionable whether existing damage models can be predictive by using conventional damage parameters only (e.g. void area fraction calculations) to predict accurate forming limits.

1.3 Goal of this Thesis

The aim of this work is to develop new experimental methodologies that allow for (i) characterization of damage micro-mechanisms and (ii) accurate quantification of damage accumulation, with a focus on industry-relevant sheet metal.

1.4 Outline of the Thesis

The thesis consists of two parts addressing the two goals stated above. In the first part, consisting of the first 4 chapters, the damage characterization problem is studied:

- In chapter 2, damage mechanisms, including their accumulation and evolution to fracture is analyzed for two typical distinct microstructures (dual phase steel and interstitial-free steel) at different strain paths and stages of deformation.
- In chapter 3, the design of a miniaturized multi-axial testing setup is presented, which allows testing of sheet metal under different strain paths up to the point of fracture, under real-time, *in-situ* microscopic examination.
- In chapter 4, using a microstructure-based digital image correlation methodology, image sequences obtained from *in-situ* SEM deformation experiments are analyzed to reveal damage micro-mechanisms within segregation bands in DP steel.
- In chapter 5, an improved brittle-fracture based experimental methodology is presented whereby deformation induced micro-events in ductile sheet metal can be visualized avoiding any specimen preparation-induced effects.

The second part consists of the following 4 chapters, addressing the damage quantification issue:

- In chapter 6, the accuracy and applicability of common direct (geometrical) and indirect (mechanical) damage quantification methodologies is analyzed and compared.
- In chapter 7, the well-known indentation-based damage quantification methodology is critically analyzed, and shown to be intrinsically-deficient due to masked plasticity effects that are probed in the experiment.
- In chapter 8, a new indentation-based methodology is developed that metallurgically resolves these masking plasticity effects existing in the original methodology through adequate heat treatments.
- Chapter 9 reports a new damage quantification methodology based on elastic micropillar compression test, that circumvent the above-mentioned plasticity effects by performing purely-elastic deformation tests.

Finally, general conclusions of the study and outlook is presented.

CHAPTER TWO

Strain Path Dependent Ductile Damage Mechanics and Forming Limits[1]

Abstract

This paper contributes to the physical understanding of sheet metal micro-mechanics by addressing the influence of damage evolution on localization and eventually ductile fracture in different strain paths. For this purpose, two steels of different microstructure are deformed in different strain paths, along which forming and fracture limit curves are measured. Microstructural damage mechanisms are characterized and compared for different strain paths (i.e. uniaxial, plane strain and biaxial tension) and at different stages of deformation (i.e. before localization, after localization and at fracture). Interesting results are obtained revealing generic relationships between microstructure evolution (e.g., damage accumulation), localization (forming limit curve) and fracture (fracture limit curve). For single phase microstructures with limited damage sources, damage is initiated as a result of a developing plastic instability (localization), and therefore does not have a significant role on the forming limits. For microstructures with more damage mechanisms, however, the damage accumulates even before localization, and significantly affects both necking and fracture limits.

[1] *Reproduced from:* C.C. Tasan, J.P.M. Hoefnagels, C.H.L.J.ten Horn, M.G.D. Geers, Experimental Analysis of Strain Path Dependent Ductile Damage Mechanics and Forming Limits, Mechanics of Materials, 41(11), 1264-1276, (2009).

2.1 Introduction

The last decades were marked by the introduction of advanced high-strength steels (AHSS) in the sheet metal forming (SMF) industry, e.g. the dual-phase (DP) and transformation-induced plasticity (TRIP) steels. Driven by strong weight reduction demands, there are also ongoing efforts to replace steel in automotive applications with low-weight aluminium alloys, especially the Al5xxx and Al6xxx series. These developments introduced new challenges to the industry [4–6].

The first challenge concerns the mechanical performance of these new alloys during forming and/or service. Although many AHSS grades are reported to have superior strength-to-ductility ratios, it is also reported that the improved strength-to-weight ratio of these steels may be accompanied by a reduction in ductility. Reduced ductility possibly results in failure without significant energy absorption, which is unacceptable for car components that are designed to absorb maximum energy upon crash. Similar problems are also encountered with aluminium alloys. [6], for example, reported significant differences in fracture behaviour of direct chill cast and continuous cast Al-Mg alloys with identical necking limits. In addition, severe roughening and cracking are reported to be critical limitations for the hemming of some Al6xxx alloys [5]. It therefore remains a challenge for sheet metal manufacturers to optimize the microstructure of these alloys using the feedback from the forming industry and, vice verse, for the forming industry to design the forming operations to yield maximum service performance for a given material. This challenge requires an in-depth understanding of the evolution of the microstructure upon deformation leading to the failure of the material.

The second challenge relates to the experimental and numerical tools that are currently employed to predict the limits of forming. The reduced ductility and the increasing risk of 'neckless' fracture hampers the predictive capabilities of the conventional tools, which rely on localized necking as the limiting criteria for SMF processes. Unpredicted fractures are attributed to the evolution of damage inside the material, i.e. microvoids [7]. To address this problem and incorporate damage and fracture into these tools, several empirical and microstructure-based fracture criteria have been proposed, many of which are compared by [8]. Furthermore, ductile damage models which aim to describe the interaction of damage growth and plastic flow have also been developed, such as the Gurson-Tvergaard-Needleman family of models [9–12]. Using such models instead of or complementary to the experimental data may result in considerably improved predictions of failure in critical applications. However, these models are still not used extensively in the industry in their present form due to the large number of material parameters involved, for which no established experimental identification method exists. Improving on this requires a better understanding of the interaction of material microstructure, forming operation and the possible failure mechanisms.

To address the above-mentioned two challenges, a coupling between the deformation history of a given sheet at a certain strain path and the evolution of its mi-

crostructure up to the point of failure is needed.

To track the strain path followed by the material and detect the limits of safe deformation along this path, forming limit curves (FLC's) are frequently used, which were initiated by the work of [13][2]. FLC's represent the point of necking in different strain paths, which is adopted as the failure criteria in present forming simulations. This is a reasonable assumption for the forming of conventional steels (e.g. high strength low alloy (HSLA) steels). AHSS's on the other hand, may fail without a neck, through premature ductile fracture. In such cases the experimentally obtained FLC's represent a combination of necking and (also) fracture limits. In an effort to separately probe these two criteria, many researchers have studied fracture limit curves (FrLC's) of relevant materials (notable examples include [8,15–21]). However, reported FLC's and the FrLC's are not coupled to the evolution of the underlying microstructure towards fracture, with the exception of the works of [8] and [20]. Even in the latter two cases the attention is primarily focused on the final microstructure and not on the evolution of the microstructure through the deformation process. It is therefore difficult to generalize these observations in particular for different materials with different microstructures that are to be formed in a variety of strain paths.

Parallel to the focus on FLC's, there have been tremendous efforts in observing and understanding the micromechanisms involved in the evolution of ductile damage leading to fracture. Predicting ductile fracture requires an adequate understanding of the physical mechanisms involved in this process, which necessitates experimental analyses of each stage of the ductile fracture process, i.e. void nucleation, growth and coalescence. Upon deformation, microvoids have been reported to nucleate and grow from: second-phase particles through matrix particle decohesion and particle cracking [22]; triple junctions between grains of identical phases [23]; interfaces between different phases [24]; slipband intersections [25]; dislocation cell boundaries [26]; etc. The anisotropic nature of these mechanisms are clearly shown [27]. Effect of damage evolution on the global mechanical behavior and failure of industrially relevant materials such as interstitial-free (IF) or dual-phase (DP) steel has also been examined, see for example [28] and [29], respectively. However, similar to the literature on forming limits, papers on damage and ductile fracture mechanisms are generally also case-specific and a connection to FLC's and forming parameters, such as the strain path, is not provided.

This brief literature overview presented highlights the gap in the literature connecting the mechanical behavior of new, advanced materials and the evolution of their microstructure, up to the point of failure. The missing link between damage and strain paths constitutes an important aspect in this sense. It is generally believed that damage evolution, for most materials, occurs only after the point of localized necking, and always faster in forming operations that involve a biaxial strain path. For advanced metals, this assumption is correctly questioned in the literature. As stated in [8] "...The works in the literature emphasize on improving the ductile frac-

[2] A detailed background of the experimentation and interpretation of FLC's are given in [14].

ture criteria available, however, a detailed examination of the effect of strain or stress state on the occurrence of a well-defined and quantitatively characterized mode of failure is needed...". The present work aims to close this gap and address the two challenges advocated. Two different steels with different formability are deformed along different strain paths and the resulting strains, FLC's and FrLC's are measured and interrelated. In addition, full characterization of microstructural failure mechanisms have been carried out using a scanning electron microscope (SEM). Through extensive fractography analyses, microstructural damage evolution mechanisms are determined. The activity of these observed damage micromechanisms are examined at different strain paths and at different stages of deformation. An intrinsic connection is therefore identified between the FLC and the FrLC of the tested sheet metals and the microstructural evolution and failure mechanisms.

2.2 Experimental Methodology

In a numerical approach, a fruitful strategy to study the influence of damage evolution on formability characteristics of sheet metal is to switch on and off damage evolution and observe its effects on the global formability of the sheet. Obviously, this is not possible experimentally. Nevertheless, with a suitable choice of the materials a similar effect can be achieved qualitatively. For this purpose, two steels at different extremes of formability are tested comparatively in this work: an advanced high strength steel (DP) and a high formability steel (IF). The initial microstructures of the DP and IF steels are presented in Fig. 2.1 and 2.2, respectively.

DP steel is composed of ferritic grains with martensite located at the grain boundaries (Fig. 2.1(a)). Limited amount of relatively soft, elongated manganese-sulfide particles and hard aluminium oxide inclusions (Fig. 2.1(b)) are also identified in the as-received microstructure. In terms of mechanical performance, these alloys are known to exhibit relatively high global formability combined with an enhanced strength due to the coexistence of ferrite and martensite phases [30]. However upon deformation, local high stresses induced by the different formabilities of ferrite and martensite is also reported to trigger damage nucleation [31]. The tested DP sheets have a thickness of 1 millimeter, and a normal isotropy ratio, the so-called 'r-value', of approximately 1 (i.e. absence of normal anisotropy).

The IF steel, on the other hand, is a single phase material with equiaxed ferritic grains (Fig. 2.2(a)). It has limited number of inclusions, which are mostly precipitated in the grain boundaries. These second-phase particles are identified as aluminum oxides (Fig. 2.2(b)) and titanium nitrides through EDX analysis. With its low carbon content, fully ferritic microstructure and relatively low amount of inclusions, IF steel is one of the most formable steels used by the sheet metal forming industry. The thickness of the IF sheet material is 0.7 millimeters, and its r-value is approximately 2 (indicating an increased resistance to thinning).

In order to deform these steels along different strain paths, specimens of different

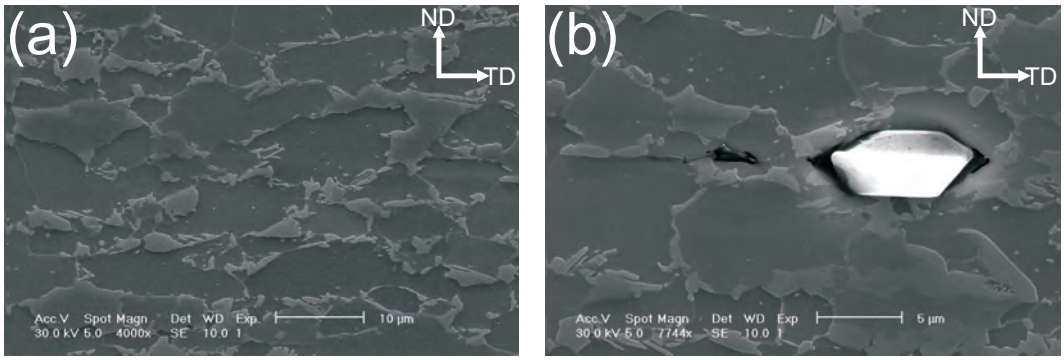

Figure 2.1: (a) Undeformed microstructure of DP steel (Transverse (TD) and normal (ND) directions are indicated with the arrows.) (b) An aluminium oxide inclusion in DP steel

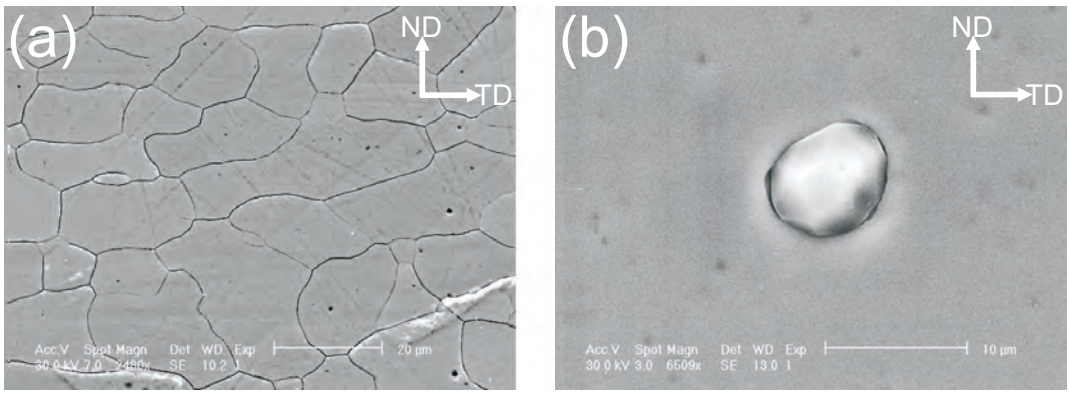

Figure 2.2: (a) SEM micrograph of the microstructure of undeformed IF steel, composed of equiaxed ferritic grains. (b) An aluminium oxide particle in IF steel.

starting geometries (i.e. Nakazima strips) are prepared (Fig. 2.3). The tests are done according to EN ISO 12004-2:2008, with the only exception that the punch diameter was 75.0mm instead of 100mm and the die inner diameter was 84.6mm instead of 105mm. For the equi-biaxial strain path, full circular blanks (radius of 166mm) are used. To achieve a wide range of strain paths, the blank width is decreased to 140mm, 100mm, 80mm and 60mm. A regular measurement grid is applied to the surface of each undeformed blank prior to deformation. The specimens are tested up to fracture using a displacement-controlled hemispherical punch. Sufficient lubricant is used to overcome friction effects between the punch and the tested sheets. All specimens are tested such that the major strain axis coincides with the "transverse direction", as this testing orientation show necking and fracture at lower strains. Along with the fractured specimens, four specimens from each geometry (i.e. strain path) are deformed to different levels of final strains, to determine the strain path followed by each geometry up to fracture. This is accomplished by adopting different

maximum punch displacements (65%, 75%, 85% and 95% of the punch displacement at fracture). Local strains are obtained by measuring the separation of the grid points using image correlation software (PHAST™). The necking strains for each strain path are plotted and together these necking strain points form the FLC.

To plot the FrLC curves, the displacement of the grid points at the point of crack initiation need to be determined in the major and minor directions. Measurement of the minor strain is straightforward and can be easily done post-fracture. However, the determination of the major strain is more challenging, and (as explained by [16]) can be done either directly from the displacement of grid points, or indirectly using the thickness at the point of crack initiation and volume conservation. Although many researchers choose the latter methodology (e.g., [8, 15, 17]), our preliminary tests showed that this approach leads to erroneous results due to the errors introduced in thickness measurement. Therefore, in this work, an improved version of the former (direct) methodology is used to determine the local major strains at the point of fracture. For this, the distance between grid points on each side of the crack is measured using the 3D position of each data point obtained from the image correlation software. Then, the crack opening width is measured directly through optical microscopy and subtracted from the calculated displacement.

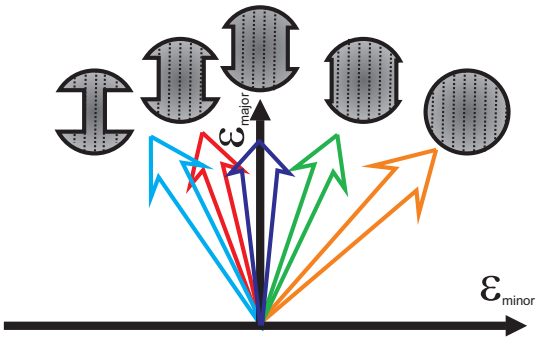

Figure 2.3: Nakazima strips of different starting geometries are deformed in a hemispherical punch test to generate the different strain paths in the center of the test specimens, as schematically indicated on the major strain versus minor strain graph.

To investigate microstructural changes in the IF and DP steels along certain strain paths (i.e. uniaxial tension (UAT), plane strain tension (PST) and equi-biaxial tension (BAT)), metallographic examination is carried out with a scanning electron microscope (Philips XL30 ESEM-FEG), using both secondary and backscatter electron modes. The specimens are deformed to different levels of final strains and microstructural analysis is carried out on their cross sections. To detect relevant changes prior to localization, the specimens that are deformed to an accumulated strain just below the FLC are prepared and analyzed from the top surface. To reveal the changes after localization, a cross section of the localized neck is analyzed in each fractured

sample (direction 1 in Fig. 2.4(b)). In order to directly measure thickness strains at necking and at fracture, and to quantify damage evolution (i.e. void area fraction), SEM images obtained at direction 1 are analyzed using a public domain image processing software (ImageJ). Furthermore, using the same samples, the final failure mechanism and the amount of damage evolution at the points of fracture is analyzed by examining the fracture surfaces (direction 2 and 3 in Fig. 2.4(c)).

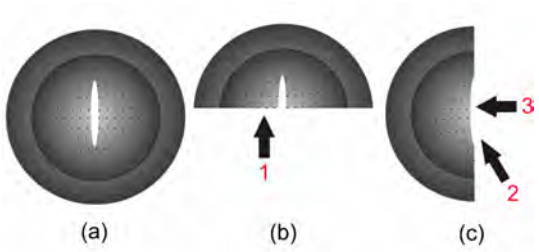

Figure 2.4: Viewing directions 1,2 and 3 for fractography analysis: (a) full FLC specimen from the top, (b) thickness cross section perpendicular to the crack, and (c) fracture surface.

2.3 Strain Path and Microstructure Evolution up to Failure

In the Nakazima test, the loads exerted by the punch on the sheet induces the deformation leading to fracture. This process involves a number of different stages, i.e. elastic, uniform plastic and localized plastic deformation, until the point of failure. In the following subsections, the changes in the microstructure of each IF and DP steel specimen is analyzed at different levels of deformation, and subsequently coupled to the strain path experienced by each specimen.

2.3.1 Deformation up to localization

The first stage in the deformation of the specimens can be referred to as the uniform deformation stage, as the strain profile remains approximately constant over the length of the sheets with an increase towards the center (see e.g. 65%, 75% and 85% profiles in Fig. 2.5 for the UAT specimens of (a)IF and (b)DP steels, and also the corresponding local strain distributions in the same samples (c)). Due to the different Nakazima strip starting geometries, each specimen experiences a different strain path, as shown in Fig. 2.6(a) for IF steel and (b) for DP steel. Note that for all geometries the deformation is initiated in a linear path towards the point of necking (FLC), however, the slope of these linear paths (i.e. strain ratios (β) up to FLC in Table 2.1)

is different for the same geometries of the two steels due to the difference in normal anisotropy. The higher r-value of IF (r=2) compared to DP steel (r=1) indicates a greater resistance to thinning for IF steel, which explains the observed lower minor strains (i.e. lower values of beta) for all strain paths except (of course) biaxial strain, as induced by the volume conservation under plastic flow.

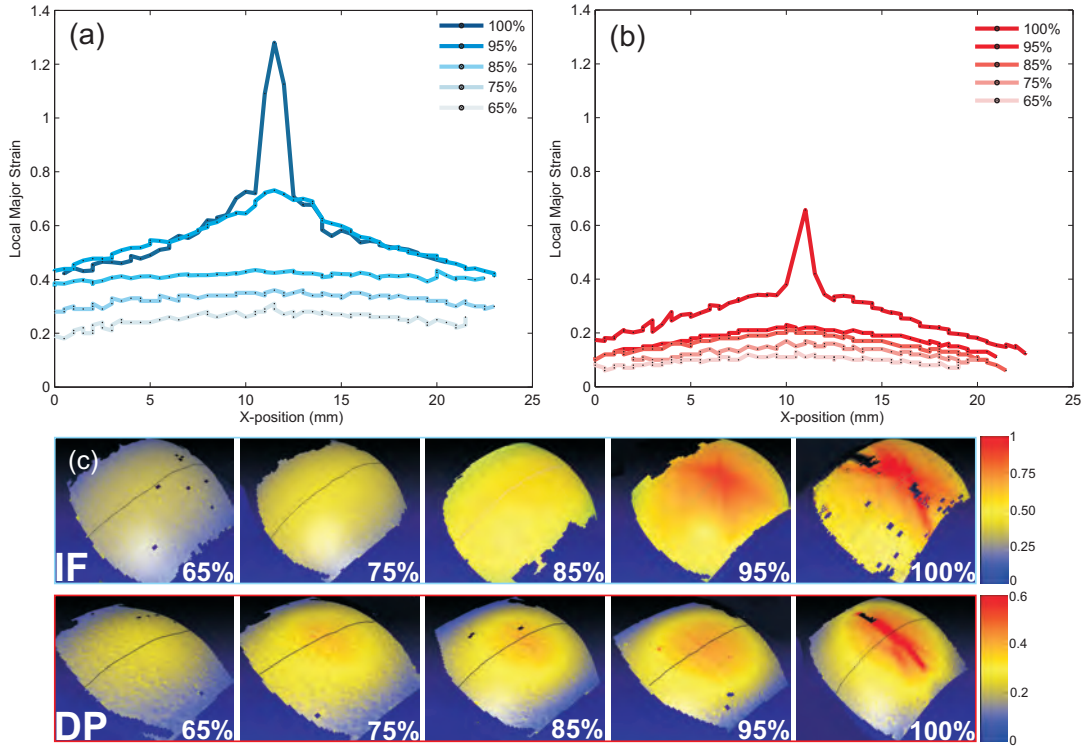

Figure 2.5: The evolution of the major strain along the longitudinal loading direction of (a) the IF specimen and (b) the DP specimen, both deformed in UAT. The major strain distribution plots of the entire samples are also given in (c).

Table 2.1: Strain ratios (i.e. ratio of minor strain to major strain) and the accumulated damage (i.e. void area fraction) of IF and DP steel samples at different strain paths. The standard deviation in the damage measurement is ∼0.02%.

Material	Stage	Strain Ratio, β			Void area fraction (%)		
		UAT	PST	BAT	UAT	PST	BAT
IF	up to FLC	-0.45	-0.07	0.86	0	0	0
	from FLC to FrLC	-0.16	-0.03	0	0.13	0.09	0.09
DP	up to FLC	-0.35	0.10	0.91	0.21	0.27	1.09
	from FLC to FrLC	-0.09	0	-0.01	0.23	0.20	0.04

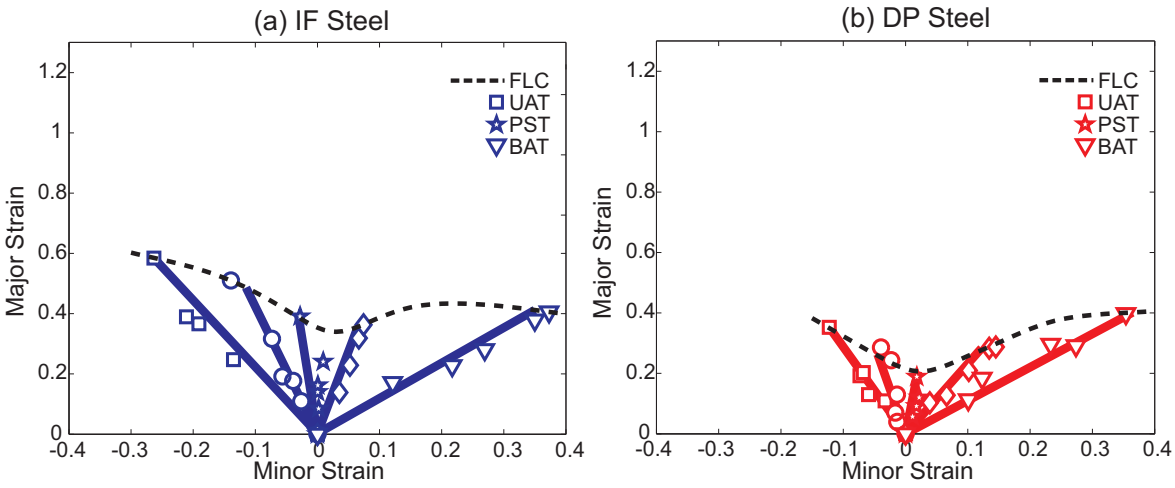

Figure 2.6: Strain paths leading towards the FLC (dashed line) of (a) IF steel and (b) DP steel specimens

The SEM micrographs at this early stage reveals the elongation of the originally equiaxed ferritic grains in IF steel specimens (e.g. UAT specimen in Fig. 2.7(a)). Difference in formability between the soft ferritic matrix and the embedded hard inclusions induces early nucleation of microvoids upon deformation (Fig. 2.7(b) and (c)). However, due to the low number of "damage sources" (i.e. inclusions), the total void fraction remains low in all strain paths and its effect on the microstructure evolution in IF steel is therefore limited. Accordingly, comparing the damage accumulation along different strain paths, no significant difference is observed between the different IF steel specimens, see Table 2.1. There is, however, a difference in the morphology of many of the analyzed microvoids: the voids nucleated in the uniaxial strain path (e.g., Fig. 2.7(b)) have less sharp tips compared to those nucleated in biaxial strain path (e.g., Fig. 2.7(c)). This is attributed to the positive minor strain in the BAT path, which drives the enlargement of the nucleated voids in the plane, forming penny-shaped voids, which are "thinner" than those nucleated in the uniaxial regime.

In the DP sheets, deformation is governed by the flow of the ferritic grains, similar to IF steel. The hard martensite phase covering the ferritic grains only constraints the ferritic deformation, while its own deformation remains primarily elastic(Fig. 2.8). The difference in flow characteristics of these two phases, along with the higher inclusion density, activates some fundamentally different damage mechanisms, resulting in significantly more damage evolution compared to IF, as tabulated in Table 2.1 and shown in Fig. 2.9 (a). Based on extensive fractographic analysis these damage mechanisms were identified as particle-matrix decohesion, particle cracking, martensite fracture, and grain boundary decohesion, see Fig. 2.9 (b) to (f). For these samples, microvoid accumulation is observed throughout the entire cross sections, however, damage accumulation is slightly higher towards the center of each sample, probably due to the slightly higher stress triaxiality in the center. Also, there is a significant

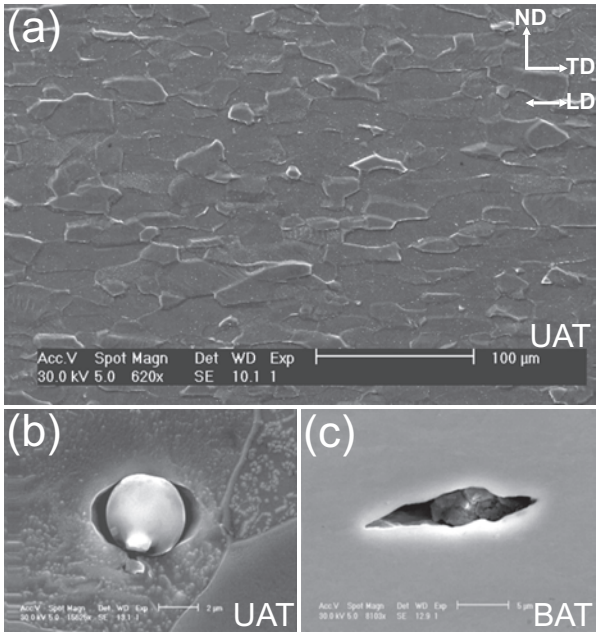

Figure 2.7: (a) The microstructure of the IF steel prior to localization (Loading direction (LD) indicated with the arrow.). (b) Void growth from aluminium oxide particle in IF steel in UAT strain path. (c) Void growth from titanium nitride particle in IF steel in the BAT strain path.

difference between the amount of damage accumulation in different strain paths already prior to localization. Near the point of necking, the area fraction of nucleated voids is more than five times larger in the biaxial-strained specimen compared to the uniaxial-strained specimen (Table 2.1). Evidently, the identified damage mechanisms for DP are more active under biaxial stress condition, as a result of the higher stress triaxiality.

2.3.2 Localization

As the strain levels increase, the deformation starts to localize near the specimen center (see, e.g., the 95% profiles in Fig. 2.5). The points of localized necking, determining the FLC's, for the tested steels are shown in Fig. 2.6.

The obtained FLC's reflect their typical 'v'-shape, i.e. the level of major strain at which localization takes place depends strongly on the strain path that is followed (Fig. 2.10). Since the IF steel develops only a negligible microvoid fraction prior to necking, the FLC is not affected by damage evolution. The v-shape of the FLC logically reveals easier necking in the PST strain path, since necking requires plane strain path to develop [32]. In the UAT and BAT strain paths, however, different constraints delay localization. In the UAT path, the negative minor (in-plane) strain is effectively reducing the thinning of the sheet (in thickness direction) with increas-

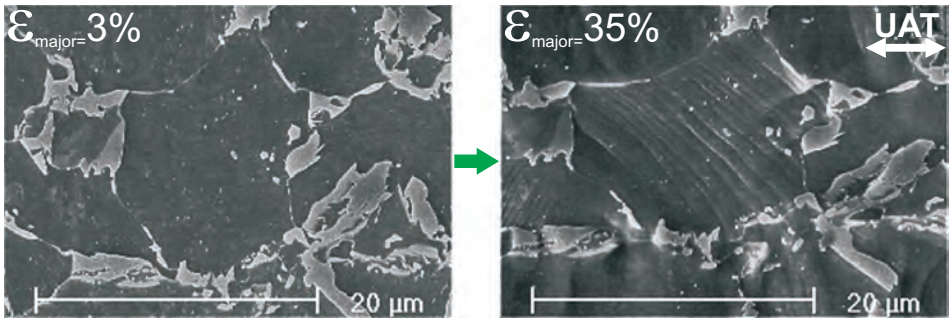

Figure 2.8: The martensite phase surrounding the ferrite grains hardly deforms and therefore constraints the deformation of ferrite. The micrographs show snapshots of the microstructure deformation in UAT, at low (left) and high (right) strain levels. The loading direction is indicated with the white arrow.

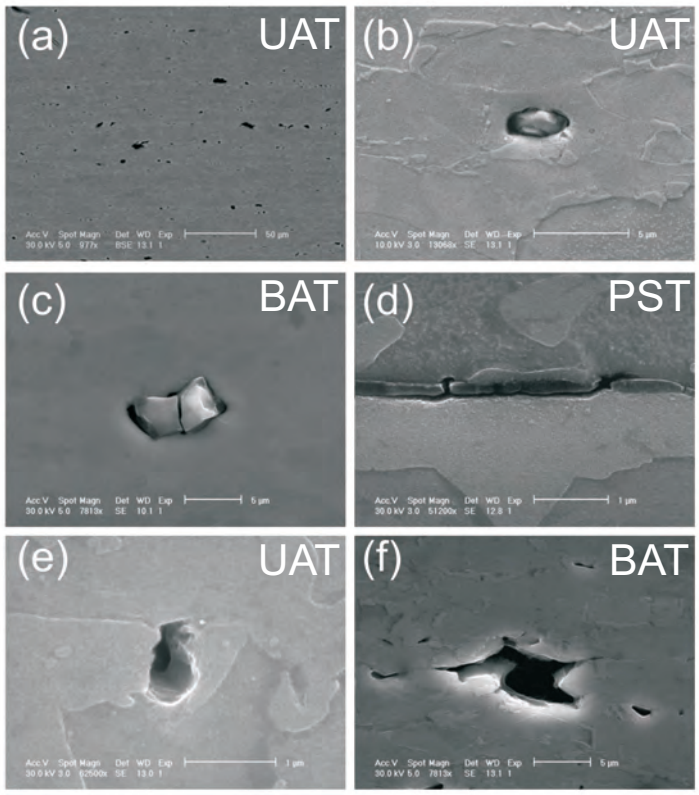

Figure 2.9: (a) Damage evolution in DP steel before strain localization: Void nucleation and growth is observed through the mechanisms of (b) particle-matrix decohesion, (c,d) particle cracking, (e) martensite fracture and (f) phase boundary decohesion.

ing major strain, giving rise to a FLC value with higher major strains. Along the BAT path, on the other hand, plastic incompressibility is expected to trigger early localization. However, Marciniak et al. argued that under biaxial straining conditions there are geometrical constraints inhibiting the localization zone to reach the plane-strain path, necessary for the neck to grow. This effectively delays localization, causing extensive thinning in the equi-biaxial path compared to UAT and PST specimens. Scaled thicknesses of these samples at localization is depicted in (Fig. 2.11).

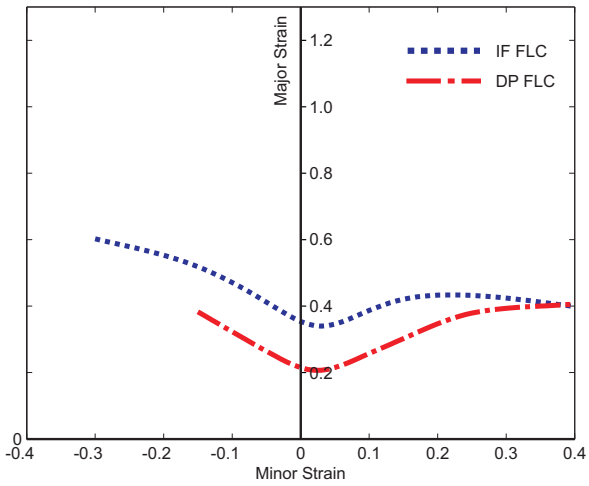

Figure 2.10: FLC's of IF and DP steels

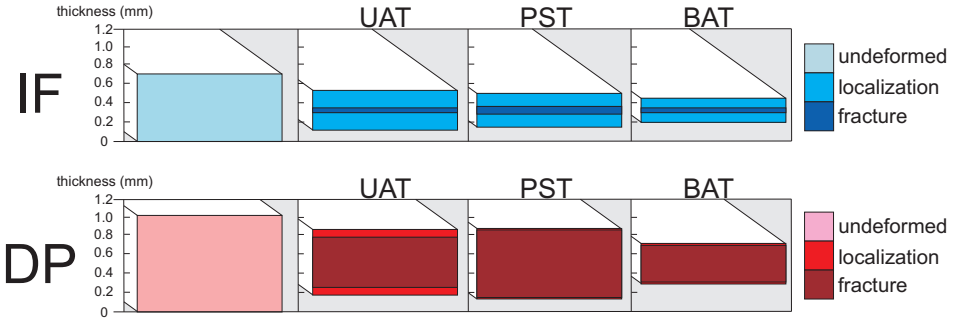

Figure 2.11: The thickness of the thinnest cross section of IF and DP specimens at different stages of deformation, and in different strain paths.

As explained earlier, DP specimens develop significant damage evolution prior to the point of localization. It is therefore reasonable to expect that damage itself triggers local softening leading to localization in this material. Correspondingly, the FLC of DP, which has a similar v-shape, reflects lower major strains compared to the FLC

of IF steel (Fig. 2.6(b)) for almost all strain paths. Only towards the equi-biaxial path, the FLC's of DP and IF steels approach each other (Fig. 2.10). This can be explained by a more pronounced geometrical constraint to reach plane strain condition (see above) for DP compared to IF steel. That is to say that since the ability to reach a plane strain state in the necking zone depends highly on the deformability of the phases that constitute its microstructure, the martensite surrounding the ferrite grains limits the deformation of ferrite thereby enhancing the aforementioned geometrical constraint. As a result, for DP more additional thinning is observed in the BAT strain path relative to the UAT and PST paths (Fig. 2.11).

2.3.3 Localized deformation to fracture

Further thinning following the formation of a localized neck eventually leads to fracture. In the case of the IF steel, a nearly vertical path is traced from the FLC to the FrLC for positive minor strains, as seen from the strain paths in Fig. 2.12(a) and tabulated strain ratios in Table 2.1. The neck is constrained in the minor strain direction (along its axis), yielding a plane-strain state in the neck and thus a vertical strain path. For the negative minor strains, however, the strain paths between FLC and FrLC are only partially bend towards a vertical path. This seems to be caused by the decrease in constraint of the neck in the minor direction with decreasing width of the Nakazima strips. However, these paths also do not continue along the same slope as that of the pre-FLC path either, as the constraint to deformation in the (in-plane) minor direction should be higher inside the localized neck (above the FLC) than in the whole specimen during homogeneous deformation (below the FLC). The non-zero negative minor strain results in a longer path from the FLC to the FrLC for the uniaxial strain path specimens compared to the other specimens. Consecutively, examining the cross sections of the IF specimens, a clearly longer neck is observed in the uniaxial strain path compared to other strain paths, confirming the relatively higher accumulated major strain in this path (Fig. 2.13(a)).

Let us now concentrate on damage mechanisms in IF steel samples. As mentioned earlier there is no damage evolution in IF steel prior to localization, however following necking, a limited amount of damage accumulates locally near the fracture surface in all strain paths (e.g. Fig. 2.13(b)). For the UAT specimen, it is mentioned above that the material is more 'formable' in the major strain direction, as a result of the less stringent constraints exerted on the localized neck in the minor strain direction. This results in a significantly higher degree of damage accumulation in the uniaxial strain path compared to plane strain or the biaxial strain paths (Table 2.1). More microvoids are nucleated and the nucleated microvoids grow to a larger size before a critical void size and density is reached at which fracture occurs. In the biaxial strain path, as shown above, the sheet goes through excessive thinning prior to the formation of the localized neck (Fig. 2.11), during which voids with relatively sharper morphologies are nucleated (Fig. 2.7(c)). As a result, beyond the point of necking, the critical size of voids at fracture is relatively smaller compared to uniaxial strain

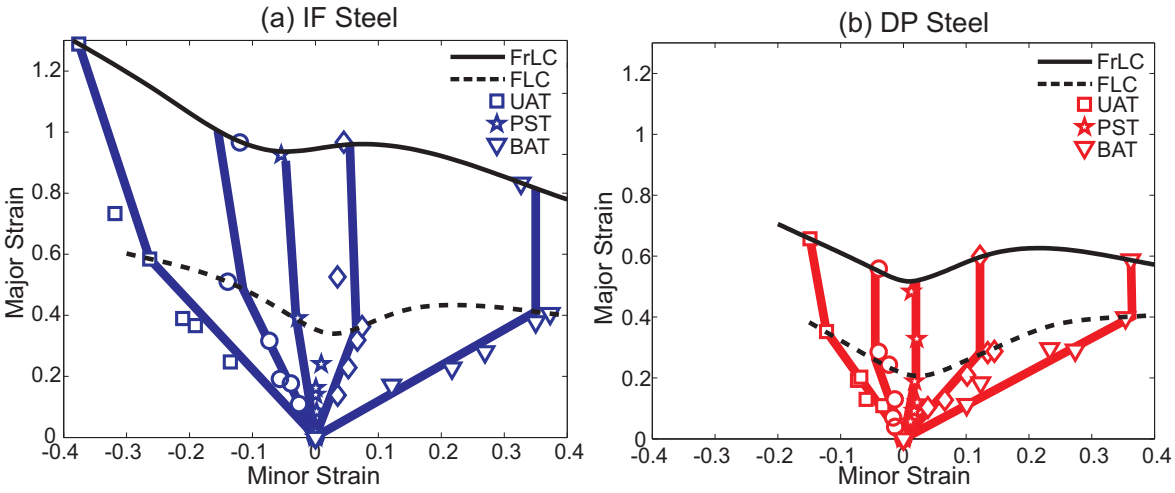

Figure 2.12: Strain paths leading towards the FrLC of (a) IF steel and (b) DP steel specimens.

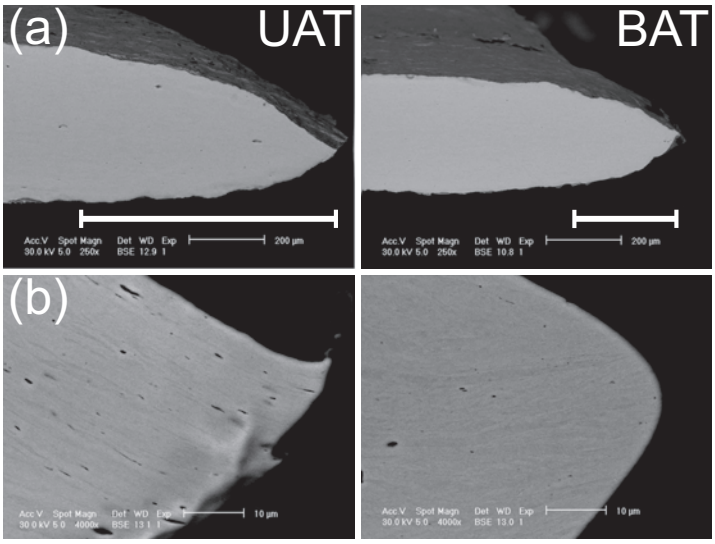

Figure 2.13: (a) Cross section of the localized neck in IF steel in UAT and BAT strain paths (The length of half localized neck is shown with the white marker), (b) Damage evolution in UAT and BAT strain paths.

path, while the spacing of the voids is relatively larger. On a more general note it should also be mentioned that the thickness at fracture is almost independent of the strain path followed, although localization occurs at significantly different thickness strains (Fig. 2.11).

Let us now concentrate on DP. Examining the strain paths in Fig. 2.12 and the tabulated strain ratios in Table 2.1, it is apparent that all strain paths turn to a plane strain path from FLC onwards for positive minor strains. However, again the UAT strain

path does not completely turn to the plane strain stress state inside the neck. But the effect described above for UAT in IF steel is relatively more pronounced for DP steel, probably due to the constraints exerted on the ferrite grains by the martensite phase.

Unlike IF steel, fracture occurs without significant thinning beyond localization in all DP steel samples (Fig. 2.11). This is understandably due to the significant amount of damage accumulation prior to localization, tabulated in Table 2.1. However, the influence of damage is observed to be different in different strain paths. For positive minor strains and especially in the equi-biaxial tension path, the FrLC is closer to the FLC (Fig. 2.12). Comparing the overall damage density in the analyzed micrographs, it is observed that damage accumulation is more pronounced in biaxial deformation compared to uniaxial tension (Fig. 2.14 (b)), although only a very small portion of this damage is accumulated after necking. Apparently, in the BAT strain path a critical damage is already reached at the point of localization, leading to failure without significant thinning or damage evolution following localization, consistent with the reduced distance between the FLC and the FrLC at that point. The relatively small length of the localization zone in the biaxial strain path specimen (Fig. 2.14 (a)) and the homogeneous damage distribution in this local neck (compared to the damage accumulation that is increasing towards the fracture surface in UAT and PST specimens ((Fig. 2.14 (b))) both agree with this analysis.

In the uniaxial strain path, on the other hand, fracture apparently occurs only at a somewhat higher damage density, causing a build up of damage towards the crack, consistent with the larger distance between FLC and FrLC and the measured damage values in Table 2.1. These observations are in accordance with the effect of the negative minor strain in the uniaxial strain delaying fracture even after the formation of the localized neck.

2.3.4 Fracture

Evidently, localized deformation of sheet metal ends in fracture. The observation of the fracture surfaces of the tested specimens at different scales completes the analysis carried out above. It should be stated, however, that the crack initiation triggers complex strain states that cannot be correlated to the strain path before fracture, in a straightforward manner. Nevertheless, this analysis has significant added-value, as many researchers use fractography as their main source of information for failure analysis.

Macroscopic fracture examination of the IF and DP sheets deformed along different strain paths reveals that, apart from the IF - UAT specimens, all specimens fail with a macroscopic crack running perpendicular to the direction of major strain (Fig. 2.15(b)). For IF - UAT specimen, localization through in-plane shear bands is observed, which triggers the final macroscopic crack fracturing the sheet.

Even when the in-plane fracture path is similar, through-thickness fracture may still proceed in different ways, e.g. cup-and-cone, through-thickness shear fracture etc.

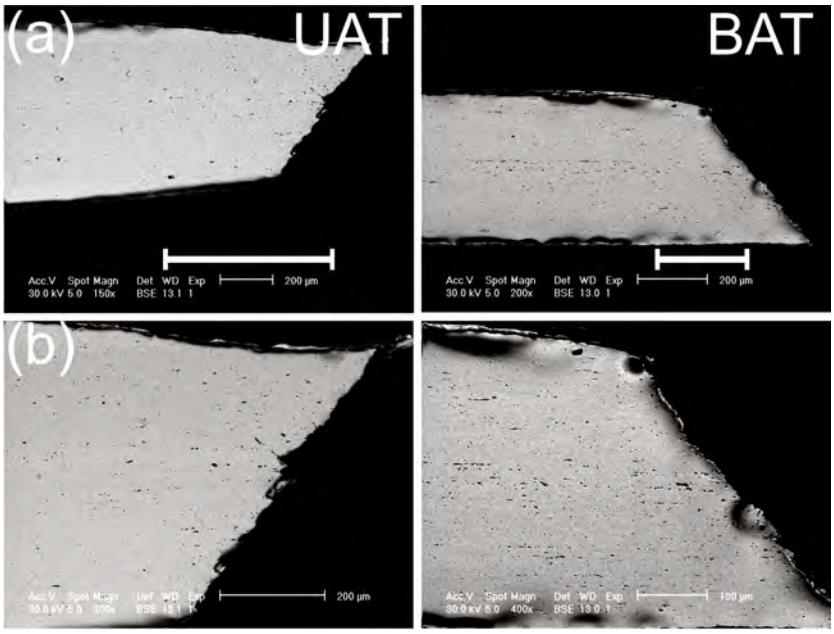

Figure 2.14: (a) Cross section of the localized neck in DP steel in UAT and BAT strain paths (The length of the half localized neck is shown with the white marker), (b) High magnification images of the same specimens showing damage evolution in UAT and BAT strain paths.

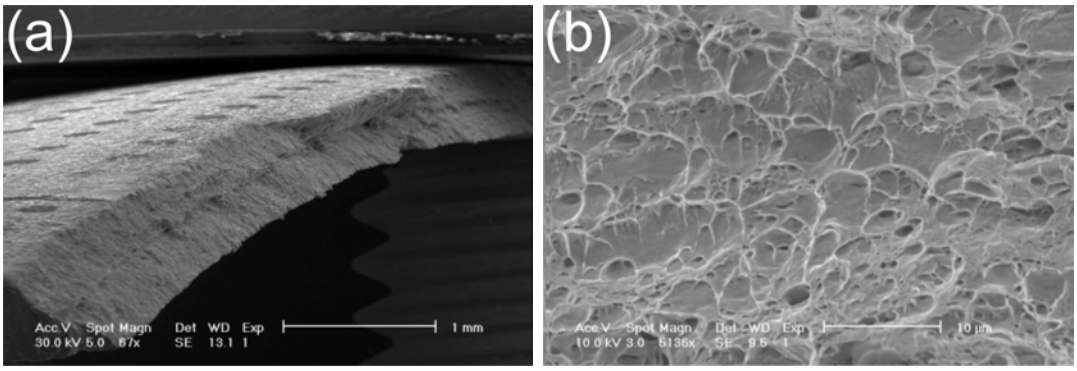

Figure 2.15: Fracture of the uniaxial strain path specimens of (a) IF steel and (b) DP steel.

For both the IF and DP sheet (Fig. 2.13 and 2.14), the final fracture predominantly occurs via a through-thickness shear fracture mechanism. However, a detailed examination of the fracture surface reveals that alternating regions of either cup-and-cone fracture or through-thickness shear fracture mechanisms can be identified, see e.g., Fig. 2.16 for the plane strain IF specimen. Micro-analysis of crack propagation (e.g. through the distortion of dimples) reveals that the fracture always initiates through a cup-and-cone crack which makes a transition to through-thickness shearing at some

point after the crack starts propagating in the minor strain direction. In the shear fracture zone the crack starts at the top or bottom of the specimen, where damage has already nucleated and weakened the material, and the crack propagates by shearing of the two specimen sides from each other.

Fig. 2.16 also clearly shows microvoid accumulation in the center of the cup-and-cone structure, but not in the shear fracture zone. These void-free surfaces could be a result of the smearing effect of the two surfaces as the fracture proceeds (as also reported by [33]), or of extensive shearing of the voids[3].

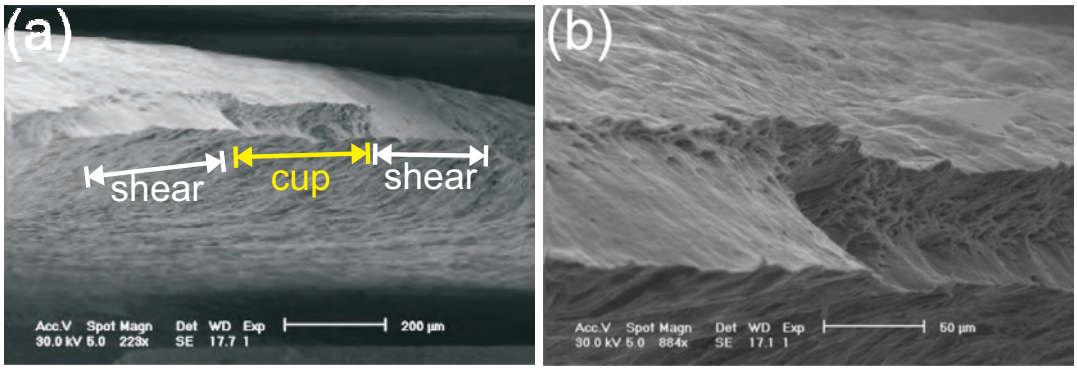

Figure 2.16: (a) The fracture surface of the PST specimen of IF steel (viewed from direction 2).(b) High magnification micrograph showing both the cup-and cone and the through-thickness shearing sites.

The examination of the fracture surface of the IF steel reveals two interesting points. First, there are two groups of dimples in the fracture surface as shown in Fig. 2.17(a). The first group of these dimples are large (10 – 20 micrometers) with visible inclusions inside and the second group of dimples are smaller (2 micrometers or below) without any inclusions inside. Second, for IF steel, the BAT specimen has an almost dimple-free surface as shown in Fig. 2.17(b). This is consistent with the observation made from the cross section images in Fig. 2.13 for IF steel, where a lower number of voids were revealed in biaxial strain path specimens.

The DP steel shows a through-thickness shear fracture in all strain paths (Fig. 2.18 (a). Unlike the IF steel, the fracture surface is completely filled with dimples (Fig. 2.18 (b)), emphasizing the effect of damage in the prior deformation. However, compared to the IF specimens the average size of the voids in the fracture surface of DP specimens is smaller ($\sim$3 micrometers). This is essentially due to the fact that IF steel is more formable around the voids. Consequently in DP steel, once the material

[3]Note that the co-existence of different fracture-induced morphologies and the reported smearing effect complicates any analysis of the failure mechanism that leads to fracture. Our observations show that it is possible to have two contradictory SEM images from the same fracture surface, one completely filled with dimples and the other without any dimples. It is therefore more objective to also examine cross sections in such specimens, even though many researchers prefer otherwise.

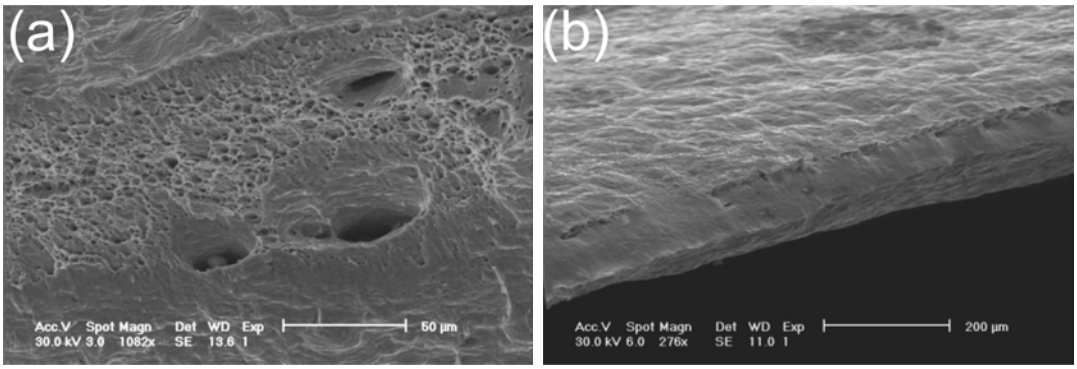

Figure 2.17: (a) Different sizes of dimples in the fracture surface of IF steel specimens. (b) Fracture surface of the IF steel specimen deformed in the biaxial strain path.

reaches the point of fracture, the high concentration of voids and the low formable character of the microstructure induced premature rupture without any significant smearing effects.

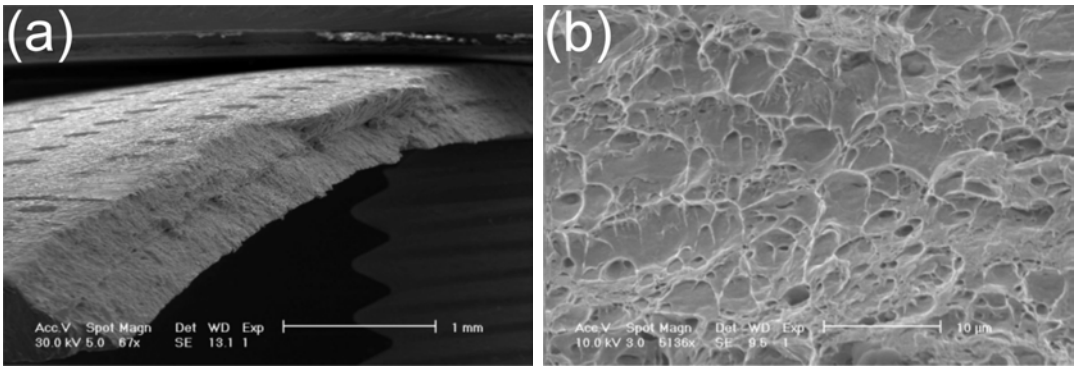

Figure 2.18: (a) Fracture surface of the DP steel specimen (uniaxial). (b) Dimples observed in the fracture surface shown in (a).

2.4 Conclusions

From the detailed analysis presented above, the following generalized conclusions can be drawn regarding the influence of ductile damage on sheet metal forming limits:

For formable, homogeneous microstructures (i.e. microstructures with few damage mechanisms):

i) Damage does not play a role before (or on) localization, but only beyond localiza-

tion.

ii) Aforementioned influence of damage is more ”critical” in strain paths with positive minor strains (e.g. equi-biaxial strain path), as geometrical constraints delaying localization causes excessive thinning and the sharp, elongated morphology of the nucleated voids cause higher stress concentration.

iii) Along strain paths with negative strain ratio, the negative minor strain effectively retains the thinning of material (even after localization), making it more damage and fracture resistant.

On the other hand, for microstructures with phases of different deformation characteristics (i.e. microstructures with easily activated damage mechanisms):

i) Damage plays a significant role on localization, and on fracture.

ii) Damage accumulation takes place even before localization, and possibly leads to inhomogeneities in local softening triggering localization, causing relatively lower forming limits (e.g. either FLC or FrLC).

iii) As significant amounts of damage accumulates prior to localization, beyond the point of localization these metals are sensitive to fracture, and fail without significant further thinning. Consecutively, fracture limit curves of these materials are very close to their forming limit curves.

iv) The overall damage accumulation is observed to be significantly higher in the strain paths with positive minor strains, already prior to localization, causing a higher fracture sensitivity upon necking.

In light of these findings, important suggestions can be made for improving the applicability of AHSS's in industrial applications. For example, FLC of these new steels can be increased to higher strains by somehow inhibiting the damage micromechanisms that are active before localization. Also, formability loss in these materials can be diminished by preventing the hard phase (e.g. martensite in DP steel) to completely cover the circumference of the soft parts (e.g. ferrite in DP steel), although this comes easily at expense of the yield strength when the martensite morphology is not controlled perfectly and becomes too open.

2.5 Acknowledgments

This research was carried out under the project number MC2.05205 in the framework of the Research Program of the Materials innovation institute M2i (www.m2i.nl), the former Netherlands Institute for Metals Research. The valuable contributions of our industrial partner, Corus, on the tests and analysis are also gratefully acknowledged.

CHAPTER THREE

Multi-axial Deformation Setup for Microscopic Testing of Sheet Metal to Fracture[1]

Abstract

While the industrial interest in sheet metal with improved specific-properties led to the design of advanced alloys (e.g. DP, TRIP, TWIP steels) with complex microstructures, predicting their safe forming limits and understanding their microstructural deformation mechanisms remain as significant industrial and scientific challenges. The main underlying cause of these challenges is the inadequacy of the existing experimental tools. The investigation of the strain-path dependent failure mechanisms of the new alloys requires miniaturized testing equipment, which can be placed in a scanning electron microscope to carry out in-situ experiments. Up to now, such tests can only be carried out in a single strain path (uniaxial tension). In this work, in order to fill this gap a miniaturized Marciniak test setup is designed, built and tested. With the new setup real-time, multi-axial tests of industrial sheet metal can be carried out up to the point of fracture within a scanning electron microscope. Proof-of principle experiments demonstrate that a realm of information can be obtained, which can be used to enhance the understanding of the mechanical behavior of these advanced alloys.

[1] *Reproduced from:* C.C. Tasan, J.P.M. Hoefnagels, E.C.A. Dekkers, M.G.D. Geers, Multi-axial Deformation Setup for Microscopic Testing of Sheet Metal to Fracture, *Submitted*, (2010).

3.1 Introduction

There is a growing scientific and industrial interest in the development of sheet metal with improved specific-properties, governed primarily by the weight-reduction motivations in the automotive industry [4]. Whereas related metallurgical research has lead to new alloys with complex microstructures (e.g. transformation induced plasticity steels, twinning induced plasticity steels, dual-phase (DP) steels, magnesium alloys, aluminium alloys, etc.), it also triggered two main challenges regarding proper character of the mechanical behavior of these alloys:

(i) Experimental (or numerical) determination of the forming and fracture limits (e.g. tensile instability, ductile fracture, shear fracture) of these new alloys in different stress and strain states,

(ii) Understanding the underlying micromechanisms that dictate the observed global material behavior and its accompanying failure mechanisms.

Although the literature has seen extensive amount of research on both aspects separately, the connection in between is only rarely established, e.g., to link the strain path dependent forming limits to the underlying microstructural deformation mechanisms [34, 35]. The major cause of this gap in the literature is the limitations of the commonly available experimental methodologies, i.e. macro-scale mechanical deformation tests for measuring forming limits and post-mortem fractography analyses for revealing microstructural-deformation mechanisms. Although these techniques have provided clear insight in the behavior of metal microstructures over the past century, thorough understanding of the deformation mechanisms in the complex microstructures of the aforementioned new alloys requires real-time analysis of microstructural deformation mechanisms. Therefore, recent studies employ miniaturized tensile testing equipment inside scanning electron microscopes, e.g., to investigate the influence of tempering [36] or segregation-induced banding [37] in DP steels. These studies clearly demonstrate the benefits of real-time microstructural analysis. In fact, a mechanical-microscopical approach makes it possible to address both challenges stated above simultaneously, by high-resolution real-time imaging enabling the investigation of the underlying deformation mechanisms and subsequent micrographic digital image correlation to enable determination of deformation limits even locally.

On the other hand, commonly used sheet metal forming processes almost always impose complex strain paths to the sheet being formed, making it unrealistic to analyze the strain path dependent behavior (and failure) of the sheet definitively through tests along a single strain path only (i.e. standard uniaxial tension test). Realistically, a full understanding of this path dependency requires in-situ examination of the deformation-induced microstructure evolution in all relevant strain paths. However, this was so far not possible due to the absence of a setup that allows in-situ multi-axial testing of sheet metal up to the point of failure. This paper presents a miniaturized Marciniak test setup that is dedicated for this purpose. In the following sections, first the choice for the Marciniak deformation concept is motivated through

a critical comparison between possible candidates. Next, the challenges related to the miniaturization of the Marciniak setup to enable real-time in-situ scanning electron microscope (SEM) visualization are explained, and the resulting final design is presented. The paper is finalized with results from proof-of-principle experiments.

3.2 Critical Analysis of Multi-axial Testing Setups for Miniaturization

Several multi-axial testings setups have been developed to study deformation of sheet metal, e.g. bulge pressure tests [38, 39], hemi-spherical punch (i.e. Nakazima) tests [19, 34], cruciform tests [40–42], flat punch (i.e. Marciniak) tests [32, 43], multiaxial compression tests [44, 45], electromagnetic forming tests [46, 47] (Fig. 3.1).

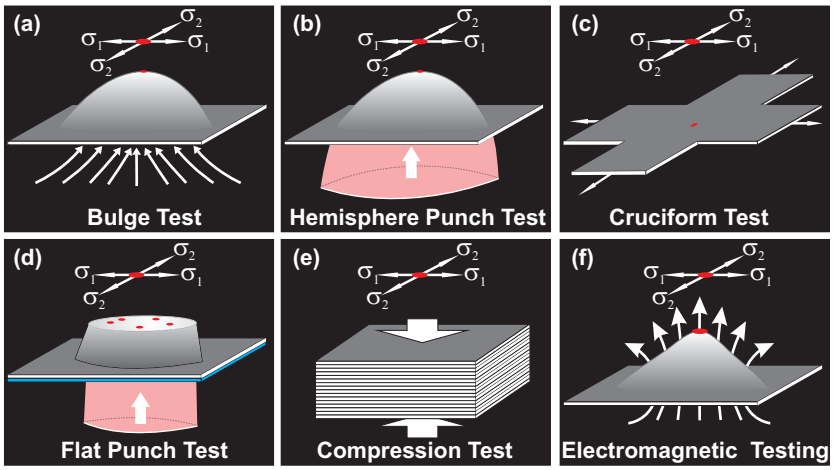

Figure 3.1: Commonly used methodologies for applying multi-axial loading, illustrated here for the case of biaxial tension testing: (a) bulge test, (b) Nakazima test, (c) cruciform test, (d) Marciniak test, and (e) electro-magnetic test

Each of these techniques have specific strengths and weaknesses regarding the degree of the control of the stress state, the quality of information provided, practicality, etc. The minimum requirement for any methodology for real-time mechanical-microstructural characterization of multi-axial deformation in a miniaturized configuration, is to:

- avoid constraining the physical deformation and failure mechanisms of the sheet being tested (i.e. to allow characterization of ”true” microstructural mechanisms),
- operate (safely) within the vacuum chamber of a SEM to allow for in-situ visualization and local strain mapping,

- produce the required level of load and displacement (i.e. to reach sheet metal failure).

Commonly used methodologies such as the compression test and the hemi-sphere punch test exert the required force through direct contact with the test piece. This makes the observed material behavior heavily dependent on the degree of friction, however, the level of its influence is difficult to assess in small-scale tests. For instance, finite element simulations[2] show that the location of fracture in the hemi-sphere punch test is directly related to the level of friction between the punch and the sheet metal being pressed (Fig. 3.2(a)). Similar concerns hold for the compression test, for which a direct view of observation in SEM is also not possible. For the hemi-sphere punch test the imposed strain path is further complicated due to the existence of a bending component, which increases with the miniaturization of the punch (Fig. 3.2(b)). As a result of these complications, characterization of the microstructural mechanisms using the hemi-sphere punch test and the compression test is not trivially possible.

Contact related problems are not an issue for bulge tests, electromagnetic forming tests or cruciform tests. However, for the former two cases, operation within SEM is not possible, due to the required fluid pressure (that is released upon sheet metal fracture) and strong magnetic field, respectively. The cruciform test, on the other hand, is an interesting candidate for miniaturization, since (at first glance) there seems to be no direct influence of boundary conditions on the region of interest (i.e. center of the cruciform). However, finite element simulations revealed that reaching high levels of deformation in the center of the cruciform is not possible, unless the thickness in the center is significantly reduced to a bowl-profile (Fig 3.3(a)). It was reported earlier that such a thickness reduced geometry may be manufactured by electro-discharge machining (or electro-chemical machining), ensuring that the failure is forced to occur at the center (Fig 3.3(b)) [40]. Unfortunately, it is well-known that industrial sheet metals have a non-homogeneous microstructure distribution along the thickness direction. Removing layers from top and bottom of the sheet render the probed microstructure not representative anymore for the as-received sheet metal. Furthermore, it is questionable whether the real material failure behavior is properly probed, since the center of the bowl, with the smallest thickness, is forced to fracture first (Note that in case of a bowl with a flat base, the fracture always occurs at the edge of the flat base, see Fig 3.3(a). Due to these reasons, the cruciform test is also regarded as unsuited for investigating large deformation induced macro and microstructural phenomena in sheet metal.

Finally, in the Marciniak test (Fig. 3.4), the load is transferred from a flat punch to the specimen via a so-called 'washer' plate, which has an opening window in the

[2] All simulations are modelled with an isotropic elasto-plastic material model of high-quality deep-drawing steel, for which the elastic and plastic material properties are determined from standard tensile tests. The sheet is modeled using solid axisymmetric elements, a four node quadrilateral element with bilinear interpolation, while the punch and the two clamps are modeled as rigid bodies. For friction the coulomb model is used, and the coefficients of friction are varied between 0 and 1.

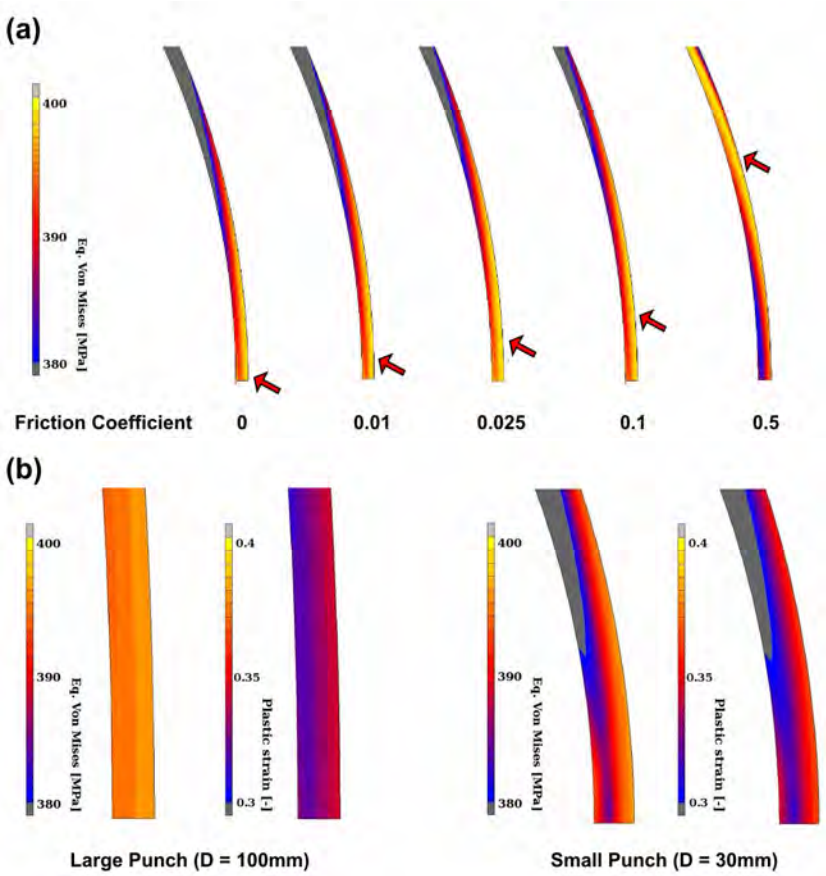

Figure 3.2: Finite element simulations of the hemi-sphere punch tests demonstrate the challenges in miniaturization: (a) friction strongly influences the strain distribution and failure, such that increasing friction causes highest strains away from the top of the punch. (b) miniaturization of the punch decreases stress and strain homogeneity along the thickness direction. Note the punch, which has been omitted from the graphs for clarity, comes in from left to right. Only half of the sheet is simulated.

middle under the region of interest (hence, there are no friction effects in this gauge region). Both the sheet and the washer are drawn simultaneously, the latter at a larger velocity due to the opening in the center. The resulting relative velocity creates friction forces on the tested sample in the opposite direction of those that occur in a normal deep-drawing experiment (i.e. without a washer). This friction force limits the level of deformation of the regions where there is contact between the washer and the sheet and, as shown by the finite element simulation in Fig. 3.4, allows the largest deformation (and failure) to occur at the center (where there is no contact) making the test fundamentally different from a standard punch test. As a result of the absence of contact a true in-plane deformation occurs and inhomogeneous material deformation is not artificially enforced. Accordingly, this test is perfectly suitable for characterizing microstructural mechanisms and, therefore, regained a lot

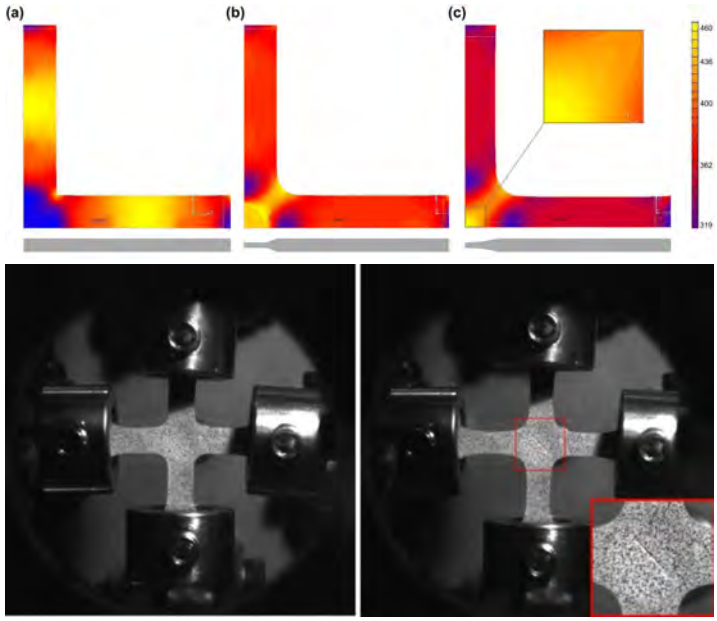

Figure 3.3: (a) Finite element simulations show that the highest stresses can only be obtained at the center, if the thickness is reduced in a bowl profile. Note that the material model used is the same as in Fig. 3.2. Further details on these simulations are given in [40]. (b) Experiments carried out using a home-built biaxial deformation setup verify that the thickness reduced cruciforms fail in their center, however, only when the thickness in the bowl is less then ∼20% of that of the as-received sheet.

of interest recently [48–51]. Furthermore, the Marciniak tests can be carried out safely in SEM (since there is no influence on the working principles of electron microscopy). All these considerations qualify the Marciniak test as the most suitable candidate for a in-situ miniaturized multi-axial deformation test, however the challenge lies in miniaturization.

3.3 Challenges in the Design of a Miniaturized Marciniak Test Setup

It was observed in preliminary macro-scale Marciniak tests that unwanted failure modes (see Fig. 3.5, and also [51]) may be triggered under certain experimental settings (e.g. too small punch radius, too small punch corner radius, too small or too large washer opening radius, too large friction etc.), all affecting the relative drawing velocity of the washer compared to the tested sheet. Of specific concern for miniaturization is a deep drawing type of failure (Fig. 3.5(b)), which occurs when the reverse friction effect is insufficient, thereby causing a stress concentration, σ_{edge}, at the corner of the flat punch, exceeding the stress level, σ_{center}, at the contactless region of the

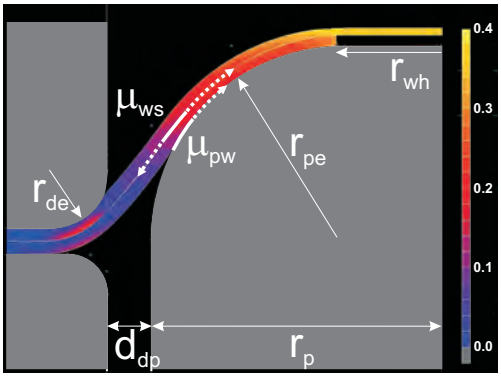

Figure 3.4: Finite element simulation of the Marciniak tests reveal that the highest level of deformation occurs at the center of the tested specimen, if the experimental parameters shown in the figure (punch radius (r_p), punch edge radius (r_{pe}), washer hole radius (r_{wh}), die edge radius (r_{de}), distance from die to punch (d_{dp})) and friction (i.e. between the punch and the washer (μ_{pw}) and between the washer and the sheet (μ_{ws})) are optimized. Note that the material model is the same as in the previous figures, and the punch comes from below.

specimen center. In order to evaluate the sensitivity of the stress ratio $\sigma_{edge}/\sigma_{center}$ to miniaturization and to provide specifications for the miniaturized Marciniak setup, finite element simulations of the Marciniak test are carried out, with a range of different geometries (0<r_{wh}<16mm; 0<r_{pe}<25mm; 0 <r_p <50mm) and friction settings (i.e. (μ_{pw}) and (μ_{pw}) between 0 and 1) (Fig. 3.4) [3].

Figure 3.5: Different failure modes in the Marciniak test investigated on IF steel (for r_p=50mm, r_{pe}=10mm): (a) washer hole initiated failure (washer hole too large) (b) deep drawing failure (i.e. the reverse friction effect not sufficiently strong) and (c) successful failure triggering a random crack in the center region.

The simulation results revealed that r_{pe} should be below ∼5mm and that the friction between the punch and the washer should be as low as possible (μ_{pw}<0.2) to keep

[3]These simulations incorporate the same material model and finite elements as the hemi-sphere punch test explained above, but with a flat punch and an additional washer sheet with am opening.

$\sigma_{edge}/\sigma_{center}$ to a minimum, while the friction between the washer and the specimen should be maximized (μ_{ws}>0.8). Furthermore, the washer hole radius, r_{wh}, also has a strong influence on the stress ratio, and has to be chosen <∼13mm (to avoid "cutting" the tested sheet at the corner (Fig. 3.5(a)) yet larger than ∼5mm (to avoid deep drawing failure at the cup (Fig. 3.5(c))). The most important choice from a miniaturization perspective is the size of the punch. For r_p <∼40mm the stress ratio rises significantly, which should be avoided in the miniaturized setup. Even though increasing the punch size would ensure failure at the specimen center, a punch larger than ∼55mm makes it impossible to produce the level of force required (>150kN) to deform two sheets simultaneously up to fracture within the limited volume of a scanning electron microscope. A final design parameter is the total stroke, which needs to be larger than 15mm to be able to reach failure in most sheet metals.

3.4 Design of the Miniaturized Marciniak Test Setup

To manufacture a Marciniak apparatus with a 15mm stroke and a load range of 150kN, a hydraulic press would be the most logical way for the small working volume available. However, this is obviously not possible in the vacuum environment of a SEM chamber. An alternative idea consists in using a spindle with a nut, driving the nut with an electric motor. Yet, the amount of friction consumes too much torque, making it impossible to select gearbox-motor combination within the maximum working volume. Even going to 16 small spindle-nut combinations around the sample does not match up the design requirements within the working volume of the SEM.

Therefore, an alternative solution is proposed, consisting in the use of a long strong string wrapped around 36 pulleys in a top plate and 36 pulleys in a bottom plate, mounted around the sample (Fig. 3.6). The force on the string is amplified by a factor 72 towards the sample. The string is divided in three parts driving three equally sized segments with rolls around the sample, providing a linear displacement without rotation between bottom and top plate. The three strings are reeled on a winch with a 22 mm brushless motor combined with a harmonic drive gearbox. The force is measured with strain gauges placed on the bottom plate.

3.5 Proof-of-principle Experiments

The capabilities of the miniaturized Marciniak apparatus are demonstrated by in-situ testing an industrial aluminium 6016 alloy to the point of fracture. Experiments are carried out in three different strain paths (i.e. uniaxial tension (Fig. 3.7(a), plane strain tension (Fig. 3.7(b)) and biaxial tension (Fig. 3.7(c)) through the use of specimens of different geometries. In all the tests, the setup operated within the determined working principles, verifying the success of the original design concept.

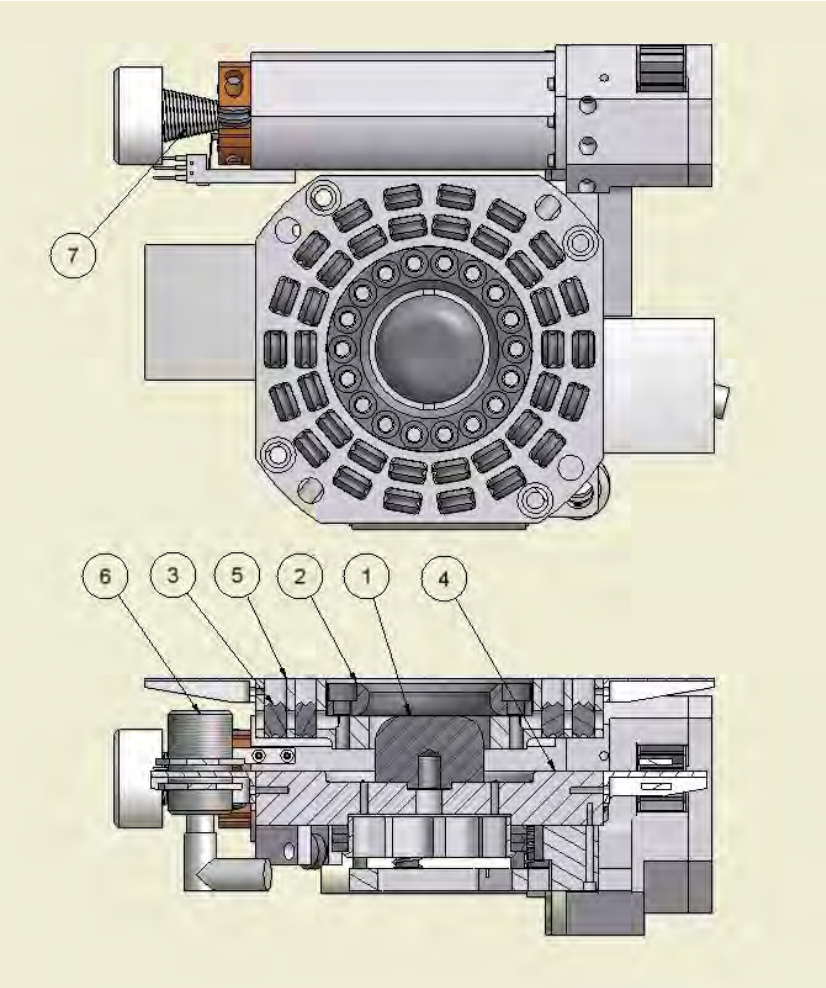

Figure 3.6: The components of the miniaturized Marciniak apparatus: (1) the punch; (2) clamping ring for sample plate and washer, (3) pulley (36 in top plate and 36 in bottom plate, all journalled in needle bearings for low friction), (4) bottom plate, (5) top plate, (6) contactless Eddy current displacement sensor, (7) winch (to reel the three cables

.

Furthermore, fracture is reached in the central (flat) region of the punch, even in the most difficult case of the biaxial tension path, proving that the critical experimental parameters (i.e. (r_p), (r_{pe}), (r_{wh}), (r_{de}), (d_{dp})), (μ_{pw}) and (μ_{ws})) are optimized, and the miniaturization related challenges in the Marciniak test are successfully overcome. And finally, the results also underline the benefits of in-situ testing: high resolution SEM images captured during deformation allow (i) carrying out micrographic digital image correlation to measure strains at the microstructure level, and (ii) studying deformation-induced microstructural mechanisms (e.g. damage evolution) from the obtained SEM image sequences (Fig. 3.7).

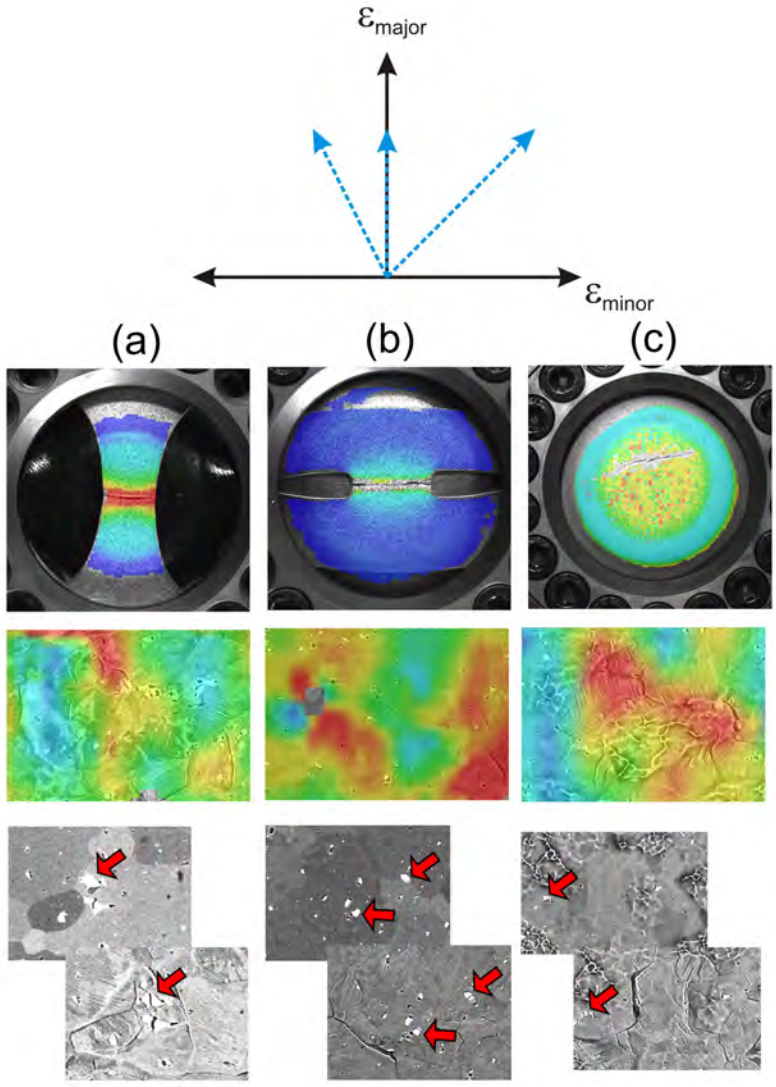

Figure 3.7: Results of the proof-of-principle experiments in (a) uniaxial tension, (b) plane strain tension and (c) biaxial tension strain paths reveal that an immense amount of data can be obtained using the setup: strain fields at the point of fracture, strain fields at the microstructure level (using images from in-situ SEM testing), damage nucleation mechanisms in different strain paths.

3.6 Conclusions

In this work a miniaturized test setup was designed, built and tested, that allows real-time, multi-axial testing of industrial sheet metal within a scanning electron

microscope. A prior numerical-experimental comparison of existing (macro-scale) multi-axial testing setups revealed that the Marciniak test concept suits perfectly to the requirements of miniaturized in-situ testing (e.g. avoiding manipulation of material behavior, operating (safely) within a scanning electron microscope, etc.). Next, miniaturization induced challenges in the Marciniak concept is investigated through finite element simulations, which led to a number of design guidelines (to avoid unwanted failure modes) for the miniaturized setup. An original design concept is developed to meet the determined guidelines within the limited volume of a scanning electron microscope. Proof-of-principle experiments reveal that the developed miniaturized Marciniak setup operates successfully within the design specifications, allowing a realm of information (e.g. high resolution SEM images of different stages of deformation, strain field at microstructure level, etc.) to be obtained.

3.7 Acknowledgments

This research was carried out under the project number MC2.05205 in the framework of the Research Program of the Materials innovation institute M2i (www.m2i.nl), the former Netherlands Institute for Metals Research. The authors would like to thank Gerard Quaak and Carel ten Horn for their contribution.

CHAPTER FOUR

Microstructural Banding Effects Clarified Through Micrographic Digital Image Correlation [1]

Abstract

Microstructural banding is commonly observed in commercial steels, but its effect on the global mechanical properties is still disputed in literature. This letter investigates the influence of band morphology and banding phase properties from tensile tests for two limit cases (continuous hard band vs. discontinuous softer band), analyzed from digital image correlation of in-situ electron microscopy micrographs. The effect of band continuity and hardness are elucidated, yielding a clear detrimental influence especially for hard bands with a continuous morphology.

[1] *Reproduced from:* C.C. Tasan, J.P.M. Hoefnagels, M.G.D. Geers, Microstructural Banding Effects Clarified Through Micrographic Digital Image Correlation, Scripta Materialia, *Accepted*, (2010).

4.1 Introduction

Nearly a century ago, researchers referred to microstructural bands with a rather intriguing name: ghosts [52, 53]. Although this nomenclature seems surprising at first, it can be understood upon closer inspection: these bands which typically appear upon hot working can only be erased with carefully designed heat treatments, only to mysteriously re-appear upon heating [54] or deformation [55].

In the following decades, intense research has elucidated the formation mechanisms of these bands[2]. Despite this qualitative understanding, the processing routes to completely avoid the formation of bands [57–59] or to permanently remove formed bands [60, 61] may not be economically feasible for all cases [55], or in some cases become thermo-dynamically impossible [62]. Yet, the band morphology (thickness, continuity, geometry etc.) depends on heat treatment [57] and deformation processes [56], and thus can be modified within economically feasible limits to remove detrimental effects of the band. Such an approach calls for clear understanding of the influence of band properties on the global mechanical behavior, which is currently unavailable. While a consensus is reached on the detrimental effects on the fracture toughness, (with small effects on yield or tensile strengths), contradictory results exist for the ductility, varying from no influence [63], a slight influence [55, 64], to a significant influence [60, 65]. Even advantageous effects of microstructural banding were reported, e.g., increase in fatigue life [66].

This apparent inconsistency in the literature essentially results from the experimental methodology commonly employed. The influence of banding on mechanical properties is typically investigated by comparing the global material behavior of a banded microstructure with an unbanded microstructure (e.g., [55, 60, 63–65, 67]. The unbanded material is generally produced by a homogenizing heat treatment from the banded material, although different starting materials have also been used (e.g., [60, 65, 67]). However, as emphasized by some authors [65], the exclusive influence of banding can only be elucidated by keeping other microstructural parameters (e.g. composition, phase fractions, grain size, inclusion morphology, etc.) unaltered. In this respect, it was pointed out that homogenizing heat treatments also change the morphology of inclusions, thereby changing the mechanical behavior [55, 63]. This illustrates the complex relation between the microstructure and the mechanical behavior in banded materials, even for carefully designed heat treatments [65].

Another explanation for the above-mentioned inconsistency in the literature emerges from the difference in the banded-phase and/or band morphologies in the studied microstructures. Banded structures occur in many types of steels (e.g.,

[2]For example for ferritic-pearlitic bands, certain alloying elements pre-segregate in the dendritic arms upon solidification, and align (almost perfectly, for still unclear reasons) upon hot working. The segregation causes either a higher or lower shift in the diffusion rate of carbon in austenite, leading to, respectively, a higher or lower carbon content around the aligned segregated elements. A higher carbon content lowers the ferrite nucleation start temperature, and vice verse, thereby yielding the final banded microstructure at room temperature [56].

ferritic-bainitic, ferritic-martensitic, pearlitic-bainitic, pearlitic-martensitic, bainitic-martensitic [56]) and the obvious difference in the mechanical properties of these phases lead to a different net effect of the band. Therefore a general understanding of the main influence of banding cannot be acquired by examining a single case of banded microstructure.

To overcome the aforementioned difficulties, we carry out an in-situ, local analysis of the deformation of two distinct banded microstructures, coupled with micro-scale strain field measurements. The behavior of the banded phase is compared with unbanded regions in the same microstructure, avoiding undesired variations introduced by band-removing heat treatments. In-situ microstructural analyses also provide improved insight in the underlying deformation mechanisms, which govern the global mechanical response. Furthermore, to probe the influence of the banded phase and its morphology, the local mechanical behavior of two carefully-chosen limit cases of banded microstructures are compared in detail: a microstructure containing a continuous, hard band (the martensitic-ferritic system) and a microstructure containing non-continuous, softer bands (the pearlitic-ferritic system), whereby both microstructures are processed from the same starting material for optimal comparison. The obtained information yields in-depth mechanistic understanding of the effect of band morphology, providing general recommendations for industry to fine-tune steel processing parameters, accordingly.

4.2 Experimental Methodology

For the martensitic-ferritic banded microstructure, a dual-phase steel (DP600) is chosen, which is composed of ferritic grains surrounded by martensitic islands at the ferritic grain boundaries (Fig.4.1). A 5μm thick martensitic band is observed in the center of the 1 mm thick sheet[3]. Tensile test samples are cut with electro-discharge machining, and the cross sections are metallographically prepared using successive grinding and mechanical polishing steps, followed by electropolishing and etching with 2 vol.% nital solution. This protocol gives optimal contrast, i.e. the best subset tracking, for the digital image correlation (DIC). The ferritic-pearlitic banded material is produced by austenizing the DP600 (at $1000\,^{\circ}\mathrm{C}$) followed by furnace cooling to room temperature. A morphologically comparable microstructure is obtained, but with pearlite replacing the martensite (Fig. 3a), i.e. with the non-continuous pearlite band replacing the continuous martensite band.

Intermittent tensile tests of these materials are carried out using a Kammrath-Weiss micro-tensile stage, placed in a FEI Quanta 600 scanning electron microscope (SEM). High resolution, low magnification micrographs are obtained in secondary electron mode at successive stages of deformation ($\triangle\epsilon_{global} \approx 0.03\%$). The gray value histograms of the obtained images were adjusted for maximum overlap, and regions

[3] A detailed description of the microstructure is provided in [34].

of interest are chosen for local strain field analysis (using Aramis software, GOM GmbH.). The subset size and spacing were carefully chosen in order to realize the best trade-off between spatial and strain resolution. Good image correlations were generally achieved, although a few subsets are inevitably lost as a result of severe surface roughening, specifically at large deformations in the ferrite grains.

4.3 Results and Discussion

The analysis starts by examining the deformation-induced morphological changes in the DP steel microstructure (Fig.4.1). Note that the global stress-strain response is also provided in the insets.

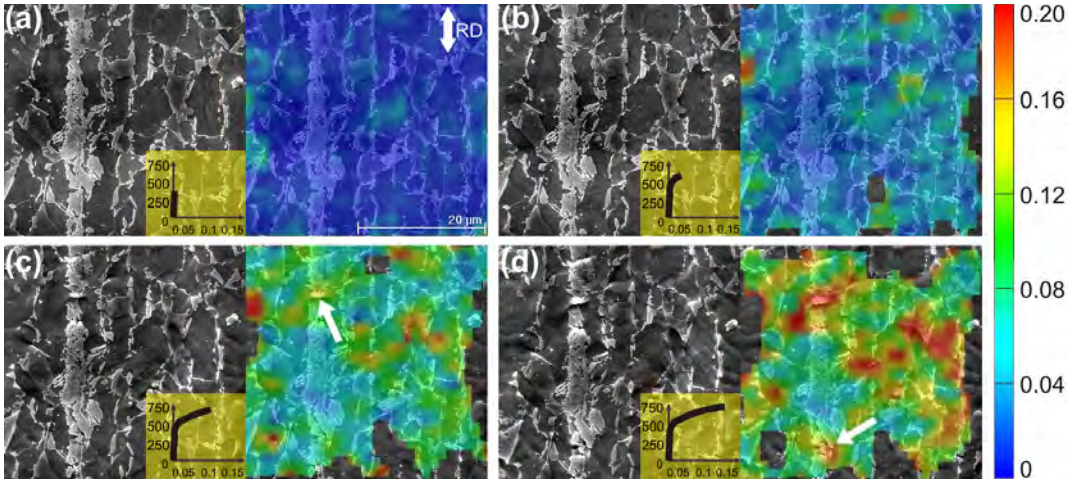

Figure 4.1: Typical example of the deformation of DP steel: SEM images (left) and von Mises effective strain field overlays (right) at four different stages of deformation. The global mechanical response is also shown in the insets (true stress (MPa) vs. DIC averaged strain). The rolling direction, i.e. the testing direction, is shown in subplot (a). White arrows indicate void nucleation sites. Color image online.

Already in the early stages of deformation, the formation of local slip lines within individual ferritic grains is observed (Fig. 1b). As the deformation proceeds, the number of slip lines increases, and the strain distribution becomes increasingly heterogeneous (Fig. 1c). This heterogeneity is caused by intra-granular formation of shear bands at approximately 45 degrees to the testing direction. Careful inspection of higher magnification images reveals that the martensitic grains are acting as obstacles to the propagation of the slip lines, and hence to the plastic deformation of the ferritic grains. In fact, the local strain fields reveal that the ferrite grains experience significant plastic deformation, whereas the martensite islands are strained only elastically at this stage ($\triangle\epsilon_{global} \approx 0.05$). In the martensite band, on the other hand, local regions of high strain are observed at those positions where the martensite band

is the thinnest, as marked with white arrows in Fig. 1c and 1d. As can be verified from the micrographs, the martensitic band is severely deformed at these particular regions up to its fracture strain, leading to void nucleation. From careful examination of the complete series of strain maps, it becomes clear that the intra-granular shear band intercepts the martensitic band exactly at these critical locations, making them the first sites where voids nucleate, while the martensite islands (and the rest of the martensite band) show hardly any deformation or void formation.

The same trends in the strain distribution within the bands are observed for other specimens of the same DP steel (Fig.4.2), i.e., the highest local strains are observed in the narrowest section of the band, leading inevitably to void nucleation at 'hot spots' in these continuous band morphologies.

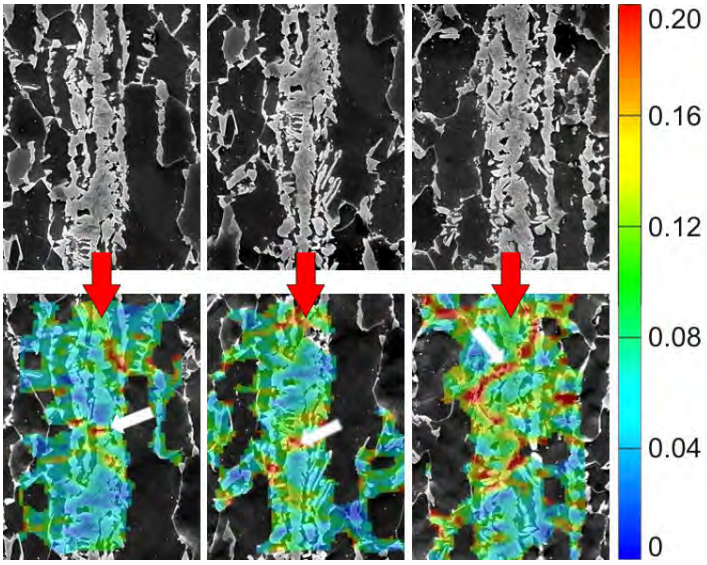

Figure 4.2: Void nucleation within the band, shown here for different martensitic band morphologies, for undeformed state (above) and deformed state (below). Note that the scale is identical to Fig. 1. White arrows indicate the void nucleation sites. Color image online.

From the observed sequence of micro-events, it is clear that the shear bands are developed in preferential paths within the microstructure. In order to accommodate the plasticity of the surrounding ferritic matrix, the martensite in the narrow regions of the band carries most of the deformation, thereby compensating the lack of deformability in the thicker parts of the band. Since martensite has a limited strain-to-fracture, the resulting high strains inevitably lead to early void nucleation.

These observations also reveal the significant role of the martensite morphology on the global material behavior, which tends to be even more important than the martensite volume fraction [68]. Similar to DP microstructures with highly-connected martensite networks, the martensite bands analyzed here are also forced to plastically deform at an early stage of deformation, deviating from "ideal" DP

steel behavior[4], and leading to a decrease in strain-to-fracture.

Let us next concentrate on the deformation-induced microstructure evolution in the pearlitic-ferritic (PF) steel (with the same overall chemical composition as the DP steel). A typical example is shown in Figure 3, where the deformation stages of the resulting PF steel are shown.

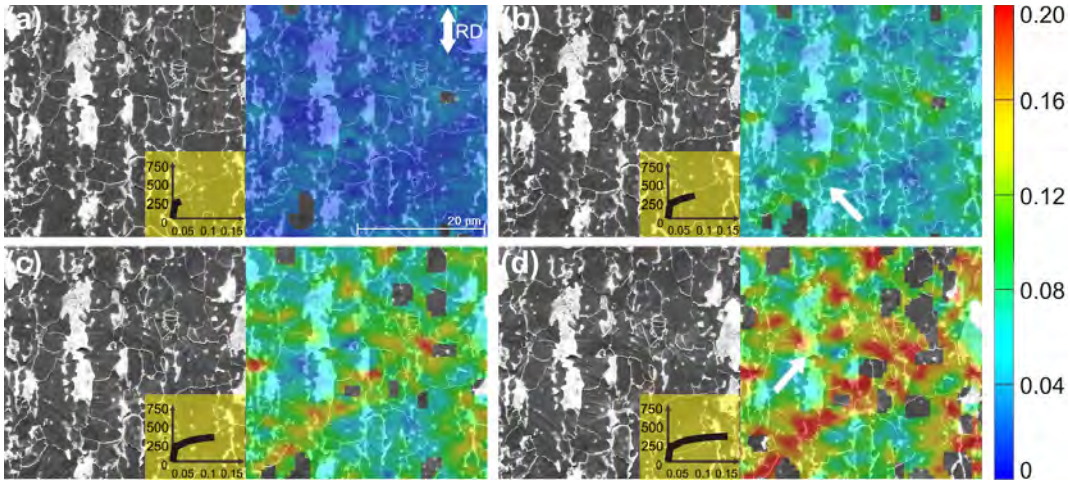

Figure 4.3: Typical example of the deformation of PF steel: SEM images (left) and von Mises effective strain field overlays (right) at four different stages of deformation. The global mechanical response is also shown in the insets (true stress (MPa) vs. DIC averaged strain). Note that all scales are identical to those in Fig. 1. The rolling direction, i.e. the testing direction, is shown in subplot (a). The white arrow in (b) points at the gap in the pearlitic band, and the white arrow in (d) shows the narrowest section of the pearlitic band, where the shear band penetrates through the microstructural band. Color image online.

As seen in the micrographs, the distribution of the pearlite phase in the ferrite-based microstructure is qualitatively similar to that of martensite in the DP steel. On the other hand, the global response of the material is significantly different, as seen from the stress strain inset figures (Fig.4.3). As expected, effectively replacing martensite with pearlite results in a decrease in strength, whereas the overall ductility improves. The main point of interest here, however, is the local deformation patterns at the level of the banded microstructure.

At the first glance, examination of the micrographs and the strain maps at different stages of deformation reveals similar trends in the deformation as found for DP steel (Fig.4.1 and Fig.4.2): initially formation of the slip lines in the ferritic grains, localized deformation at approximately 45 degrees to the testing direction, and the evolution of the strain distribution from homogeneous to increasingly heterogeneous with in-

[4]Ideal DP performance is obtained when ferrite deforms purely plastically and martensite deforms purely elastically [66].

creasing deformation.

However, more detailed analyses reveals a significant difference at a rather early stage, see Fig.4.3b. The first shear band initiates at a discontinuity in the pearlitic band (shown with a white arrow in Fig.4.3b. As confirmed by additional measurements, when the band (morphology) is not continuous, the preferential path for the shear bands is through the gaps in the band. With further deformation, this shear band deforms steadily while the rest of the pearlitic band experiences only a limited amount of deformation (Fig.4.3c). Only at much higher global strain, another shear band is developed that percolates through the narrowest section of the pearlitic band (shown with an arrow in Fig.4.3d), in the absence of any void nucleation. This marked difference in microstructural behavior between DP and PF steels is quantified in Fig.4.4, which compares the local strain evolution of martensite and pearlite to the local strain evolution in the ferrite grains outside the band, as a function of DIC averaged strain.

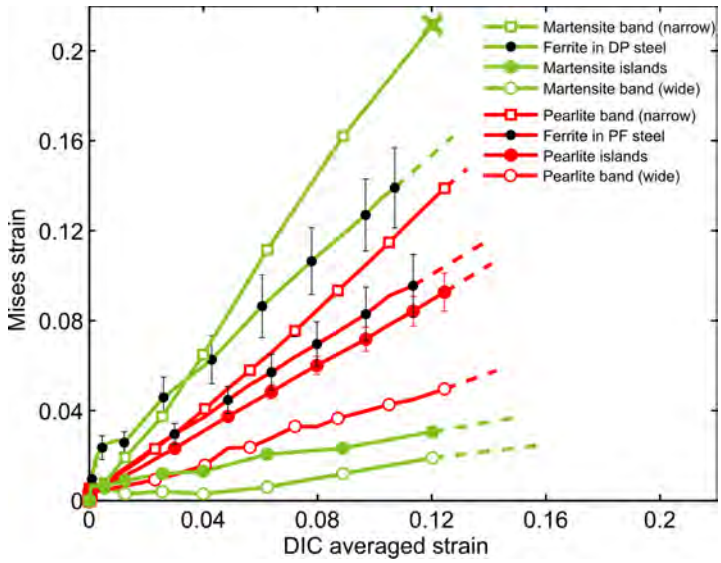

Figure 4.4: Local strain evolution in martensitic and ferritic grains in DP steel (green), and pearlitic and ferritic grains in PF steels (red). High and low deformation zones within the bands in each steel are also shown, with square and circle markers respectively. Martensite cracking is indicated with a X. Note that the error bars represent the standard deviation of the average strain in the specific constituent.

First concentrate on the phases outside the band. The strain partitioning between martensite and ferrite is obviously more pronounced than between pearlite and ferrite. For the DP steel, the narrow band sections show high deformations and eventually cracking to compensate for the relatively low deformation in the wide sections of the band. Note that the strains in these critical band regions are significantly higher than even the most severely deforming ferritic grains. For the PF steel, the strain partitioning is less significant since the pearlite phase well accommodates the ferritic

deformation. Therefore, the amount of excess deformation of the narrow sections of the pearlitic band remains relatively limited. Hence, the probed pearlitic band (which has a large variance in its thickness similar to the martensitic band) experiences no void nucleation at the same level of (global) strain. Even though this observation is consistent with the larger ductility of pearlite compared to martensite, it clearly shows that the influence of band morphology on global mechanical behavior is strongly dependent on the mechanical properties of the banded phase.

4.4 Conclusions

In summary, the obtained reproducible results of the local analysis on two limit cases of banded structures support the following conclusion for the mechanical behavior of banded microstructures: The influence of a banded structure on the global properties (YS, UTS, ductility, etc.) of metals is critically dependent on the morphology of the band, as well as the mechanical behavior of the phase that composes the band. In microstructures where there is a continuous microstructural band, shear bands are forced to develop through the band, therefore they percolate through the narrowest section of the band. This forces the banded phase to deform beyond its plastic limit, especially if there is a significant difference in the ultimate strains of the phases composing the banded microstructure (e.g. the case of martensitic-ferritic dual phase steel). For discontinuous microstructural bands, shear bands naturally cross at the gaps within the band, thereby delaying early damage initiation.

Obviously, the strength of the banded phase also plays an important role, e.g. a continuous band of a high fracture strength phase may accommodate high local stresses without damage initiation, whereas a low fracture strength phase may not.

From an industrial point of view, it is obviously complex to eliminate the banded phase. However, even for cases where complete removal of banding is not economically feasible, presented results reveal that the detrimental influence of a banded microstructure can be significantly reduced by altering the morphology of the band in order to (i) avoid microstructures with continuous bands, and (ii) decrease the thickness variation of the band. For the critical case of reducing the severity of banding in DP steels, for example, this may be achieved by optimizing the reported critical production parameters (e.g. rate of cooling during hot rolling, intercritical annealing temperature, soaking duration, etc. [57–59]) that have a significant influence on the degree of banding.

4.5 Acknowledgements

This research was carried out in the framework of the Research Program of the Materials innovation institute, the former Netherlands Institute for Metals Research. The authors would like to thank Bart Vossen for his contribution.

CHAPTER FIVE

A Brittle Fracture Methodology for 3D Visualization of Ductile Deformation Micro-Mechanisms [1]

Abstract

An improved experimental methodology is developed and successfully evaluated to visualize deformation induced micro-events in ductile sheet metal. This easy-to-use methodology consists in a well-controlled brittle separation of samples previously deformed in a ductile manner, whereby a coupled-analysis of the two fracture surfaces permits to re-combine 3D features from the ductile pre-deformation. Obtained results show a realm of information regarding grain deformations, microvoid nucleation sites and growth mechanisms, and other micro-events induced by ductile deformation.

[1] *Reproduced from:* C.C. Tasan, J.P.M. Hoefnagels, M.G.D. Geers, A Brittle Fracture Methodology for 3D Visualization of Ductile Deformation Micro-Mechanisms, Scripta Materialia, 61(1), 20-23, (2009).

5.1 Introduction

In 1900, Ewing and Rosenhain [69] stated "The microscopic study of metals was initiated by Sorby, and has been pursued by Arnold, Behrens, Charpy, Chernoff, Howe, Martens, Osmond, Roberts-Austen, Sauveur, Stead, Wedding, Werth, and others". About 100 years later, this list would be exponentially longer, revealing the importance of bridging a metal's microstructure to its mechanical, chemical and physical properties. Major part of the progress made can be attributed to the new and steadily improving multitude of microscopes used to examine these microstructures. Meanwhile, the basic principles of metallographic specimen preparation, i.e. removal of the material adjacent to the layer of interest have hardly evolved. This leaves a number of fundamental complications in the analysis of complex micro-phenomena in modern metals (e.g. advanced high strength steels) unresolved, even though cutting-edge fully automated material removal systems are nowdays at hand.

These complications originate from the fact that ductile damage micromechanisms (e.g. void nucleation, growth and coalesence) are masked since they are intrinsically located inside the metal (i.e. not revealing essential details at the surface). The common approach in analyzing these micro (and increasingly nano) constituents consists in the advanced use of several experimental techniques (e.g. mechanical polishing, electro-polishing, etching, etc.) for material removal[2]. This can be achieved with acceptable precision with each of the techniques, however, reports in the literature show that the revealed microstructure is also modified, and in some cases deformed significantly [71–74]. While mechanical polishing cause subsurface hardening [71–73] and smearing effects [74], electro-polishing and etching processes by definition round of sharp edges (e.g. edges of the specimen, microvoids etc.), effectively altering the dimensions of the microstructural features. These adverse effects are well known in the metallography community, and hence lengthy specimen preparation protocols are generally designed to reduce surface manipulation effects to acceptable levels, and carried out in different viewing directions (i.e. in order to visualize the 3D nature of the microstructure). Such procedures, however, are unpractical, expensive and not fully conclusive, as it remains experimentally difficult to assess the influence of deformation, alteration or modification due to a preparation process. Moreover, regardless of the type of the technique used, the material that is removed is "lost", i.e. no data can be obtained from the removed part of the examined microstructure.

Many of the problems mentioned above are solved with the development of the focused ion beam (FIB) technology, which allows 3D analysis of microstructures (and crystal orientations) with almost no manipulation . However these measurements

[2]Ductily deformed microstructures can also be visualized without material removal by the use of radiography techniques (e.g. x-ray tomography, [70]), which allow bulk analysis with high energy penetrating radiation. However, limitations regarding both practical (e.g. availability, time, costs, expertise etc.) and technical aspects (e.g. resolution, specimen size etc.) restrict their applicability for a large class of problems.

are by no means practical, i.e. in most cases only very limited areas (or volumes) can be investigated due to time or economic constraints. In the case of ductile deformation analysis, for example, these limitations make it significantly difficult to get an overview of the multitude of acting damage mechanisms.

In this short paper, we propose and explore an experimental methodology that overcomes the above mentioned difficulties, in a simple, fast and cheap but precise manner, allowing the visualization of the 3D microstructure. As a first step, we ”open-up” fractured tensile test specimens making use of a well-controlled brittle-fracture separation technique which hardly alter the large deformations and damage traces left behind by the previous ductile deformation. The advantage of using brittle fracture to open up inner surfaces was recognized before (i.e. for the investigation of critical void nucleation strains in a C-Mn structural steel [75]), however, this is the first time that the strength of the concept is demonstrated in all its facets. Upon separation, the two surfaces are studied by SEM (or with surface profilometry tools) to reveal the original 3D ductile deformation microstructure by correlating the observations from both surfaces.

The advantage of brittle fracture approach depends on two critical factors; the control of the crack path and the absence of plastic deformation upon opening. Controlling the brittle fracture in a preferential cross section may be challenging due to the nature of brittle-crack growth . A dedicated setup is developed to trigger the brittle fracture of, e.g., a previously fractured tensile test specimen (Fig.5.1(b)) in any cross section of interest. To keep the propagation of the crack fully brittle, specimens are opened-up under conditions that inhibit ductile deformation [76], i.e. high stress concentrations and strain rate, and low temperature .

5.2 Experimental Methodology

The experimental procedure starts with a (ductile) mechanical test whereby the specimen is loaded up to complete ductile failure (Fig.5.1(a, b)). For the proof of principles, uniaxial tension tests are used even though the methodology can be extended for other test specimens via some minor adjustments. A scratch is made on the surface of one of the fractured parts (Fig.5.1(c)). The location of this scratch can be chosen at any angle to the test direction, depending on the cross section of interest. The specimen is next placed in clamps specially designed to maximize the stress intensification in the scratch, and cooled down in a container of liquid nitrogen well below the ductile-to-brittle transition temperature. The sample is then fractured into two parts ((Fig. 5.1(d)) by using a conventional charpy-impact test hammer. Microstructure and topography analyses are carried out simultaneously on both sides of the brittle-fractured specimen, to visualize the 3D microstructural characteristics of the previously ductile deformed test sample.

To assess the applicability of the methodology to different microstructures, four different steels are studied: interstitial-free (IF), re-phosphorized interstitial free, dual-

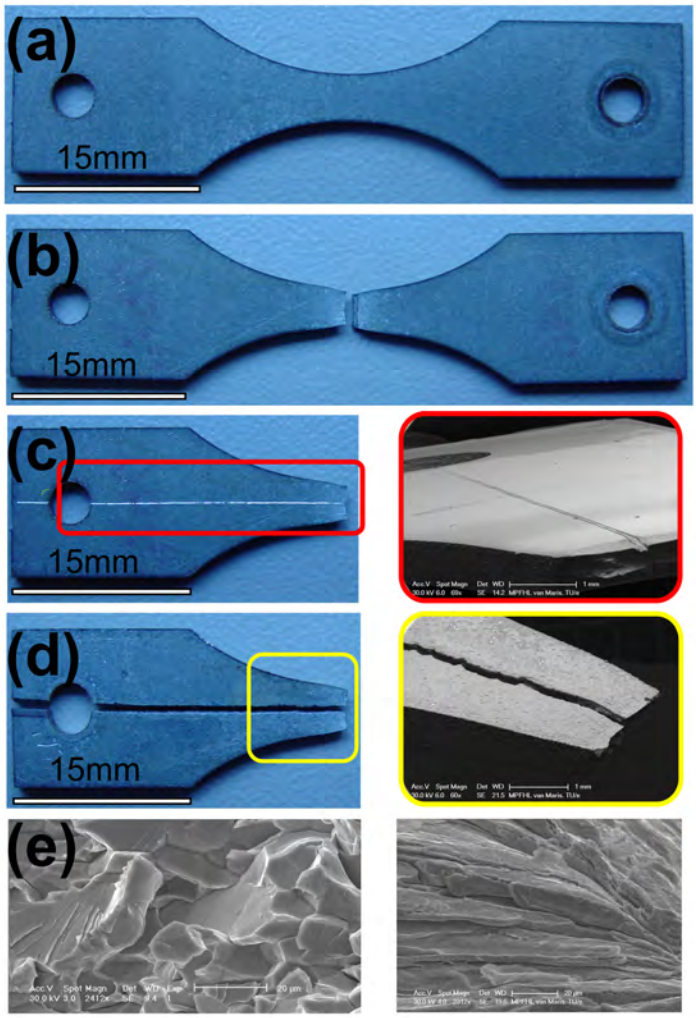

Figure 5.1: Experimental methodology used on tensile samples. (a) Initial geometry of tensile test specimen. (b) Fractured specimen. (c) A sharp, $\sim 10\mu$m. deep scratch is carved with a razor blade on the fractured sample to select the cross section of interest. The insert image shows the scratch as observed in SEM. (d) The specimen is separated into two pieces along the scratch using the brittle fracture process. Insert image shows the two fractured pieces. (e) SEM images of the obtained morphologies away from the fracture surface (left) and in the neck (right).

phase and low carbon steel. Three samples from each material are analyzed to the check reproducibility. In all of the metals investigated, complete brittle-fracture is achieved and fracture always occurred along the scratch. In this paper, however, focus is on the analysis for an IF-steel. IF steel is a perfect case study, since it is not trivial to achieve brittle fracture in such a ductile material. Furthermore, the use of conventional polishing methodologies for this material lead to significant void smearing effects (i.e. due to its high ductility), making the visualization of the true nature of microvoid growth in this material a challenging task.

5.3 Results and Discussion

Let us start with some general observations regarding the brittle crack propagation. Interestingly, when the opened surfaces are examined a smooth transition is observed in the brittle fracture mode along the tensile axis, i.e. as a function of the deformation history. While the brittle crack is dominantly transgranular away from the neck (i.e. at relatively low local pre-strains), the fracture is dominantly intergranular close to the ductile fracture surface of the tensile test sample (along the elongated grains in the neck (Fig. 1 (e))). This transition is more pronounced in more formable steels with (IF, plain carbon steel), compared to less formable steels (DP600, Stainless Steel, IF-r).

The brittle fracture approach provides a clear visualization of the prior (severely deformed) ductile microstructures, as shown in Fig. 2 where SEM images from the neck regions are compared for different preparation techniques. The conventional strategies, obviously, lead to unrepresentative surface finishes that reveal little microstructural information. Mechanical polishing (Fig.5.2(a)) provides a nice representation of the fracture surface morphology (i.e. ”cone”) but smearing effects limit void analyses, and observation of grains or grain boundaries is not possible. Electropolishing (Fig.5.2(b)) removes smearing effects, whereby more voids are visible, but rounding effects change the morphology of the cross section and these voids, as well as of the fracture surface. Grains are poorly visible, making them difficult to analyze. Etching (Fig.5.2(c)) makes grains somewhat more visible, but voids also are also affected by etching, or even completely removed. With the brittle-fracture approach (Fig.5.2(d)), on the other hand, the specimen is separated through the grain boundaries, allowing a clear analysis of elongated grains in three dimensions, while keeping the cross section and fracture surface morphologies undistorted, to the extent that it can be checked.

This 3D visualization also allows for a clear analysis of void nucleation sites (e.g. the microvoids nucleated at grain boundary triple points in Fig.5.3(a)) due to the unique property of the methodology allowing both surfaces to be available for observation (Fig.5.3(d)). This is another important advantage of the brittle-fracture based methodology, i.e. the separation is achieved without any noticeable plastic deformation, leading to true 3D morphologies obtained by assembling the micrographs of both sides of a grain (Fig.5.3(a)), a microvoid (Fig.5.3(b)) or other microstructural constituents, either qualitatively (e.g. by SEM observation) or quantitatively (e.g. by using confocal microscopy or atomic force microscopy). The nearly perfect complementary nature of the features in both surfaces in Fig.5.3 supports the hypothesis on the absence of plastic deformation in the separation of these two surfaces, enabling quantitative (three-dimensional) measurements of single voids or cracks and (area-averaged) surface fractions of damage. Note that the brittle crack tends to propagate along the internal surfaces of highest damage concentration, which are of prime importance to the failure of a deforming ductile sheet.

Furthermore, important information about ductile damage evolution and accumula-

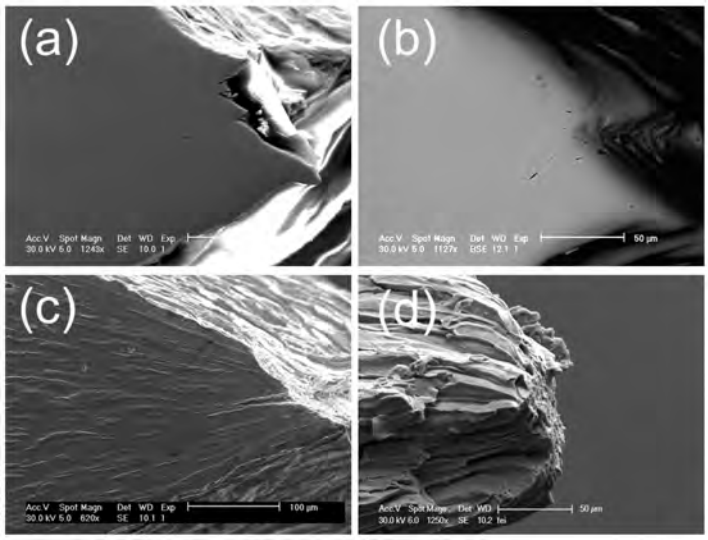

Figure 5.2: Comparison of different specimen preparation methodologies to analyze ductile deformation. Neck regions of fractured tensile test samples examined in SEM following (a) mechanical polishing, (b) electro-polishing, (c) etching and (d) brittle-fracture methodology.

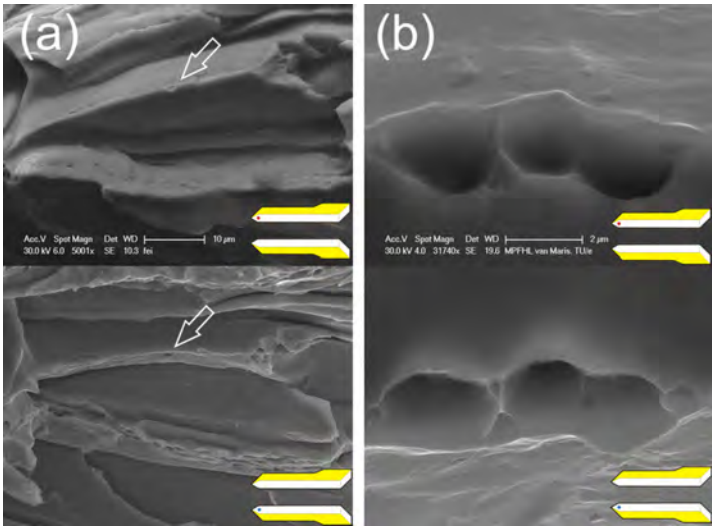

Figure 5.3: Analyses on both complementary brittle-fractured surfaces allow the reconstruction of the true 3D morphology of deformation induced microstructures. (a) Elongated grains in the neck region of a tensile test sample, showing void nucleation at grain boundary triple points. (b) Void growth with deformation leads to the partial coalescence of three microvoids. Note that both bottom images are flipped vertically.

tion mechanisms can be gathered upon the examination of complementary surfaces. Such an observation is shown in Fig. 4, which is an SEM image from the neck region of a ductile fractured tensile test specimen (fracture surface towards right) of an IF

steel. Note that a portion of the SEM image is highlighted and the high magnification insert images show different snapshots of the deformation process leading to fracture. The figure shows that microvoid nucleation, growth and coalesence take place at the triple junctions of the elongated grains. Nucleation starts at relatively lower local strains (i.e. further away from the fracture surface) as seen in Fig.4 (i). At higher local strains (i.e. closer to the fracture surface) these microvoid grow such that they begin to ”touch” each other (Fig.4 (ii)). At even higher strains, these microvoids coalesce to form larger voids (Fig. 4 (iii)) leading to fracture.

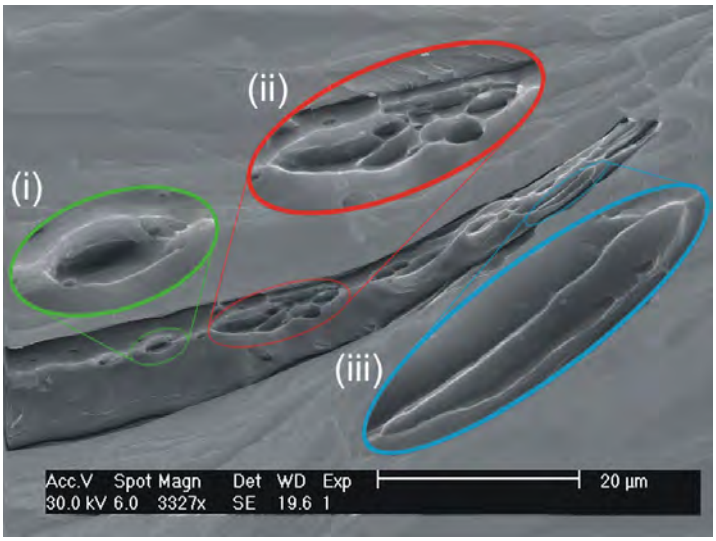

Figure 5.4: Void nucleation (i), growth (i-ii) and coalasence (ii-iii) observed together in one image approaching the neck of a tensile test sample. Insert images show enlarged views of these steps. Rest of the image is shadowed for visualization.

5.4 Conclusions

In summary, the proposed brittle fracture based methodology provides significantly more details needed for microstructure characterization, compared to traditional techniques. More data can be obtained from a given cross section of interest (which can be chosen freely), as both separated surfaces can be examined comparatively. This data presents a significantly higher quality (in the sense that it is more representative for the true microstructure) since preparation-induced deformation is prevented. Finally, these achievements are obtained through an economic and practical methodology that is highly suited for practical and even industrial applications.

5.5 Acknowledgements

This research was carried out under the project number MC2.05205 in the framework of the Research Program of the Materials innovation institute M2i (www.m2i.nl), the former Netherlands Institute for Metals Research.

CHAPTER SIX

Comparative Analysis of Damage Quantification Methodologies [1]

Abstract

Continuum damage models require experimentally-determined material specific damage parameters, for which a wide variety of experimental methodologies following different strategies are proposed. However, the critical influence of the methodological differences on the measured damage evolution parameter is so far not fully investigated. This work aims to fill this gap by an in-depth comparison of the most common and/or promising methodologies (i.e. by considering damage measurement accuracy, precision, damage spectrum, spatial resolution, practicality, etc.), in an effort to determine the most suitable damage parameter identification strategies for continuum damage models. Obtained results clearly indicate that methodologies that quantify ductile damage through its influence on a mechanical property (such as hardness or elastic modulus) have significantly higher accuracy than damage morphology-based measurement methods that aim to quantify damage geometrically.

[1] *Reproduced from:* C.C. Tasan, J.P.M. Hoefnagels, L.C.N. Louws, M.G.D. Geers, Comparative Analysis of Damage Quantification Methodologies, *Submitted*, (2010).

6.1 Introduction

Over the last decades, continuum damage mechanics has proven to be a useful toolbox for modeling the failure behavior of damage-susceptible materials, e.g. concrete, fiber-reinforced composites, advanced high steel steels, etc. Accordingly, significant research has been conducted to allow the implementation of continuum damage models in industrial operations (e.g. sheet metal forming simulations for dual phase or transformation-induced plasticity steels) addressing both theoretical [77–79], and numerical aspects [80–82]. However, continuum damage models also require significant experimental input: i.e. the evolution of a material specific damage parameter. The importance of a damage parameter is best illustrated conceptually through the strain equivalence principle and the effective stress definition, which form the basis of commonly-used elasticity-based continuum damage models. The strain equivalence principle states that the constitutive relations for undamaged materials can be used for a damaged material by replacing the stress term with the effective stress, which is defined as:

$$\sigma_e = \frac{\sigma}{1 - D}. \tag{6.1}$$

For instance, in Kachanov's description, the damage parameter represents the surface density of cracks and cavities in the deforming material [83]. For the case of an isotropic matrix material with homogeneous distribution of voids and cracks, this refers to:

$$D = \frac{S^D}{S} \tag{6.2}$$

where D is the damage parameter, S^D is the total 'damaged' area (i.e. of voids, cracks, cavities, etc.) and S is the total area of the surface.

The damage parameter, D, is sensitive to material microstructure and deformation conditions, and hence, can only be measured experimentally. Many of the experimental techniques used for proving damage parameters for continuum damage models are proposed in the pioneering work of Lemaitre and Dufailly [84], where a distinction is made between *damage morphology-based damage quantification methodologies* (which aim for a measurement of the geometry of voids either in a 2D or in a 3D manner) and *material property-based damage quantification methodologies* (which measure D through its effect on physical, often mechanical, properties of the material)[2]. While techniques following both approaches are used commonly in literature

[2]Note that Lemaitre and Dufailly prefer to name these two groups as 'Direct' and 'Indirect' techniques, respectively.

for damage parameter identification, in most of these papers it is assumed that all damage effects are successfully quantified by the chosen technique, without verifying the resulting damage parameter by alternative methodologies. The reason lies in the fact that the influence of the methodological differences in damage definition, experimental accuracy (resulting from intrinsic systematic errors) and in experimental precision (resulting from random errors) on the measured damage evolution parameter have so far not been investigated in detail. Such an analysis requires the measurement of the damage evolution on the *same* deformed material, using a number of distinct representative techniques. This work aims to fill this gap by addressing the influence of the chosen methodology on the measured damage parameter, in an effort to determine the most suitable damage parameter identification strategies for continuum damage models. Evidently, it is an unfeasible task to compare all damage techniques on all different types of damage (e.g. brittle, ductile, creep, fatigue, etc.) and for all different types of materials. Therefore the choice is made to:

- Place the focus is on ductile damage in sheet metal, which remains a significant challenge for newly developed advanced high strength steels;
- Analyze the most common and/or promising damage quantification methodologies from each category (i.e. 3D damage morphology-based methods, 2D damage morphology-based methods, non-mechanical material property-based methods and mechanical material property-based methods) in a comparative manner;
- Focus this comparative study to the case of dual phase steel, which is a industrially-relevant (automotive) steel with many active damage micromechanisms due to its low yield point and different ductilities of martensite and ferrite phases that compose its microstructure [34,37].

In the subsequent sections, first the selection of the investigated damage quantification methodologies is motivated. Then, the uniaxial tension test to deform the sample and the post-mortem processing of the deformed samples are explained. Next, the detailed methodology of each damage quantification technique is presented, and the obtained results are discussed. Finally, the damage parameters obtained from all techniques are comparatively analyzed in the discussion chapter, and the conclusions are presented.

6.2 Damage Quantification Methodologies for the Comparative Analysis

The classification of different ductile damage quantification methodologies are presented in Fig.6.1. We start by reviewing different damage morphology-based and

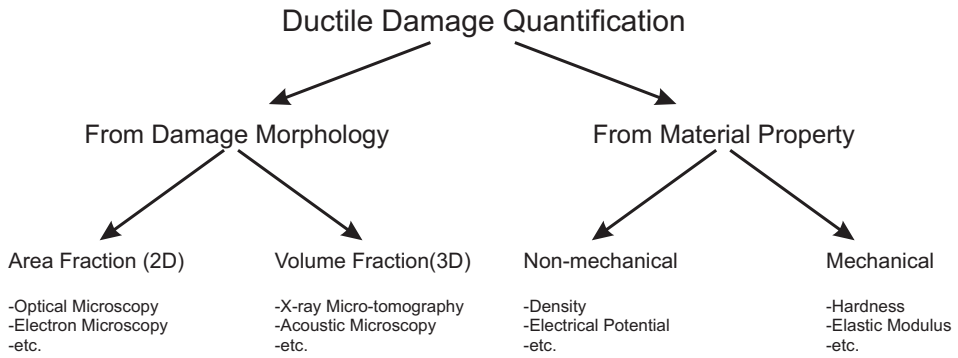

Figure 6.1: The classification of ductile damage quantification methodologies.

material property-based damage quantification methodologies, to determine the most suitable candidates from each category for the present comparative analysis.

Damage morphology-based quantification of ductile damage can be carried out in two ways. Deformation is a 3D process, therefore the ideal approach is to carry out a 3D measurement of the deformed metal microstructure to determine the exact geometry of the deformation-induced defects, and to extract the *volume fraction of damage* [70, 85–88]. A number of different techniques can be applied for this type of analysis (neutron imaging, scanning acoustic microscopy, thermal imaging, scanning positron microscopy, x-ray tomography, etc.). All of these techniques follow a similar strategy incorporating a 2D sensor array where every pixel detects a probe (e.g. photons) that is sensitive to changes in local density, in order to obtain a line-integrated projection image of the sample with microscopic voids. Obtained projection images can be further processed to reconstruct a 3D image using computed tomography (CT). Among these options, X-ray micro-CT tomography is the most suitable for the current purpose of quantifying ductile damage in sheet metal, due to its relatively higher resolution ($\sim 1\mu$m), ability to measure many types of damage, and availability of highly-established computed tomography software. Therefore, x-ray micro-tomography is chosen as the 3D damage morphology-based quantification methodology used in this comparative study[3].

Damage morphology-based quantification of ductile damage can also be carried out with 2D surface measurements on the deformed metal to extract the *area fraction of damage* as a damage parameter [84,90–92]. A number of surface characterization techniques can be used for this purpose, including optical microscopy, atomic force microscopy, scanning tunneling microscopy, scanning electron microscopy, etc. Among these techniques, optical microscopy is the most practical technique, however, the

[3]Recently, X-ray micro-tomography using synchrotron radiation has received significant interest, also for ductile damage in metal [70, 89]. While it is a scientifically powerful tool, practical difficulties make it impossible for industrial applications. Here, the choice is made to perform X-ray micro-tomography using a high-resolution lab-scale equipment, which are now commercially available and therefore a better candidate for a practical damage quantification tool.

maximum resolution is intrinsically limited to $\geq$300nm. Tools such as atomic force microscopy and scanning tunneling microscopy allow nanometer-scale resolution, however, the field of view is too limited. Scanning electron microscopy, on the other hand, combines high resolution with a large field of view, and hence is the most suitable technique for 2D damage quantification. Accordingly, it is chosen as the 2D morphology-based quantification methodology used in this comparative study.

Material property-based methodologies for the quantification of damage can be classified into two groups, depending on the material property that is probed: non-mechanical methods and mechanical methods. Non-mechanical methods aim to quantify damage through its effect on a non-mechanical physical property of the metal, such as the density [93–95], ultrasonic wave attenuation [96,97] or the electrical resistance [98–100]. The use of the latter two properties to obtain damage evolution is practically difficult in cases where damage is heterogeneously distributed, e.g. in the localized neck of a tensile bar, whereas for ductile damage it is this region that needs the most precise measurement. The density measurement methodology, on the other hand, exploits the direct relation of the density with the void volume fraction and therefore has been used frequently. Generally, Archimedes' principle is the technique used for density measurement in the field of experimental damage mechanics [93–95]. Two significant measurement sensitivities exist in this strategy. First, the density of the liquid is changing as a result of temperature variations, and second, the measurement in a fluid requires a wire to hold the sample and the resulting capillary forces will introduce an error. As a result, density kits are only available for balances with a reproducibility larger than 1 mg. In this study, density measurement is chosen as a non-mechanical material-property based methodology, and alternative density measurement strategies are investigated to decrease experimental inaccuracy. Preliminary investigations revealed that, of the three main sources of inaccuracy for density measurements,i.e. the cutting process, the volume measurement and the mass measurement, the error introduced due to the former two factors are far more critical than the error introduced due to mass measurements. However, it is difficult to assess which of these two steps introduce the largest error. Therefore, two different sets of rectangular-prism shaped specimens are electro-discharge machined out of the deformed samples, to test two different strategies. In the first strategy, the volume measurements are circumvented by electro-discharge machining specimens of equal length, width and thickness out of deformed tensile test samples. The damage-induced density change is then measured using mass measurements only. In the second strategy, the total surface area affected by the cutting processed is minimized, by developing a highly sensitive volume measurement methodology for small samples. In this new method, a high-resolution 3D surface profilometer is used to measure the displacement of a liquid surface induced by submersion of a deformed cube in the liquid. By measuring the liquid surface twice, i.e. before and after inserting the cube, the volume of the cube can be determined by subtracting both measurements.

Material property-based quantification of damage can also be carried out by measuring the influence of the deformation-induced damage on the mechanical behavior.

In earlier works, this was achieved by monitoring the elastic modulus degradation, which was quantified from the slope of the unloading curve in the stress-strain diagram at different stages of tensile deformation [101, 102]. This approach is severely limited in resolution especially at regions with high strain gradients, due to the use of strain gauges. Even when digital image correlation is used to determine the unloading strains, it is still challenging to measure the modulus with a few % accuracy. Additionally, early drops in Young's Modulus are triggered due to a elasto-plastic coupling effect [101], which makes the damage-induced drop difficult to distinguish. A more suitable approach is to resort to a mechanical method with a controlled high precision displacement, instead of strain, measurement. For this purpose, the z-resolution of the currently available nano and micro indenters are perfectly suitable, and the Oliver-Pharr methodology enables a local measurement of the elastic modulus from the unloading stiffness during indentation [103]. Furthermore, it is also proposed that hardness measurements can also be used as a mechanical probe for ductile damage [84]. Accordingly, the indentation-based damage quantification, which probes the amount of damage from the degradation of hardness and modulus, is chosen as the mechanical material property-based methodology used in this study. It was recently shown that the elastic modulus can also be measured locally through elastic compression tests on micro-pillars [104]. As a second mechanical technique, this method is also analyzed in this study.

6.3 Preparation of Damage Analysis Samples

Tensile specimens of dual-phase steel are cut (in rolling direction) by electro-discharge machining (Fig.6.2a), covered with a speckle pattern and deformed using a micro-tensile testing stage up to the onset of fracture (Fig.6.2b). Digital images are captured during deformation with an optical camera, and used afterwards in digital image correlation analysis to determine the local equivalent strains on the deformed sample (Fig.6.2c). Following the tensile tests, at least 3 specimens (i.e. 6 specimen halves) are further processed for damage quantification, to reveal the final geometries shown in (Fig.6.2d-h):

For the volume fraction methodology with x-ray micro-tomography, a pillar of $0.25\text{x}0.25\text{mm}^2$ cross sectional area is electro-discharge machined from the center line of each deformed sample, spanning the whole deformation range (Fig.6.2d). The machined specimen is glued on a glass rod prior to x-ray image acquisition.

For the area fraction methodology with scanning electron microscopy, central cross sections of the deformed tensile specimens are inspected using two different surface preparation protocols based on mechanical polishing and electro-polishing (Fig.6.2e). Each protocol is optimized (through previous test runs and follow-up microscopic analyses) to reveal the best visualization of the metal microstructure and limit the smearing (i.e. in case of mechanical polishing) and edge rounding (i.e. in case of electro-polishing) effects to a minimum.

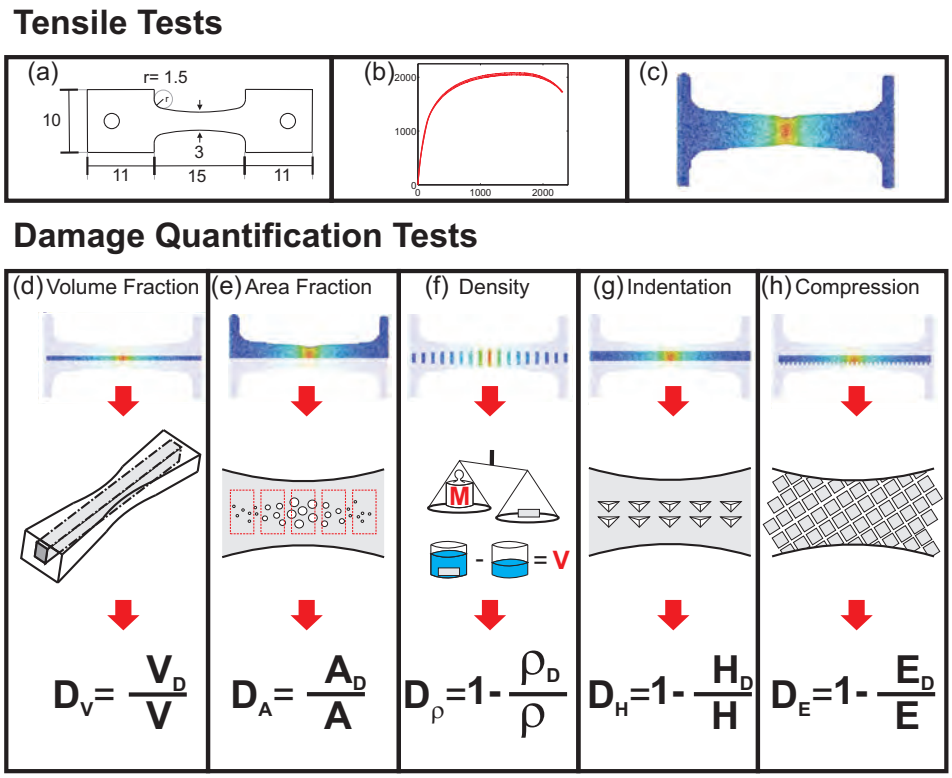

Figure 6.2: Comparative analysis of damage quantification methodologies summarized: (a) Dimensions of the tensile test specimens (in mm), (b) Load (in N)-displacement(in μm) curves resulting from the tensile tests, (c) Local equivalent strain data obtained from digital image correlation analysis, and final specimens after cutting (and optional grinding, polishing) for the (d) volume fraction methodology, (e) area fraction methodology, (f) density measurement methodology, (g) indentation methodology , and (h) micropillar compression methodology.

For the density measurements, sub-millimeter sized rectangular prism samples are to be machined from the deformed tensile test specimens. For the first set of samples, the density is measured from only mass measurements, whereby the thickness of the samples is reduced homogeneously (with electro-discharge machining) to the thickness at the neck, prior to cutting of the rectangular prisms. On the other hand, the width and length of the rectangular prisms are maximized (within reasonable limits) to reduce the experimental inaccuracy of mass measurements to a minimum. As a result, all of the electro-discharge machined specimens of the first set have constant dimensions of 1x2x0.6mm^3. For the second set of specimens (shown in Fig.6.2f), the density is measured from mass and volume measurements. These specimens have a constant width of 0.5mm and a linearly changing length (from 2mm in the neck, to 1.2mm just out of the clamps) to compensate for the deformation induced thickness reduction.

For the indentation methodologies, the cross section of the samples are prepared to

a final RMS roughness of $\sim$0.1 μm using successive grinding and polishing steps. To limit the statistical uncertainty due to preparation-induced surface hardening, all samples are mounted and polished collectively, and to avoid any bending effects of the sample during the indentation experiment, the clamped regions are also removed by grinding (Fig.6.2h).

Finally, for the micropillar compression methodology, deformed samples are split in half along their cross sectional plane using electro-discharge machining (with a wire diameter of 0.1mm). Pillars of square cross section (i.e. 0.2x0.2mm^2) are produced at the cross sections of both specimen halves, as a result of two perpendicular sets of 0.4mm-deep parallel electro-discharge machining cuts (Fig.6.2g), revealing a field of pillars. Prior to the compression tests, the surface roughness of the pillars is reduced by electro-polishing.

6.4 Morphology-based Volume Fraction Methodology

6.4.1 Experimental Set-up

High resolution X-ray micro-tomography measurements are carried out using a Nanotom μCT scanner (Phoenix). During the acquisition, the sample (an electro-discharge machined pillar, placed on a glass rod) is rotated 360° while it is exposed to the X-ray beam. The acquisition is set to the highest possible resolution while keeping the signal-to-noise ratio within useful limits. This corresponds to a minimized source-to-sample distance of 3.6mm, maximizing the sample-to-detector distance to 350mm. Preliminary optimization tests revealed that the highest signal-to-noise ratio is achieved using a X-ray tube voltage of 60kV and current of 240mA. To further improve the signal-to-noise ratio, 4 images (taken with an acquisition time of 3 seconds) are averaged at each rotation position. A total of 1080 averaged images are made for the reconstruction. As a result, a voxel size of 0.5 μm is obtained.

Following the acquisition, a volume of 50x50x400μm^3 (enclosed within the sample) is reconstructed at different axial locations in the specimen (i.e., at different strain levels). The volume fraction of voids is calculated in post-processing, using two different methods. The first method, which is the commonly used method in the literature, consists of visually setting a threshold in the gray value histogram to distinguish between air and material in order to calculate the volume fraction of the damage. In the second method, a peak fitting routine is employed to fit two (Gaussian) peaks (i.e. representing solid and air in the solid) in the gray value histogram of the 3D reconstruction[4]. The damage parameter is then calculated by comparing the relative

[4]Since the typical scale of damage is in the order of the resolution of the system, the transmission peaks of the solid and the air enclosed in the solid inevitably overlap (especially for lab-scale X-ray micro-tomography equipment for which the energy dispersion of the incoming X-ray beam is significant).

area underneath the peaks. Both methods are shown in Fig.6.3.

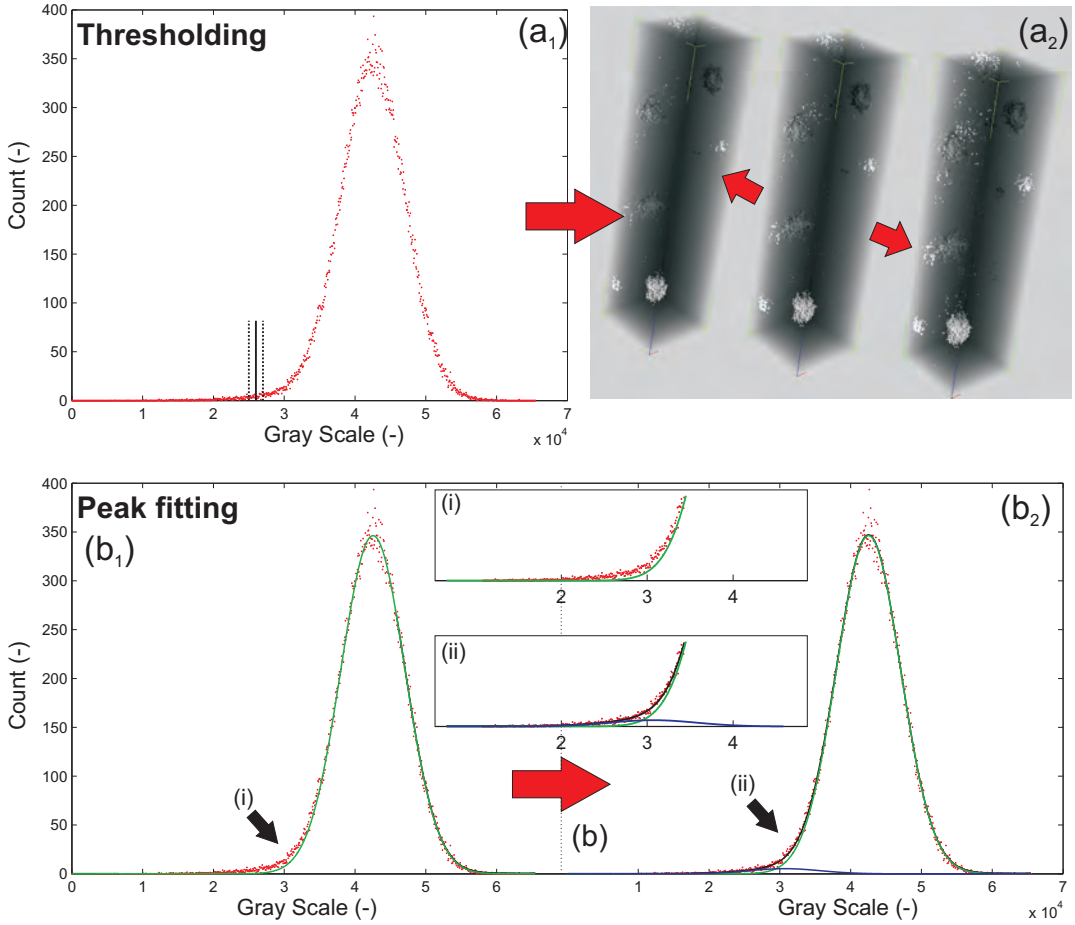

Figure 6.3: The two strategies adopted to obtain the damage volume fraction from X-ray tomography measurements: (a) In thresholding, a threshold level between air and solid in the gray value histogram is selected (a_1), by examining the reconstructed morphology of the voids, microcracks (a_2). Small changes in the threshold may induce strong changes in void quantity as shown (with the red arrows) in the 2D projection of the 3D reconstructed 50x50x400μm^3 volume enclosed within the neck of the pre-deformed sample. (b) In peak fitting, two Gaussian peaks representating air and solid are fitted to the gray value histogram of the 3D reconstruction. Even in the case of hidden peaks(b_1) this strategy can be applied successfully (b_2) to determine damage parameter.

6.4.2 Results and Discussion

Results obtained from both strategies are presented in Fig. 6.4. At equivalent strain levels lower than 50%, damage evolution remains within the experimental inaccu-

racy of X-ray micro-tomography measurements for both analysis strategies. At larger strains, damage evolution is captured with both thresholding and peak fitting, however, leading to significantly different damage values. Although it is a popular strategy, thresholding seems to be a less reliable approach than peak fitting, as the amount of damage strongly depends on the value of the threshold, which for most cases is subjective (visual interpretation of the operator). This constitutes an unacceptable source of inaccuracy, as demonstrated clearly in Fig.6.3a_2 in the reconstructed volumes, and in Fig.6.4 with the large error bars. With peak fitting the error is lower, as the strategy optimizes for a minimum residual of the combined two-peak profile, thereby eliminating operator-induced errors. Peak fitting routine still yields an uncertainty in the determination of the area of the two peaks, which is used to calculate the error bar in the damage as shown in Fig.6.4.

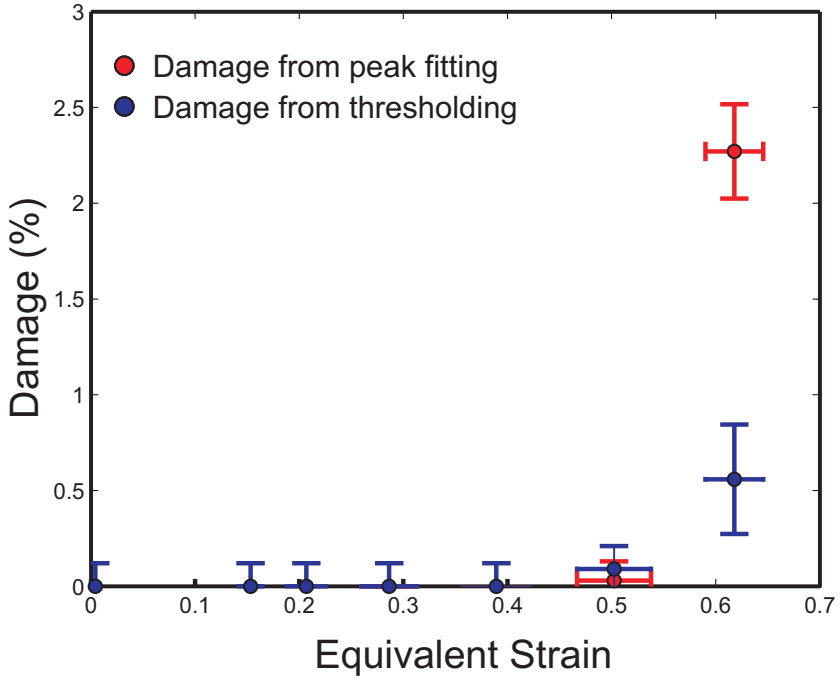

Figure 6.4: Damage vs strain diagram obtained from X-ray measurements.

6.5 Morphology-based Area Fraction Methodology

6.5.1 Experimental Set-up

The SEM analysis is carried out using a FEI Quanta 600 scanning electron microscope, in the backscatter electron mode. First, high resolution micrographs are obtained from the cross section along the axis of the deformed samples using a mag-

nification of 400X and an acceleration voltage of 30kV. These images are combined afterwards in the image processing software, and the area fraction of damage is calculated over an area of 0.15x04mm^2 at different positions (i.e. strain levels) on the specimens, as shown in Fig. 6.5. To accurately determine the location of the material-air threshold that corresponds to the real area fraction of the voids at the surface, the threshold is set through examination of much higher magnification images of the same voids, yielding an operator-induced error that is significantly smaller than other error sources of this methodology. To assess these other error sources, the complete procedure is repeated following different preparation protocols (i.e mechanical and electropolishing) and for different SEM-operating settings (contrast/brightness, magnification, beam voltage/current).

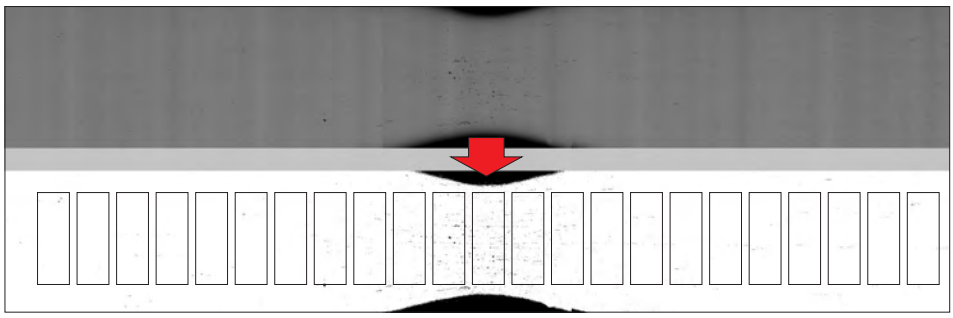

Figure 6.5: For the measurement of the area fraction of damage, high resolution SEM images of the polished specimen cross section are taken along the central axis of the deformed sample, and then combined together (above). With an image analysis software the reconstructed area fraction of voids at different positions is determined.

6.5.2 Results and Discussion

The results presented in Fig.6.6 reveal that scanning electron microscopy analysis is able to capture the damage evolution already at relatively low strains of $\sim$0.1. The damage increases almost linearly up to a strain of $\sim$0.35, and then enters into a exponential increase regime towards the onset of fracture.

In terms of measurement reliability, it is clear from the set of data presented that a significant inaccuracy may be introduced due to the selected specimen preparation method. In fact, mechanical polishing and electropolishing have opposite effects on the porosity in the metal microstructures. In mechanical polishing, voids are smeared out such that an under estimate of the total damage area fraction is measured, whereas in electro-polishing voids are enlarged (due to edge rounding) such that an over estimate of the total damage is measured. Additional inaccuracies are introduced due to a number of imaging (e.g. magnification, contrast adjustment, etc.) and image analysis (e.g. thresholding) parameters. As a result, the overal inaccuracy

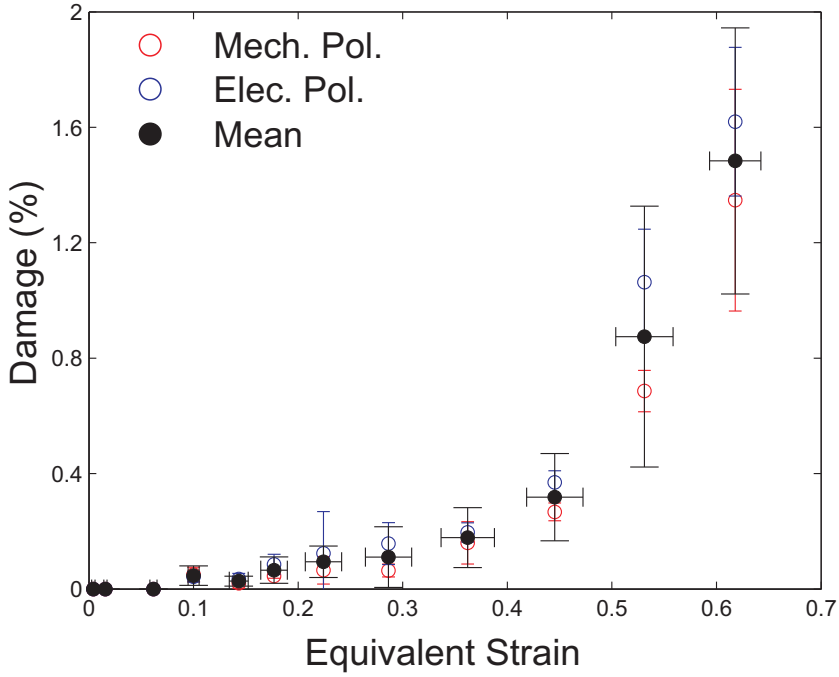

Figure 6.6: The damage at different equivalent strains, obtained from void area fraction measurements using SEM. Red data represents mechanical polishing, blue data represents electro-polishing, both shown with error bar representing standard deviation of the individual measurement. The black data corresponds to the overall average including all random and systematic errors, with its error bars representing the uncertainty in the determination of the mean value.

may reach a factor of 2 of the measured damage value.

6.6 Material Property-based Density Measurement Methodology

6.6.1 Experimental Set-up

For the first set of specimens (with equal-volume), only mass measurements are carried out, using a Mettler Toledo XP2U. This micro-balance has a maximum reproducibility of 0.25 μg, depending on the laboratory conditions. All cubes are measured three times to get more accurate averaged mass values and to check the reproducibility. Before the measurements, all cubes have been cleaned with acetone. For the second set of samples (i.e. specimens with geometry shown in Fig.6.2f), both the mass and volume are measured. The mass measurements are carried out as for the first set, and the volume measurements are carried out using a 3D surface pro-

filometer from Sensofar, PLμ2300. For this purpose, thin paraffin oil is identified as the ideal liquid, which meets the requirements (e.g. low vapor pressure, ideal viscosity and surface tension to prevent overflow while allowing the sample to sink, low thermal expansion, non-hygroscopic nature, etc.). A reservoir for the oil is made from PMMA, which is an ideal material for this purpose[5]. The size of the reservoir is minimized and the optical profilometer is enclosed in a climate box that is kept at 23.0$\pm$0.1°C to reduce the effect of thermal expansion of the liquid (Fig.6.7a). Finally, the surface of the polymer is polished to prevent liquid overflow.

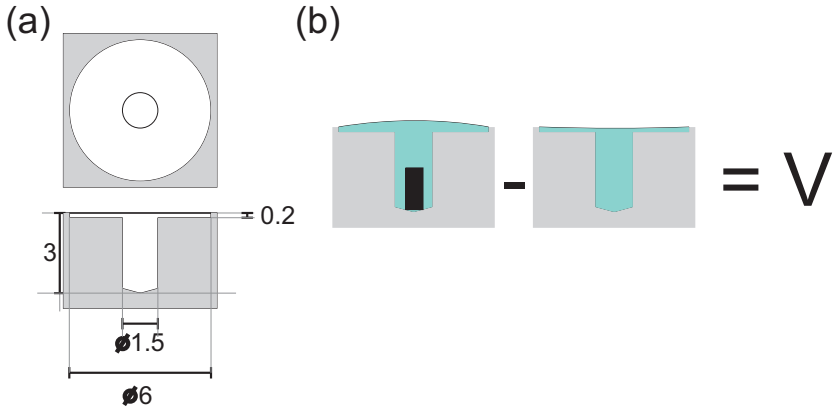

Figure 6.7: (a) The dimensions (in mm) of the polymer reservoir where the paraffin oil is placed. (b) Volume measurement principle.

For the measurement, paraffin oil is inserted into the reservoir with an injection needle, and the resulting 3D surface profile is measured using the confocal microscope, with a 10X objective. Right after the measurement, the specimen is placed in the reservoir with clean tweezers, and the measurement is repeated with the same parameters, except for an increased z-range. Finally, both profiles are subtracted (Fig.6.7b) to obtain the volume of the specimen (Fig.6.8).

6.6.2 Results and Discussion

The results obtained from both sets of specimens are shown in Fig.6.9.

A first observation is that the experimental error in the mass measurements of the first set of specimens is unacceptably high, preventing any damage trend to be captured. This is somewhat surprising, as mass measurements on undeformed specimens revealed a standard deviation of 0.5μg, which should be sufficient to capture the damage in the specimens. In-depth analysis of the specimen surface roughness and final dimensions reveal the causes of this scatter. First, as shown by the SEM

[5]PMMA is transparent, has a coefficient of reflection close to the paraffin oil, it can easily be machined and is relatively hard. Water absorption is low and the material is dimensionally stable.

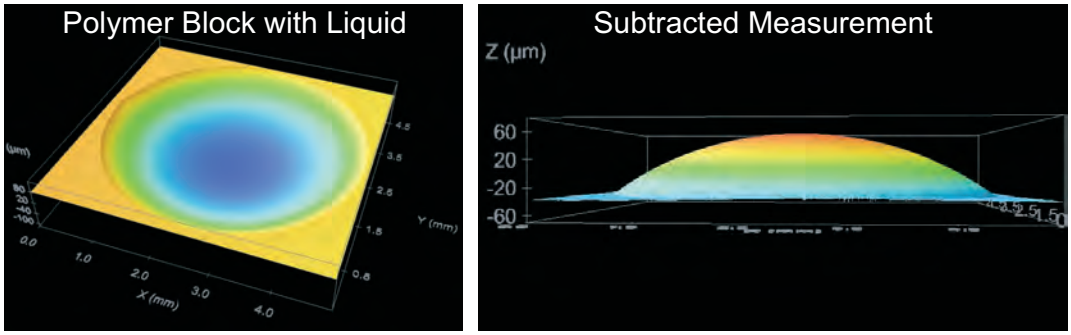

Figure 6.8: Typical volume measurement results: the 3D profile of the paraffin oil within the polymer reservoir (left), and the difference between the profiles before and after the placement of the specimen, corresponding to the volume of the specimen (right).

image of a cut surface resulting from electro-discharge machining in Fig.6.10, the cutting process creates an affected zone on the surfaces of the specimens with high roughness. The degree of roughness may evolve during the EDM process leading to different roughness values for different specimens. Secondly, a more important error is limited to the positioning accuracy of the EDM cut, which in the case of the mass samples is present for all six surfaces[6].

The density measurements on the second set of specimens are also shown in Fig.6.9 revealing a more promising result towards damage quantification. Apparently, the EDM-induced errors can be overcome by the developed volume measurement methodology, revealing a clear trend in density, and hence damage. These results lead to a preliminary conclusion that accurate volume measurements are nevertheless required for quantification of ductile damage from density measurements.

6.7 Material Property-based Indentation Methodology [7]

6.7.1 Experimental Set-up

Indentation experiments are carried out on specimen cross sections at two different scales. Using a MTS Nano-Indenter shallow indents ($\sim$3.5 μm) and using a CSM Instruments Micro-indenter deep indents ($\sim$15 μm) are made with a Berkovich tip.

[6] As the cubes thickness is limited to that of the sheet metal, further enlargement of the cube's in-plane dimensions to compensate for the position of the electro-discharge machining cut would reduce the error by a theoretical maximum of 66%, while considerably sacrificing its local resolution (e.g. at the neck)

[7] This methodology is investigated in more detail in Chapter 7.

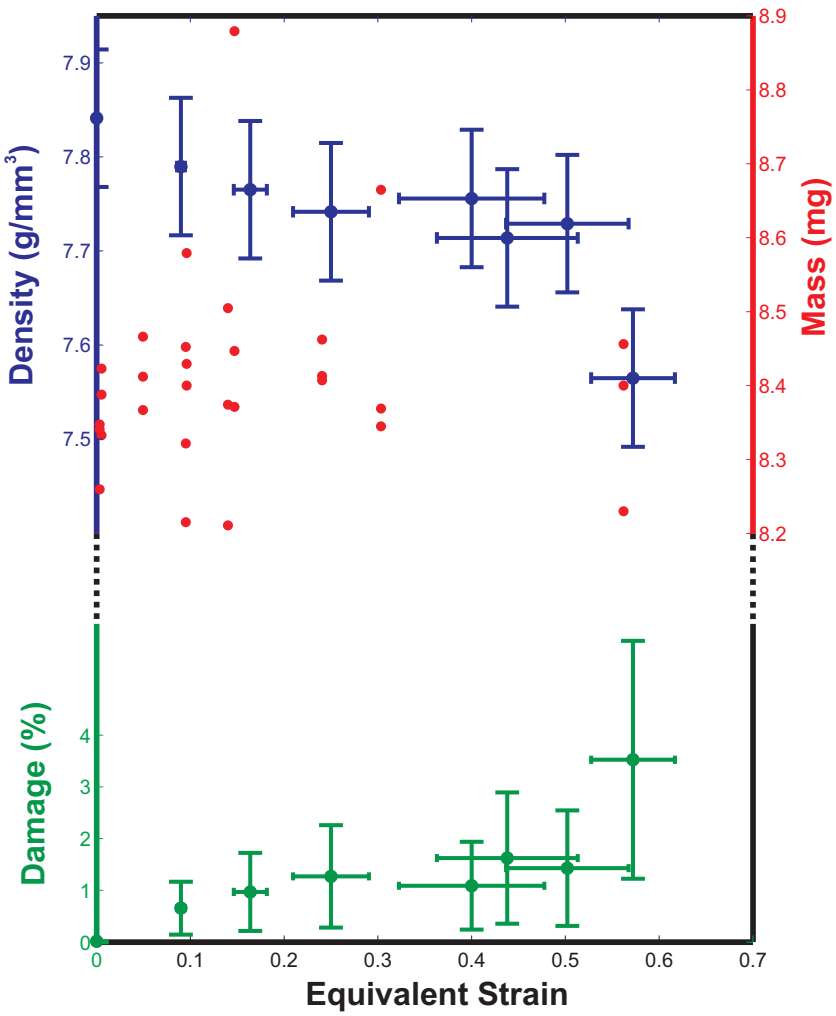

Figure 6.9: Results of the density measurements from two sets of specimens. Only mass measurements (set 1) lead to significant amount of experimental scatter (red data points), while for the mass measurements combined with volume measurements (set 2) the density shows a clear decrease with increasing strain (blue data points), from which the damage accumulation can be determined (green data points).

Typical examples of the results of indentation experiments are shown in Fig.6.11. Nanoindentation enables a larger number of indents at each strain level, whereas microindentation allows to probe the mechanical response of a larger interaction volume. Along with the hardness, the elastic modulus upon unloading is also extracted, using the Oliver-Pharr methodology [103]. Finally, both are coupled with the local strain data to investigate their coupled evolution with increasing deformation.

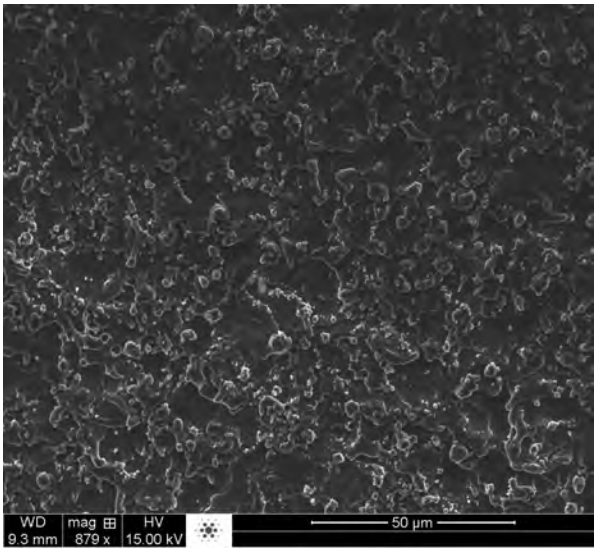

Figure 6.10: Electro-discharge machined surface of dual phase steel

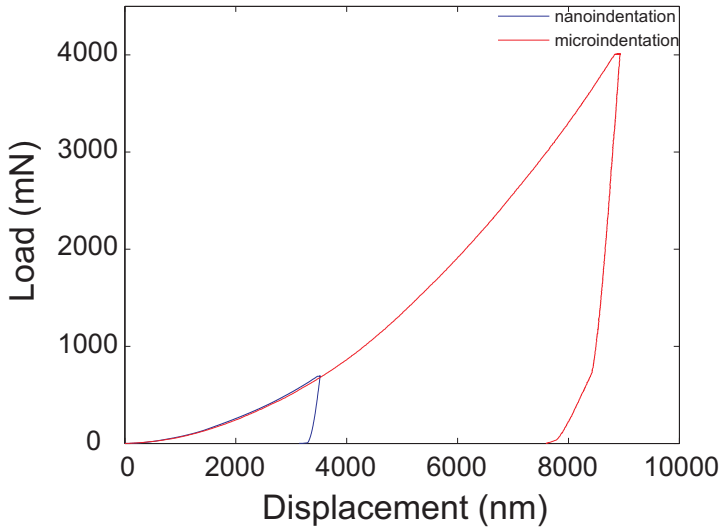

Figure 6.11: Typical micro- and nanoindentation curves.

6.7.2 Results and Discussion

The deformation-induced hardness and modulus evolution in DP steel is shown in Fig.6.12. Let's first concentrate on the hardness evolution with deformation.

As demonstrated in the work of Lemaitre and Dufailly [84], quantification of damage from hardness degradation is only possible if a clearly recognizable, damage-induced decrease exists in the hardness evolution curve. Results shown in Fig.6.12 clearly indicate that there is no such distinct noticeable decrease in the DP steel due to

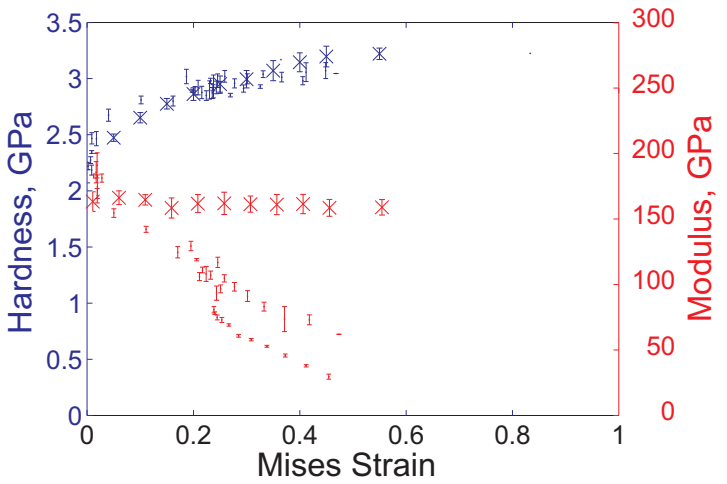

Figure 6.12: Hardness (blue) and modulus (red) evolution in DP steel with deformation.

damage evolution. Additionally, also no drop in hardness was found for interstitial-free steel, stainless steel and an aluminium alloy [105]. This may seem surprising, since the scanning electron microscopy, X-ray micro-CT scanning and density measurements (shown in Figures 6.4, 6.6 and 6.9, respectively) reveal that there is significant damage present in the microstructure. To investigate the underlying reasons for this apparent discrepancy, finite element simulations of the indentation experiments are carried out[8], confirming that porosity should indeed cause a drop in both the indentation hardness and modulus (Fig.6.13).

These results emphasize that there are other deformation-induced mechanisms in the microstructure, such as strain hardening, texture evolution, grain shape change, etc., which mask the expected damage-induced softening. These mechanisms are active in any deforming metal to different extents, whereby it is not trivial to measure their exact influence. As a result of this systematic error, it was concluded in [105] that hardness based damage quantification from indentation experiments are not reliable in their original setting.

Concentrating on the modulus evolution presented in Fig.6.12, a different trend is observed. Modulus does drop with increasing deformation, giving the first impression that a damage parameter can be quantified. However, the presented data also reveals that the interspecimen reproducibility is extremely poor, despite the fact that the data is obtained from the same indentation experiments from which the hardness data (showing good reproducibility) is obtained. An equally poor reproducibility was also found for modulus data of interstitial free steel, stainless steel, and an

[8]For the simulations, elasto-plastic material behavior is assumed, with isotropic hardening, and mechanical properties obtained from uniaxial tensile tests are used directly as a table-input in the FE simulations. The actual Berkovich tip used in the experiments is modeled as a rigid body. More details are provided in [105].

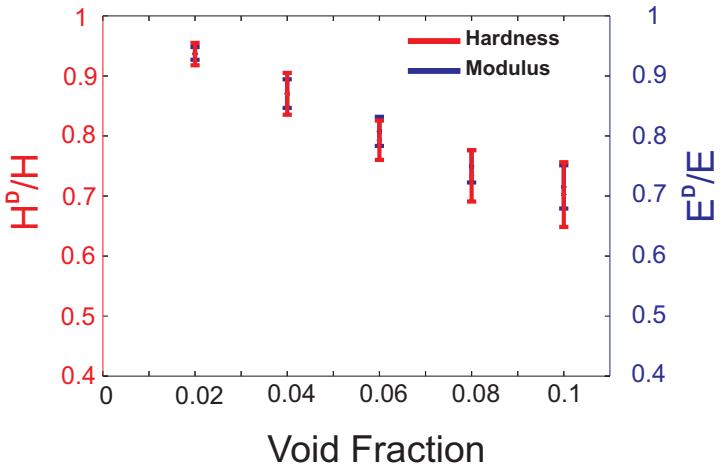

Figure 6.13: Indentation simulations predict a noticeable (relative) decrease in (a) hardness and (b) elastic modulus with increasing void fraction. Note that H^D and E^D represents the damaged state, and H and E represents the damageless state.

aluminium alloy [105]. As was explained in [105], this low reproducibility is due to slight tilts of the specimens with respect to the indenter tip, for which the Oliver-Pharr methodology is reported to be sensitive [106]. Additionally, the unloading stiffness, from which the modulus is obtained is known to be quite sensitive to plasticity [103]. The large error bars for modulus data (for both nanoindentation and microindentation results), and the significant difference in the indentation moduli from nanoindentation and from microindentation tests (for equal hardnesses) are both triggered by this sensitivity. A further complication was revealed from surface profilometry analyses of the indentation marks, which show that indentation causes the material to sink-in at regions of low (or no) deformation, and pile-up at regions of severe deformation (Fig.6.14). The Oliver-Pharr approach assumes a sink-in behavior and takes into account a correction factor for pile-up, thereby overestimating the elastic modulus (i.e. on average 8%) [107]. Finally, the elastic modulus may also be influenced by deformation induced texture evolution or residual stress development. Therefore, it was concluded in [105] that all of these complications makes the indentation based elastic modulus also an unreliable probe for damage quantification.

Obviously, the indentation based damage quantification (from the degradation of hardness or modulus) is not applicable in its original conception. However, the indentation based damage quantification may be used after all upon erasing all microstructural masking effects via a (material-specific) heat treatment, which completely removes the deformation history and all associated microstructural plasticity effects while leaving the damage unaltered. This approach is discussed in the next section.

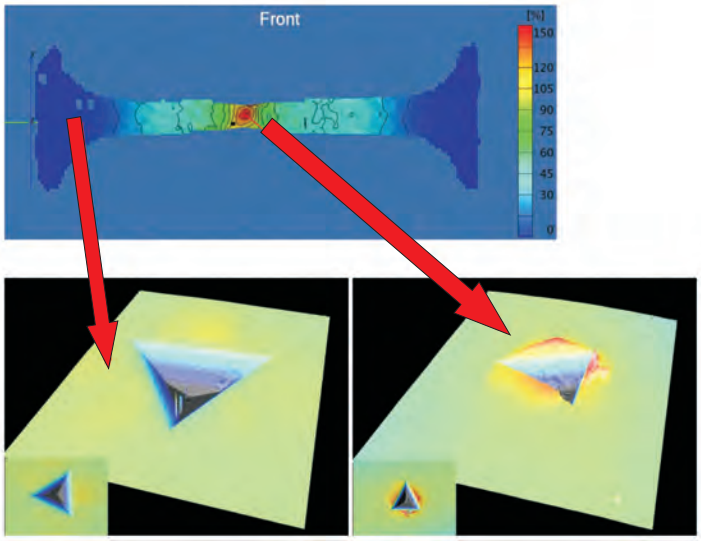

Figure 6.14: Indentation causes sink-in at regions of low deformation, and pile-up at regions of severe deformation.

6.8 Material Property-based Modified Indentation Methodology [9]

6.8.1 Experimental Set-up

The intrinsic deficiencies of the indentation based damage quantification methodology can only be resolved upon removing all non-homogeneous deformation-induced microstructural changes from the as-deformed material, i.e. by an extensive deformation-history erasing heat treatment that yields a spatially homogeneous matrix surrounding the voids (which themselves should remain unaffected). Indentation experiments on such a partially-homogenized microstructure should reveal a constant hardness and modulus at low deformation levels (prior to damage nucleation) and drops in both hardness and modulus with increasing deformation as caused by the onset of damage. Damage can then be calculated using D_H = 1-H_D/H or D_E = 1-E_D/E, as in the original indentation methodology [84].

The main challenge in developing such a heat treatment is the strong heterogeneity in the metal microstructure due to its deformation history, which significantly affects the recrystallization or phase transformation kinetics. To overcome this obstacle for the case of DP steel, first, the heterogeneity in strain energy is reduced with a prolonged recovery step (24 hours at 500°C). Next, sufficient time is allowed upon a recrystallization step for grain boundary migration to minimize the grain size distribution via extended grain growth (24 hours at 700°C). Finally, microstructure (partial)

[9] This methodology is investigated in more detail in Chapter 8.

homogenization is further assured through repeated eutectoid transformations (at 1000°C) for 24 hours and is cooled below the eutectoid transformation temperature and held at 600°C for 24 hours, before cooling to room temperature for indentation experiments. Microstructure analysis following this heat treatment reveals that a homogeneous matrix is obtained, while the deformation-induced damage is preserved in the material [Chapter 8].

Load-controlled microindentation experiments are carried out on the cross sections of the heat treated samples, using a CSM Instruments Micro-indenter with a Berkovich tip, up to a load of 4 N, and the local hardness and elastic modulus are obtained using the Oliver-Pharr methodology [103]. All tests are repeated on six specimen parts to assess inter-specimen reproducibility. Hardness and modulus data are then coupled with the local strain data to investigate their coupled evolution with increasing deformation.

6.8.2 Results and Discussion

The indentation results on heat-treated samples in Fig.6.15 show that a much higher measurement reproducibility is obtained in both hardness and modulus measurements compared to the original indentation methodology. Furthermore, the expected trend (i.e. a constant hardness and modulus regime at low strains, and a decrease in both after a certain strain level) is successfully obtained. This observed trend also indicate the effectiveness of the adopted heat treatment, as in the as-deformed case a monotonous increase in hardness and a clear decrease in modulus before the onset of damage was observed. Hardness and modulus based damage parameters can now be quantified, which are also shown in Fig.6.15. Another promising note is on the comparison of the two damage parameters obtained from indentation hardness and modulus: These two different measurements methodologies reveal approximately equal damage values, within their statistical uncertainties.

6.9 Material Property-based Micropillar Compression Methodology [10]

6.9.1 Experimental Set-up

In this section, another mechanical damage quantification methodology is presented with which damage can be quantified directly using the degradation of modulus. In this methodology, plasticity-induced microstructural effects which render the conventional indentation-based methodology useless are overcome by probing only the elastic response and thereby eliminating all undesired plasticity effects. In this way,

[10] This methodology is investigated in more detail in Chapter 9.

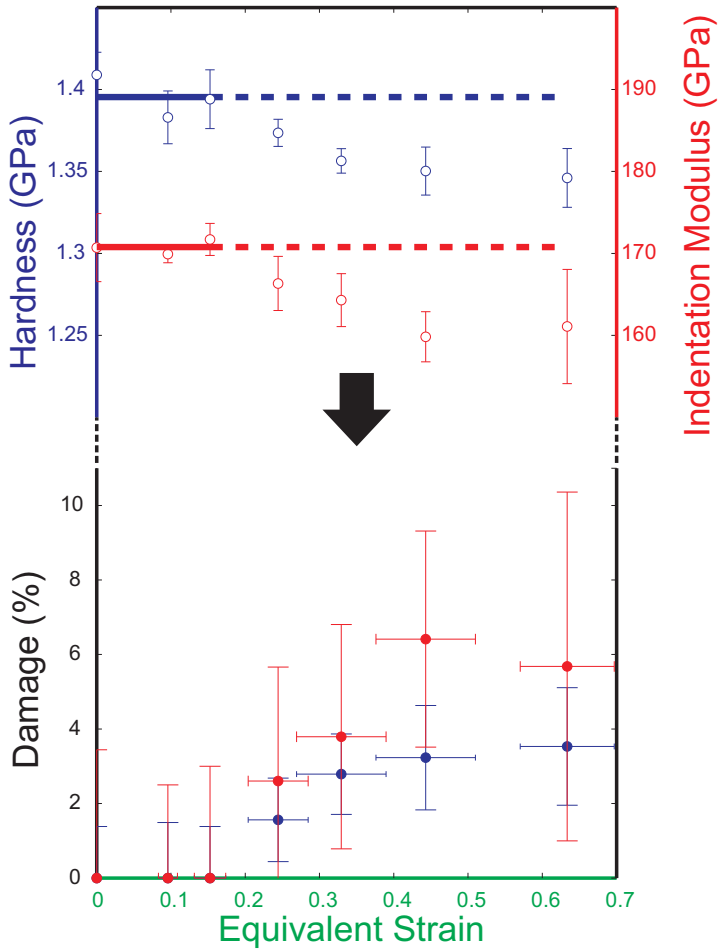

Figure 6.15: Results of the indentation measurements on the heat treated, partially homogenized microstructure: hardness (blue), modulus (red) and the corresponding damage values are also plotted for the same strain levels and with the same color coding. The error bar represents the standard deviation of the mean.

the pure damage-induced degradation of the modulus is probed in a local sense from flat punch compression tests on electro-discharge machined micropillars (Fig.6.16), at load levels sufficiently lower than the point of yielding. The manufacturing methodology and the dimensions of the micropillars are explained in section 1.3.

Compression tests are carried out using a micro-indenter (CSM Instruments Micro-Indenter) in a load-controlled manner, with a flat punch of 0.35mm diameter. The pillars are first compressed up to approximately half the material yield strength (which corresponds to 2N), subsequently unloaded to 0.4N, and then three times reloaded and unloaded between 0.4N and 1N. The modulus is calculated using the initial 60% of the unloading data from 1N, to minimize surface plasticity effects. The obtained modulus data is used to calculate the damage parameter D^E (Fig.6.2h), where the modulus in the undeformed state is measured on the pillars outside the specimen

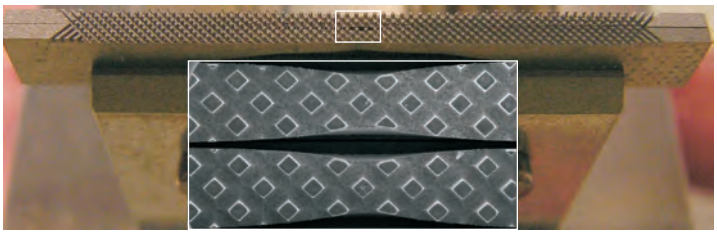

Figure 6.16: The pillars for the micro-compression test. the inset shows the SEM image of the pillars from top.

gauge section. Finally, D^E is coupled to the measured local strains to reveal its evolution with deformation.

6.9.2 Results and Discussion

The measured modulus evolution and the corresponding damage evolution is shown in Fig.6.17, which show acceptable experimental accuracy. The major source of inaccuracy is due to the electron-discharge machining process, which (due to the positioning inaccuracy of the EDM wire) lead to small differences in the cross sectional area. The damage value that is obtained from the modulus evolution shows a realistic trend: a constant regime within experimental accuracy up to a strain level of $\sim$0.25, followed by an increase to 4-5% damage at 50% strain, and subsequently followed by a final rapid grow to approximately 20% damage close to fracture.

6.10 Discussion

The damage evolution parameters measured by the considered five methodologies are plotted collectively in Fig.6.18 for a comparative analysis of the accuracy and precision of each technique.

This overview of all results reveals that the general damage evolution trend is qualitatively similar (i.e. two different regimes of damage evolution are captured with each technique: an initial regime of slow damage accumulation followed by a later regime of accelerated damage accumulation). A more detailed analysis reveals that there are significant differences between damage evolution curves obtained with mechanical material property-based methods (i.e. indentation, elastic compression) and (material property-based or morphology-based) non-mechanical methods (volume fraction, area fraction, density). All three mechanical methods measure a rather late damage initiation strain (approximately 0.25), followed by an accelerated damage accumulation and ending in a higher final damage level. Apart from the same trends, there is also a pronounced cross-methodology reproducibility between the damage evolution trends obtained from these three different mechanical method-

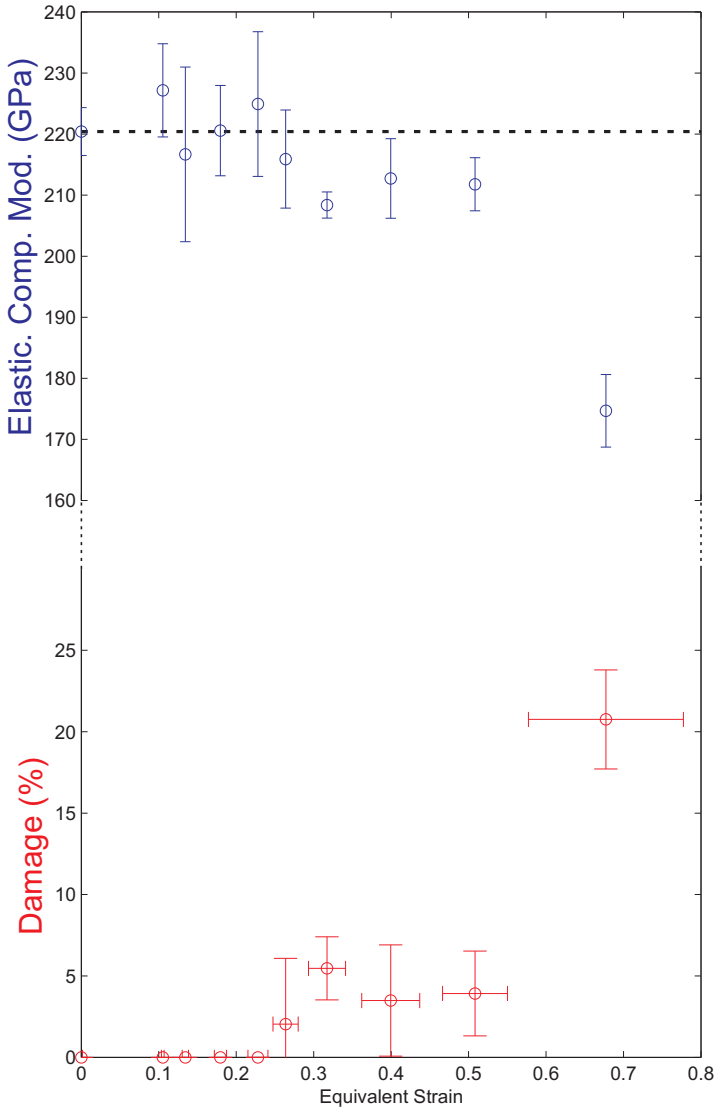

Figure 6.17: Compression modulus and damage evolution in DP steel (The reference modulus value at zero strain [measured at specimen pad, outside the clamp] is shown with a dashed line.) The error bar represents the standard deviation of the mean.

ologies (although the measurement precision is not as high in each of them). On the other hand the non-mechanical methods, especially the morphology-based techniques, miss out an important portion of the damage at intermediate strains measured with the mechanical techniques. The reasons of the limited damage spectrum of the non-mechanical techniques are two-fold: First, damage morphology-based methods (i.e. volume or area fraction techniques) have limited spatial resolution, and hence can only capture voids, cracks with one dimension larger than roughly twice their resolution. Second, non-mechanical methods (including the density methodology) are fundamentally incapable of capturing deformation-induced 'volumeless'

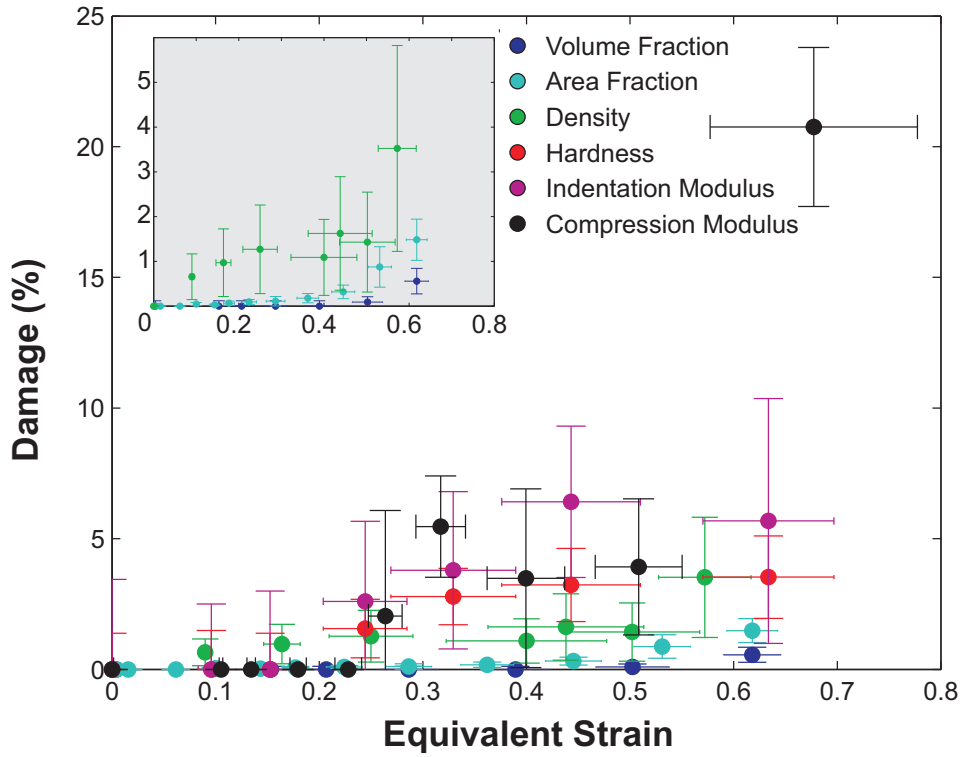

Figure 6.18: Damage evolution in DP steel measured by the different methodologies used in this study: X-ray microtomography to measure void volume fraction, SEM imaging to measure void area fraction, mass and volume measurements yielding the density, indentation measurements of heat treated (partially homogenized) microstructure to measure hardness and indentation modulus and compression tests on electro-discharge machined micropillars to yield the modulus of compression. Inset image shows the trends of damage morphology-based techniques at higher magnification.

damage (e.g. microcracks), which may induce a strong overall softening effect. In fact, the results shown here (in particular the relatively large difference between the damage captured by the mechanical and non-mechanical methods) reveal that this effect is significant even for uniaxial tension, which is more suited for void growth than microcracking compared to other strain paths (e.g. shear, torsion) or deformation modes (e.g. high-cycle fatigue). Whereas the non-mechanical methods are limited to the resolvable geometric damage spectrum only, the mechanical methods are more sensitive to different damage morphologies (e.g. cracks) and alternative strain path (e.g. shear). Both hardness and modulus based damage quantification methods probe the overall mechanical response from the measurement volume investigated, thereby including the influence of all defects that have a noticeable effect on the mechanical response. Overall, these considerations lead to the conclusion that the mechanical methods have much better accuracy then the non-mechanical methods.

Interestingly, in terms of measurement precision (e.g. reproducibility) the mechanical methods are not as strong (as seen from the larger error bars in Fig.6.18), possibly due to the more challenging specimen production routes necessary (i.e. involving more electro-discharge machining steps) compared to, e.g., the 2D direct damage quantification methodology. Another factor that limits the precision in all methodologies (especially at high strains) is strain localization. In most fracture modes, strong strain and damage gradients develop (whether or not inside a neck), which effectively requires the damage quantification methodology to probe a very small material volume. On the other hand, a minimum measurement volume needs to be probed to measure the representative mechanical response of the microstructure and to acquire significant precision. In most cases, due to these considerations a relatively smaller number of data points can be obtained from the neck region, leading to larger error bars due to statistical uncertainties.

Isotropic damage models assume that the effect of the damage is equal for all directions in a material point, enabling the use and experimental determination of a single (scalar) damage parameter instead of the full damage tensor. However, this is rarely the case in engineering materials. For example, it is obvious that crack enlargement under tensile loading will have a different mechanical softening effect in the direction of loading compared to the transverse direction. Consequently, it is also relevant to compare the damage quantification strategies presented here for their ability to provide different components of the damage tensor. To this end, the geometry-based damage quantification methodologies can obviously provide information over the directional differences in the geometry of deformation-induced damage[11]. Accordingly, the damage-induced anisotropy can be captured (at least in the principal directions), however, limitations due to the experimental methodologies presented (e.g. low accuracy) and especially due the underlying assumptions (e.g. volumeless micro-crack effects are not captured fully by the effective stress concept) still complicate the identification of all parameters of the damage tensor. Mechanical property-based methodologies, on the other hand, capture the mechanical response directly, and if carried in different directions (e.g. by producing pillars in different cross sections) provide information about damage-induced anisotropy. The assumption in this case is that the difference in the mechanical damage effect due to the differences in the loading conditions between the damage quantification technique (e.g. compression for the micro-pillar based methodology) and the deformation process of interest (e.g. a deep drawing) is insignificant.

Finally, the strengths and weaknesses of all methodologies are summarized in Table 6.1. Among the criteria considered here, accuracy (i.e. low systematic errors) and damage spectrum are the most critical for ductile damage quantification. Apart from the original indentation methodology which shows intrinsic shortcomings, mechanical material-property based techniques score relatively higher in both of these aspects, compared to non-mechanical techniques, due to their higher accuracy and

[11] For the 2D area fraction methodology this requires specimen preparation and analysis in multiple directions

sensitivity to volumeless cracks. The density methodology also performs well in accuracy, however it has the same damage spectrum limitations as the damage-morphology measurements, and the most limited spatial resolution among all methods. Damage morphology-based methods (especially 2D measurements with scanning electron microscopy) provide practical, high-resolution and high-precision measurements of ductile damage. However, due to the low accuracy and limited damage spectrum, obtained data is more useful for damage characterization rather than damage quantification.

Table 6.1: Review chart for ductile damage quantification methods, compared according to different criteria. Note that 'Accuracy' refers to the accuracy with which a method measures the parameter from which damage is quantified. 'Precision' refers to reproducibility. Methodologies with a high 'Damage spectrum' captures the influence of many different damage morphologies (from elliptical pores to volumeless micro-cracks). 'Spatial resolution' and 'practicality' are self-explanatory. Apart from damage quantification capabilities of each method, the damage micro-mechanism *characterization* capabilities are also compared, at the bottom row.

	Vol. Frac.	Area Frac.	Density	Ind.	Mod. Ind.	Compression
Accuracy	*	**	*****	-	****	****
Precision	***	*****	***	***	***	***
D. Spectrum	*	**	**	****	****	****
Spatial Resolution	***	*****	*	****	****	***
Practicality	***	*****	**	*****	***	***
OVERALL	*	***	***	-	****	****
D. Mechanisms	****	****	-	-	-	-

6.11 Conclusions

In this work, an in-depth analysis of different damage quantification strategies and methodologies is carried out. The strengths and limitations of each methodology in terms of damage measurement accuracy, precision, damage spectrum, spatial resolution, practicality, etc., are comparatively investigated by aiming to quantify ductile damage evolution in an industrially-relevant steel sheet (dual phase 600 steel). The obtained results clearly indicate that methodologies that quantify ductile damage through its influence on a mechanical property (such as hardness or elastic modulus) have significantly higher accuracy than damage morphology-based measurement methods that aim to quantify damage geometrically. Furthermore, the mechanical material property-based techniques also probe a larger damage spectrum,

as the detrimental influence of any damage morphology (from voids to cracks) can be captured mechanically. Morphology based methods (such as X-ray microtomography or scanning electron microscopy) are limited in both damage measurement accuracy and damage spectrum, yet provide significant information about damage mechanisms, which is obviously not possible by the mechanical methods.

CHAPTER SEVEN

Critical Assessment of Indentation-Based Ductile Damage Quantification[1]

Abstract

This paper scrutinizes the reliability of indentation-based damage quantification, frequently used by many industrial and academic researchers. In this methodology, damage evolution parameters for continuum damage models are experimentally measured by probing the deformation-induced degradation of either hardness or indentation modulus. In this critical assessment the damage evolution in different sheet metals was investigated using this indentation approach, whereby the obtained results were verified by other experimental techniques (scanning electron microscopy, X-ray micro-tomography and highly-sensitive density measurements), and by finite element simulations. This extensive experimental-numerical assessment reveals that the damage-induced degradation of both hardness and modulus is at least partially but most likely completely masked by other deformation-induced microstructural mechanisms (e.g. grain shape change, strain hardening, texture development, residual stresses and indentation pile-up). It is therefore concluded that hardness-based or modulus-based damage quantification methods are intrinsically flawed and should not be used for the determination of a damage parameter.

[1] *Reproduced from:* C.C. Tasan, J.P.M. Hoefnagels, M.G.D. Geers, A Critical Assessment of Indentation-Based Ductile Damage Quantification, Acta Materialia, 57(15), 4957-4966, (2009).

7.1 Introduction

The introduction of advanced high strength steels (e.g. dual phase steels and transformation-induced plasticity steels) into the automotive industry triggered extensive research to improve the predictive power of forming simulations [4, 108]. These materials have desirable formability coupled with high strength, which makes them extremely suitable for many components in modern vehicles [109]. However, weight minimization motivated use of these materials is limited by the unpredicted failures observed, due to deformation-induced damage evolution in the multi-phased microstructures [70]. These damage mechanisms are triggered typically due to different deformation characteristics of the phases in the microstructure (e.g. ferrite and martensite in dual phase steels). To understand and resolve these problems with unpredicted failure in steels, the industry typically resorts to continuum damage models to be able to model damage evolution and ductile fracture. The classical basis of elasticity-based damage models is the strain equivalence principle, which states that constitutive relations for undamaged materials can be used for a damaged material, under the condition that the effective stress tensor is used instead of the conventional stress tensor [83]. The effective stress, in its most elementary form, is defined as

$$\sigma_e = \frac{\sigma}{1 - D}. \tag{7.1}$$

To this purpose, most models require an accurate assessment of a damage parameter, D, which depends on the material microstructure and deformation characteristics (e.g. strain path, stress state etc.). As also pointed out by other researchers (e.g.,in [84, 89, 90, 110, 111]) accurately determining the damage is a challenging task as the typical size of microvoids is only a few microns, and the critical microvoid volume fraction reached before fracture is typically only 1-2% of the deforming volume [90]. In their pioneering work, Lemaitre and Dufailly suggested a number of direct and indirect experimental techniques for the quantification of damage [84].

7.2 Geometrical and Mechanical Damage Parameters

Direct methods interpret damage as a purely *geometrical* characteristic, and aim to quantify D through density [84, 93–95], surface area [84, 90–92] or volume fraction [70, 85–88] measurements. Although quite popular, it is questionable whether these methods may reach the required high levels of accuracy in quantitative analysis of ductile damage. This concern is essentially based on two arguments. First, direct methods have rather limited accuracy due to their intrinsic experimentation errors. In the density route, for example, volume measurements show significant scatter even when high precision equipment is used [112]. Surface area fraction measure-

ments, on the other hand, suffer from errors introduced by the specimen preparation (i.e. smearing or enlargement of voids)[2] [114]. Direct volume fraction measurement (e.g. using X-ray tomography) avoids these effects as specimen preparation is not required, however, limitations in spatial resolution affect the accuracy, especially when voids are smaller than a few micrometers [70]. Second, all geometrical methods are (intrinsically) incapable of yielding any information on the correlation between damage morphology/distribution and the resulting mechanical behavior (e.g. void interactions [115] or void morphologies [116]).

As an alternative to the geometrical methods, Lemaitre and Dufailly qualify two indirect, *mechanical* methods as the most promising routes for the determination of the D parameter [84]: probing of ductile damage through its effect on the hardness or the elastic modulus, both of which can be obtained from a micro-indentation test[3]. Hardness based damage quantification assumes that the hardness is linearly proportional to the flow stress. Therefore, this methodology monitors the hardness degradation to assess the damage-induced changes in the flow stress [118]. The damage parameter is determined through

$$D_H = 1 - \frac{H_d}{H} \tag{7.2}$$

where H_d is the measured damaged hardness and H is the undamaged hardness, which is extrapolated from the hardness values at low strains in the undamaged regime (Fig. 7.1(a)).

In a similar way, elastic modulus based damage quantification is based on the stiffness degradation due to the evolution of damage, and calculated by

$$D_E = 1 - \frac{E_d}{E} \tag{7.3}$$

where E_d and E are the elastic modulus in the damaged and undamaged states, respectively (Fig. 7.1(b)).

[2]With use of focused ion beam technology (FIB) (e.g. in [113]) such microstructure manipulations may be avoided. However, in practice, damage quantification using FIB is unfeasible due to the (relatively) large surface area that needs to be scanned to obtain a statistically relevant damage value.

[3]Lemaitre and Dufailly originally measured the modulus using strain gauges from unloading curves. Later, Guelorget *et al.* used the modulus obtained from the more practical Oliver-Pharr indentation methodology, to calculate the damage parameter [117]. The well-studied Oliver-Pharr methodology uses the unloading stiffness to calculate the material compliance and the amount of sink-in, which is required to find the exact contact area (assuming no pile-up) [103].

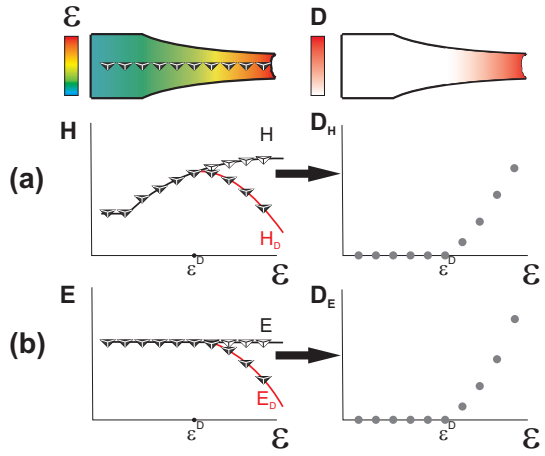

Figure 7.1: Schematic representation of an idealized measurement of ductile damage using the indentation-based methodology. (a) Damage evolution as a result of deformation is expected to cause a sudden drop in the hardness, which is compared to the extrapolated "damageless" hardness curve to calculate the D parameter. (b) In the absence of damage the elastic modulus does not change with deformation, but the modulus is expected to decrease after damage initiates, which can also be used to calculate the D parameter.

7.3 Current Status and Goal

Although the microscopic damage morphology is not captured using these indentation-based damage quantification methodologies, sudden drops in both hardness and modulus presented in the work of Lemaitre and Dufailly visualize a clear effect of damage evolution, which they used for the quantification of the damage parameter using Eqs. 7.2 and 9.1. Therefore, this methodology resolved at least one of the above-mentioned concerns for the direct damage measurements, since the mean effect of all voids and discontinuities on the mechanical behavior is captured in the average flow response of the material under the indenter. As a result, and considering the practical nature of the methodology (e.g. local character, quasi-non-destructive, widely available, etc.), many contributions in the literature selected one of the two indentation based methodologies to analyze deformation-induced effects in different materials (e.g. [90, 117, 119–123]). Note that most technological tests and assessments made by and for the industry are never published.

However, in contrast to the results of Lemaitre and Dufailly, some of these works revealed no sharp drop in the hardness as a function of strain [90, 117, 121]. For instance, Alves reported that hardness based methodology gave good results with an aluminum alloy but not with a mild steel, and questioned whether the methodology is in fact a general technique [90]. Cotterell *et al.* [121] and Guelorget *et al.* [117] both observed an increase in hardness for steel and copper, respectively, and claimed that it is due to the influence of higher density of dislocations close to the fracture sur-

face. Other authors [123] have calculated hardness-based D parameters even when the transition from the undamaged to damaged regime appeared to be completely obscured, resulting in interpretation-dependent damage values.

In the indentation based elastic modulus route, Guelorget *et al.* reported a decrease in the elastic modulus (calculated during the loading process of indentation) of copper sheet, from which they calculated the damage evolution [117]. However, it is also mentioned that a larger scatter is observed for the same specimens when the modulus is calculated from the unloading curves, whereas the opposite trend would be expected [103]. Furthermore, Alves tabulated void area based and elastic modulus based damage values from the literature, and underlined that for many materials common values were not obtained [90]. There are, therefore, clear grounds to question whether an accurate damage quantification can be carried out at all with this methodology in a reproducible manner for different materials.

The present paper aims to critically assess the applicability and reliability of indentation based methodologies, aiming for an accurate damage quantification method. To achieve this, micro-indentation experiments are carried out on three rather different steel alloys and one aluminium alloy. The obtained results are carefully analyzed and confronted with measurements obtained through alternative damage analysis techniques, including scanning electron microscopy, sensitive density measurements, and X-ray micro-tomography. In addition, the micro-indentation results are compared with finite element simulations to verify the separate effect of microvoid density on the degradation of hardness and indentation modulus. Using the gathered data from this experimental-numerical analysis, the accuracy and overall applicability of the indentation-based damage quantification methodology is critically assessed.

7.4 Methodology of Comparative Damage Assessment

Experiments are carried out on interstitial-free steel (IF), X30Cr13 stainless steel (SS), dual phase 600 steel (DP) and aluminium 6016 alloy (AL). Dog-bone shaped tensile samples (of 12 millimeter gauge length) are electro-discharge machined from these sheets, and tested (at a strain rate of $0.25\text{x}10^{-3}$ s^{-1}) using a Kammrath-Weiss microtensile stage to determine the global mechanical behavior. Local strain fields are measured using digital image correlation (Aramis software, GOM GmbH.). Cross sections of these specimens are polished to a final roughness of $\sim$0.1 μm. Indentation experiments are carried out on these cross sections with a MTS Nano-Indenter (for shallow indents of $\sim$3.5 μm) and also with a CSM Instruments Micro-indenter (for deep indents of $\sim$15 μm), both using a Berkovich tip. The local hardness and elastic moduli are obtained using the Oliver-Pharr methodology [103]. With the nanoindenter, at each strain level, at least three indentation experiments are performed over the thickness of the cross section (with sufficient spacing), which allowed to assess the

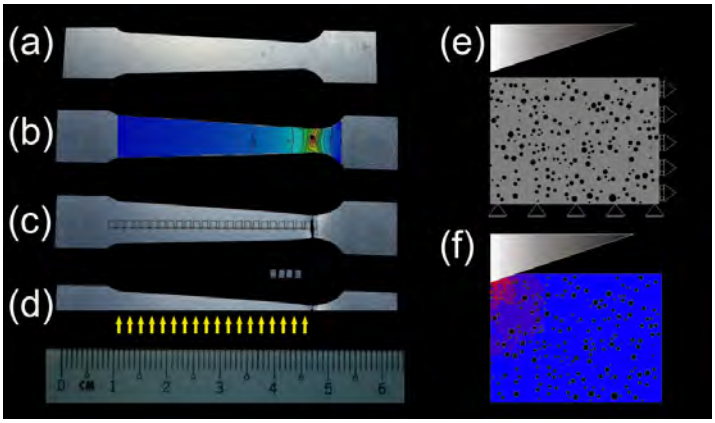

Figure 7.2: (a) Non-homogenous tensile test specimens tested. (b) Local strains are measured using digital image correlation. (c) First, 1 mm^3 cubes are cut by electro-discharge machining (EDM) from the fractured samples. (d) Subsequently the cross sections of the tapered specimens that result after the EDM process are polished for metallographic analysis and indentation experiments (at the positions of the yellow arrows). (e) The finite element mesh (using mirror-symmetry around the indenter axis) showing the randomly generated void distribution and the indenter geometry that are used for the indentation simulations. (f) Typical computed local strain distribution as a result of the indentation.

scatter in the hardness data. The microindentation experiments, on the other hand, allowed to probe the mechanical response of a larger, i.e. more representative, interaction volume. Furthermore, measurements with the microindenter are repeated on at least 3 fractured specimens of each material to assess the inter-specimen reproducibility. Hardness and modulus data are then coupled with the local strain data to investigate their coupled evolution with increasing deformation.

To analyze the damage accumulation directly, tapered tensile samples (Fig. 7.2(a)) are also tested while local strain measurements are carried out (Fig. 7.2(b)). Scanning electron microscopy (Philips XL30 ESEM-FEG), high-resolution micro-CT tomography (Nanotom, spatial resolution of $\sim$0.6 μm) and highly sensitive density measurements (i.e. mass measurement by Mettler Toledo XP2U mass balance with a sensitivity of 0.25 microgram, combined with highly sensitive volume measurement using a Sensofar PLμ2300 profilometer) are used to assess the damage accumulation[4]. For the micro-tomography and density measurements, small ($\sim$1mm^3) cubes are cut out of tensile test specimen using electro-discharge machining (Fig. 7.2(c)). For the scanning electron microscopy analysis, the polished surfaces are electro-polished to reveal the microvoids (Fig. 7.2(d)).

It is important for the purpose of the critical analysis to assess the sole influences

[4]Note that volume measurement using the Archimedian method is not nearly sensitive enough for the present purpose.

of pre-existing damage and plastic hardening on the indentation response. This can not be done experimentally, therefore in support of the experimental analysis, simulations of these indentation tests are performed. However, quantitative prediction of the complex physical mechanisms underlying indentation experiments requires modeling efforts outside the scope of this work. Therefore here, more practical 2D FE simulations are carried out to qualitatively investigate the influence of pre-existing voids (with a certain void volume fraction) and plastic hardening on the measured hardness and modulus. In fact, both plane-strain and axisymmetry simulations are performed (using MSC Marc Mentat). Clearly, the assumptions of plane strain and axisymmetry do not reflect the true 3D geometry of the indentation test (the plane strain response yields an overestimation (upper limit) of the hardness and modulus, whereas axisymmetry is realistic for a homogeneous material and conical indenter tip but surely not when including toroidal voids). Nevertheless, the same trends in hardness and modulus as a function of void volume fraction are observed for both cases, which assure that the observed trends are representative of the real 3D geometry.

For the simulations, elasto-plastic material behavior is assumed, with isotropic hardening. Mechanical properties are obtained from the uniaxial tensile tests of aluminum, as shown in Fig. 3, and the measured hardening behavior is used directly as a table-input in the FE simulations. The actual Berkovich tip used in the experiments is modeled as a rigid body and the thickness in the plane-strain simulations is taken to yield the same 3D indentation volume. The voids are modeled explicitly with a random spatial distribution (taking into account a minimum distance between the voids of 0.5 μm) and a void size distribution, which is sampled from the actual void size distribution measured through SEM and micro-CT analysis; a typical FE mesh is shown in Fig. 7.2(e,f). The voids are modeled as having no material inside, hence, it was generally observed that the voids under the indentor tip close under the compression force, while the voids besides the tip elongate due to the shear force. The simulations yield force-displacement indentation curves, from which the hardness and elastic moduli are obtained using the Oliver and Pharr methodology, in the same way as is done in the indentation experiments. It was verified that smaller element sizes or more nodes in the elements surrounding the voids had a negligible influence on the obtained indentation curves. Ten indentation simulations are performed for each void fraction to obtain averaged values for the hardness and elastic moduli.

7.5 Results and Discussion

Tensile curves of the dog-bone specimens of the four tested materials are given in Fig. 7.3, revealing significant differences in the mechanical behavior. Let us first focus on the hardness versus strain data which is obtained from the indentation tests carried out on the cross sections of these specimens. As shown in Fig. 7.4, these results show a high degree of reproducibility.

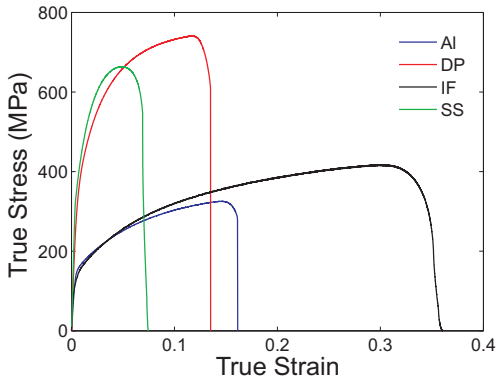

Figure 7.3: True stress versus true strain data of the four tested sheet metals, as measured under uniform tension. The strain hardening coefficients of all steels are approximately 0.29, while that of the aluminium is 0.24.

It is striking to observe that none of these metals show a decrease in nano-hardness or micro-hardness, as was observed by Lemaitre and Dufailly [84]. In the absence of a noticeable drop in hardness, constructing a virtual damageless hardness curve (as was schematically depicted in Fig. 7.1(a)) is virtually impossible. The data suggests that only a minor amount of damage, if any at all, is accumulated in each of these materials, therefore not revealing any sudden decrease in hardness.

However, this is a misleading result and conclusion, since damage in these materials is clearly observed with other experimental tools: Fig. 7.5 shows SEM images revealing damage in both the cross sections (also at those positions where the indentation tests are carried out) and the fracture surfaces of all specimens. Even for IF, a fully ferritic steel which has only a few active damage micro-mechanisms [34], some microvoid growth occurs away from the fracture front. Moreover Fig. 7.6 shows the reconstructed 3D X-ray micro-tomography image of the neck region of the deformed AL specimen, which shows coalesced voids of more than 50μm in diameter. Finally, the sensitive density measurement - with a spatial resolution of 1 mm^3 - also revealed a noticeable drop in the density towards the fracture surface (e.g., 0.87% for AL [112]).

In order to quantify the relative impact of the measured voids on the hardness and modulus, numerical indentation simulations are carried out to complement the experimental observations (Fig. 7.7). For a given microvoid density, the indentation simulations reveal a continuous decrease of the hardness with increasing void fraction. This was expected, as hardness degradations of equal order were reported earlier for other materials where the influence of an increasing porosity on the hardness in an otherwise constant microstructure was monitored (e.g. sintered ceramics [124, 125], coatings [126], porous films [127], sintered porous metals [128], etc.). It is however interesting to note that the drop in hardness is limited to 5-10% for the typical void fractions in industrial alloys, which calls for a challengingly high reproducibility in indentation measurements to achieve the required sensitivity to void

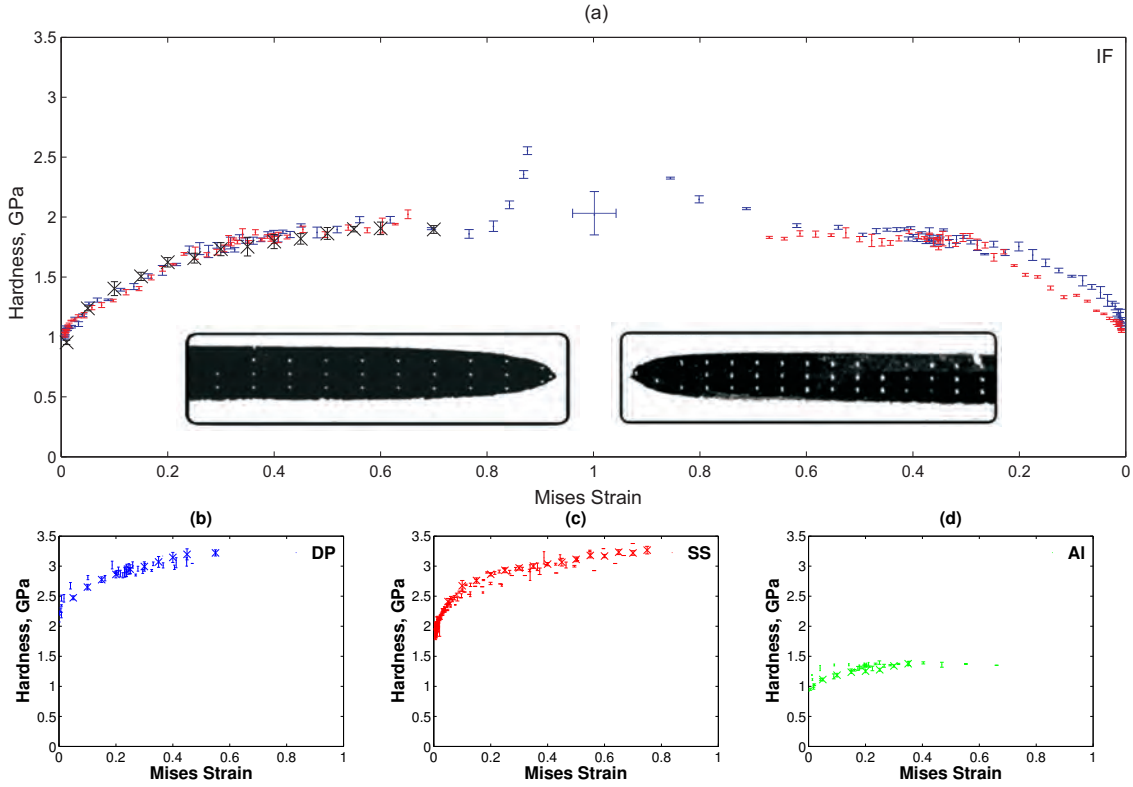

Figure 7.4: Coupled hardness vs. local strain data for (a) IF (b) DP (c) SS and (d) AL. The indentations are carried out at the cross sections of the tensile specimens as shown in the inset images for the IF samples. Microindentation results overlap with the nanoindentation results of separate specimens, and thus for clarity, only the mean value calculated from of all microindentation specimens is shown (i.e. data points with cross). Note that the x-axis in subfigure (a) has its maximum strain in the center, to allow better visualization of hardness profile along a tensile test sample. Also note the large error bar of the data point very close to the crack tip (strains of ~ 1).

fractions of approximately 0.1%.

To summarize, the existence of damage in the form of microvoids, in the neck region is clearly confirmed from three different types of measurements (SEM, X-ray microtomography, and density), and the numerical analysis shows that the measured void density should cause a noticeable decrease in the hardness (and elastic modulus) at least if other effects in the non-voided material are ignored. This apparent inconsistency can only be explained when the decrease in hardness due to damage evolution is partially or fully obscured by other underlying mechanisms (that induce an increase of the hardness) arising from the evolving microstructure. These mechanisms are next investigated in more detail.

The different possible mechanisms that can cause an increase in hardness are best studied on the interstitial-free steel, as this material exhibits a late increase in

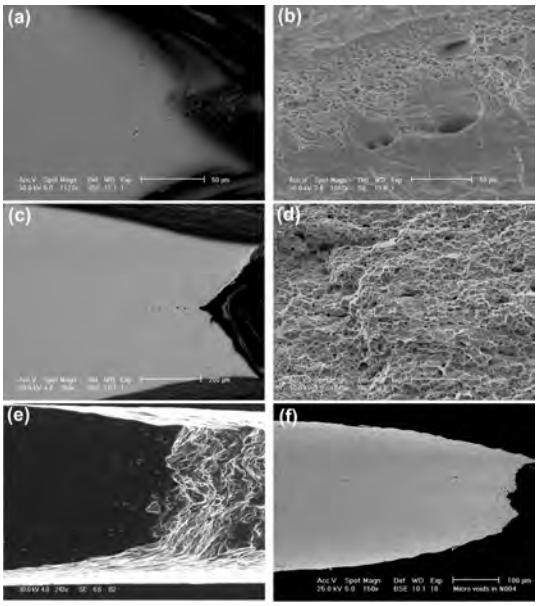

Figure 7.5: Significant damage accumulation is observed in SEM images of IF specimens ((a) cross section, (b) fracture surface), DP specimens ((c) cross section, (d) fracture surface), AL specimens ((e) cross section and fracture surface), and SS specimen ((f) cross section).

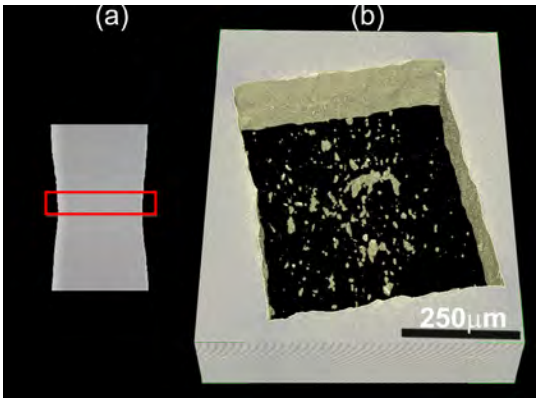

Figure 7.6: Microvoid coalescence leads to internal microcracks in a AL specimen after strain localization, as shown in this reconstructed X-ray microtomography image: side view (a), and cross section (b). Note that the colors in (b) are inverted for visual clarity, i.e., material is shown fully transparent whereas the air surrounding the specimen and in the voids are colored.

hardness followed by an apparent decrease in hardness at ultimate strain of ~ 1 (Fig. 7.4(a)).

First, a perhaps trivial mechanism of interest is the increase of hardness due to *strain*

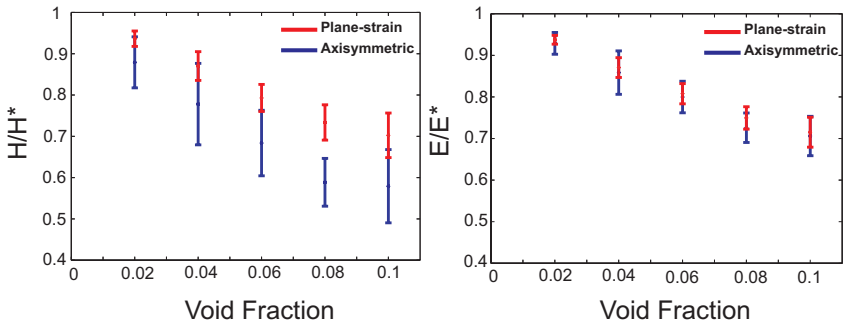

Figure 7.7: Plane-strain and axisymmetric indentation simulations predict a noticeable (relative) decrease in (a) hardness and (b) elastic modulus with increasing void fraction.

hardening, as it seems (highly) plausible that for low amounts of damage accumulation strain hardening effects do obscure the damage-induced decrease of the flow stress and hardness in metals. Numerical simulations of indentation experiments carried out with different initial levels of plastic strains (and no voids) shows this effect in Fig. 7.8. As expected strain hardening has a strong influence at low strain levels, but this influence decreases with increasing deformation (as the strain hardening rate decreases with increasing strain). Since strain hardening is intrinsically coupled to evolving damage, resulting in the largest strains locally around the voids, the influence of strain hardening on the hardness may well dominate the damage-induced effects even for large voids close to fracture.

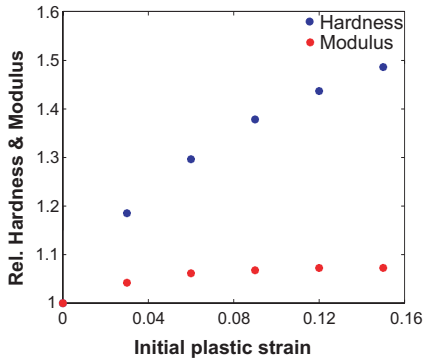

Figure 7.8: Numerical indentation simulations reveal the expected increase in relative (a) hardness and (b) modulus as a function of initial (homogeneous) plastic pre-strain. These simulations are carried out without voids.

A second mechanism of interest that can cause an increase in hardness is the significant *change in grain shape* at large deformations. Force-controlled nanoindentation tests on undeformed IF specimens reveal that the grain boundaries are significantly harder than the bulk of the grains (see, e.g., Fig. 7.9(c)). In the deformed sample

the amount of grain boundaries underneath the tip is substantially different in different regions of a tensile test specimen: away from the neck, where the grains are more-or-less equiaxed, the plastically deforming volume underneath the indenter tip contains much less grain boundary surface than at the neck, where the grains are severely deformed and elongated. As interstitial free steel is the most deformable of the four metals tested, the grains near the fracture surface will be most elongated for this metal (Fig. 7.10), which will induce a significant Hall-Patch effect. This well explains why IF-steel shows a clear increase in hardness for strains over 0.8 (Fig. 7.4(a)). Nevertheless, as for the other metals, where a clear increase in hardness for large deformations is not seen (Fig. 7.4(b), (c) and (d)), this does not mean that the effect of the grain shape change is not present or irrelevant. For these metals it is much more likely that the effect of grain shape change is masked such that its relative influence on the hardness is essentially not known.

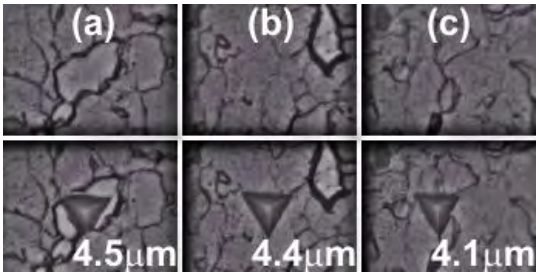

Figure 7.9: Examples of indentation experiments up to a constant load of 500 mN, carried out at different locations on the IF specimen: (a) deeply etched grains, (b) lightly etched grains and (c) grain boundaries. The images on top show the sites before the indentation. Analysis of at least five such indentation experiments shows a statistically significant difference in the indentation depth of (a) 4.5, (b) 4.4, and (c) 4.1 μm, respectively. Note that the different etching behavior (deep or light) is due to orientational differences of the ferritic grains.

A third mechanism is the texture development, which also has an influence on the measured hardness. The influence of the grain orientations on the hardness was shown by analytic and experimental analyses of single crystals [129, 130]. A similar effect was also shown in this work for IF steel (Fig. 7.9(a) vs. (b)). The strong elongation of the grains at large deformations (Fig. 7.10) results in a strong change in texture, which undoubtedly has a profound effect on the measured hardness.

The highlighted mechanisms, and possibly other unidentified mechanisms contribute to the final hardness value at any given level of deformation. The effect of each is different in different microstructures (and therefore in each material), which is the reason why this indentation hardness-based damage quantification methodology, in its present form, is not applicable to most materials as no drop in hardness is observed. Moreover, even in those cases where some drop in hardness is observed,

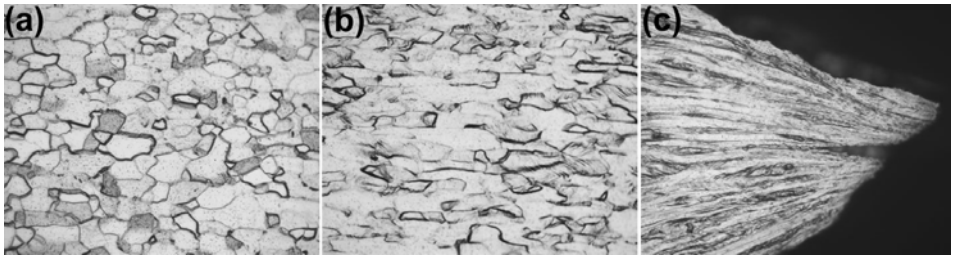

Figure 7.10: Initially equiaxed grains of IF (a) are severely elongated as a result of tensile deformation to different levels of local strains: (b)$\sim$0.3 and (c)$\sim$1. All images are shown at same magnification.

one should be aware of the masked effects of strain hardening, grain shape change and texture development on the hardness values, which can easily cause a large systematic error in the obtained value of the assumed damage parameter D.

It is also worth mentioning that even in the presence of a fully damage-driven drop, extrapolation would be a crude way of setting the damageless hardness curve. The authors have, therefore, also considered a number of alternative options for the determination of the damageless hardness curve. The main idea here would be setting test conditions such that the same strain levels are achieved (as in the investigated test) while no damage nucleation mechanisms are being triggered. Such conditions may be achieved by carrying out tensile tests under hydrostatic pressure [131, 132], compression experiments [111] or bending experiments, such that with subsequent indentation experiments on these samples, new reference curves can be obtained[5].

However there are significant problems in these routes rendering this strategy worthless. First, although most damage nucleation mechanisms are suppressed in these tests, it is still be very difficult to prove that the material is fully "damageless". Second, especially in the latter two experiments, it is not possible to reach the same strain levels observed in tensile tests. And most importantly third, the influence of the different strain path and stress states in these reference tests are not taken into account. As a result of these considerations, the use of alternative methods to obtain the damageless hardness curve fail to provide the required reference state.

Next, the elastic moduli versus strain history is investigated in Fig. 7.11, where the elastic modulus is determined from the same indentation experiments as used to determine the hardness in Fig. 7.4. Whereas the hardness results showed very good reproducibility (inter-specimen and between nano- and microindation), the modulus results show large systematic variations between different specimens and between nano- and microindation. These large systematic variations are attributed to slight (unavoidable) tilts of the specimens with respect to the indenter tip, as it is known that the Oliver-Pharr methodology for obtaining the elastic modulus from

[5]For the case of bending, indentation tests need to be carried on the compression region of the bent samples

the unloading slope of the indentation experiment is very sensitive to even small tilt angles [106]. Such a significant problem of reproducibility already make the elastic modulus an unpractical probe for damage quantification.

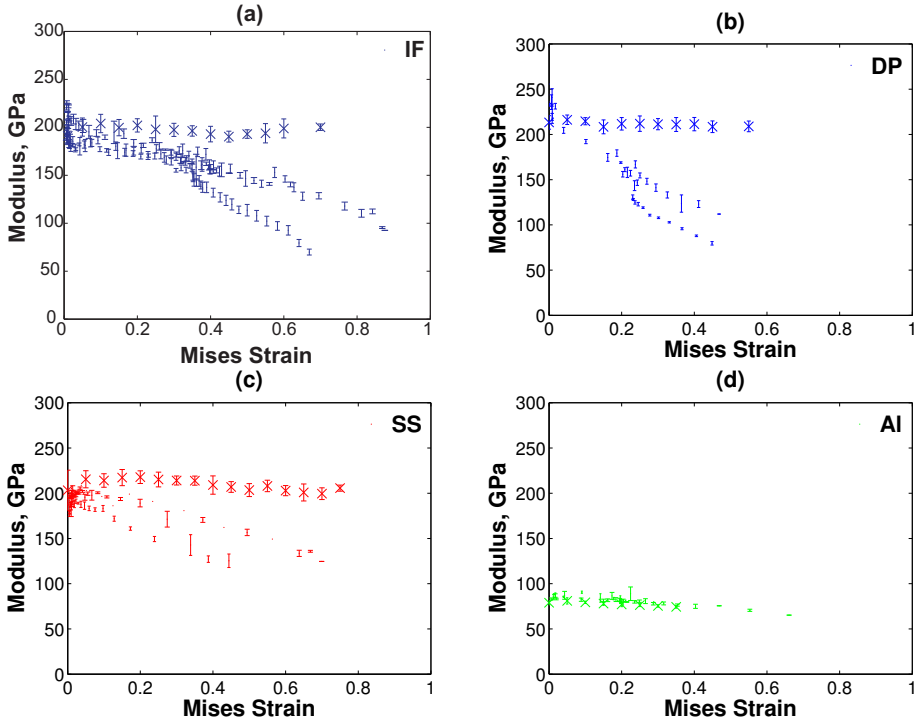

Figure 7.11: The elastic indentation modulus (obtained from microindentation (data points represented by crosses) and nano-indentation (data points represented by dots)) vs. local equivalent Von Mises strain data for the tested materials: (a) IF, (b) DP, (c) SS and (d) AL.

For the present purpose, it is more interesting to focus on the systematic decrease in the elastic modulus with increasing strain (visible for each individual specimen) and its correlation to damage evolution and other deformation mechanisms. Similar to the hardness curves, a sudden decrease in the elastic modulus does not occur, which prohibits the identification of a marked onset of damage. Moreover, irrespectively of the specific data set or specimen considered, the observed continuous decrease in modulus would mean an increase of damage from the onset of deformation which is in contradiction with the known slow evolution of damage at low strains followed by a sharp increase in damage towards localization (Fig. 7.5) [34]. It is more plausible that the observed decrease in elastic modulus is (at least partially) caused by other microstructural deformation mechanisms, similar to the case of indentation hardness as is discussed next.

Surface profilometry revealed for all four materials that indentation causes the material to sink-in when the material was undeformed or only moderately deformed

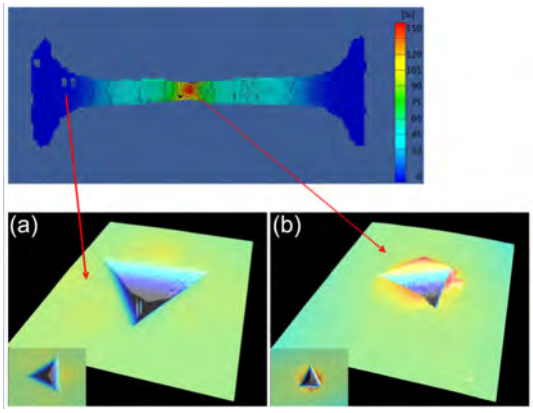

Figure 7.12: Field data of the local equivalent Von Mises strains for an IF steel specimen at the point of fracture and the profile of typical indents at different regions on this specimen. Indentation in undeformed or barely deformed regions causes a so-called 'sink-in' behavior (a), whereas in severely deformed regions 'pile-up' occurs (b).

prior to indentation (Fig. 7.12 (a)), which is a basic assumption in the Oliver and Pharr methodology to allow determination of the elastic modulus from the unloading indentation curve. However, it is shown in Fig. 7.12 (b) that indentation causes the material to pile-up if the material is severely deformed prior to indentation. In the Oliver and Pharr methodology, pile-up can cause a large underestimation of the elastic modulus due to the significant underestimate of the contact area under the indenter tip [103]. The Oliver and Pharr methodology takes into account a correction factor for pile-up, but nevertheless yields a significant overestimation of the Youngs modulus [103,107]. The overestimation of the Youngs modulus is approximately 8% on average for hard and soft materials but increases for our relatively soft materials; for instance, for IF steel the overestimation is as high as 24% [107]. In fact, pile-up also gives a significant systematic error in hardness [107], which is another argument against the indentation-hardness damage quantification technique. The elastic modulus also depends on the texture [130], and especially due to the strong grain rotations associated with the observed elongated grains (Fig. 7.10 (c)) this could be a significant effect. Finally, the elastic modulus measurements with the Oliver-Pharr methodology is possibly affected from local residual stresses present in the material at high deformations resulting from dislocation pile-ups at grain boundaries and second-phase particles.

In conclusion, a measured decrease in the elastic modulus has many contributing sources (not excluding other mechanisms not considered here, such as, a decrease in grain boundary connectivity at higher strains). Since it is strictly impossible to quantify the separate contributions of all these sources on the decrease of the elastic modulus, the use of the elastic modulus as a reliable probe of the accumulated damage is unjustified.

7.6 Conclusions

This paper critically analyzed the reliability and applicability of a frequently used damage characterization methodology, in which indentation tests are carried out to measure the degradation of the hardness and elastic moduli as a function of the accumulated strain, from which a damage variable is extracted. Four sheet metals of different formability were analyzed using a combination of indentation, scanning electron microscopy, micro-CT tomography, sensitive density measurement, as well as supporting finite element simulations. The following conclusions can be formulated:

i) For increasing degree of deformation, both the hardness and the elastic modulus not only change due to damage, but also due to a number of additional microstructural mechanisms, such as strain hardening, grain shape change, texture development, residual stresses and indentation pile-up.

ii) This clarifies why for the investigated four metals, the hardness does not decrease for increasing deformation even though (a) all other experimental techniques clearly reveal the presence of damage at indentation locations, and (b) accompanying simulations emphasize that the measured density of voids suffices to induce a significant decrease in hardness for the case that no other mechanisms would contribute to the hardness.

iii) For the obviously less frequent case that a marked reduction in the hardness and the elastic modulus is observed for a certain material subjected to indentation, a reliable quantitative characterization of damage is still not justified, since the masked factors will modify the hardness and elastic moduli in an unknown and unpredictable manner.

Despite the described complications which render the indentation-based methodology useless, aforementioned advantages of mechanical methods for damage quantification over geometric methods still motivate an effort for improvement. It is obvious from our results, however, that as long as the drop in hardness or modulus due to damage accumulation is masked by other microstructural effects, the methodology cannot be used. Accordingly, one strategy to improve the indentation-based methodology is by erasing all other microstructural effects to be able to capture damage-induced softening; this could be achieved by designing a (material-specific) heat treatment, which completely removes the deformation history while leaving the damage unaltered. A second strategy for an improved damage quantification technique is by probing the local mechanical properties in the fully elastic regime, thus remaining far away from the plastic regime; this is not possible with indentation but could be accomplished by performing sensitive compression tests on (EDM-machined) micropillars. Both strategies are currently being investigated and results will be reported in future publications.

7.7 Acknowledgments

This research was carried out under the project number MC2.05205 in the framework of the Research Program of the Materials innovation institute M2i (www.m2i.nl), the former Netherlands Institute for Metals Research. The authors would like to thank Mark Heeren, Erica Coenen, Paul van Beers and Nard Louws for their contributions.

CHAPTER EIGHT

Indentation Based Damage Quantification Revisited[1]

Abstract

Efforts in implementing continuum damage models in forming simulations are hampered by the absence of experimental techniques to provide reliable and accurate damage evolution parameters. The widely used indentation approach, whereby deformation-induced damage is quantified through the degradation of indentation hardness and modulus, was shown to be intrinsically deficient (Chapter 7). Here, a new indentation-based methodology is developed and evaluated, allowing damage-induced degradation of hardness and modulus as a reliable probe for damage quantification .

[1] *Reproduced from:* C.C. Tasan, J.P.M. Hoefnagels, M.G.D. Geers, Indentation Based Damage Quantification Revisited, *Submitted.*, (2010).

8.1 Introduction

In the last decades, continuum damage mechanics frameworks [80,83,133–135] have evolved towards a useful toolbox to predict failure behavior for a wide range of materials (e.g. metals [136], composites [137], polymers [77] etc.). This interest is most pronounced in the sheet metal forming industry, where the damage evolution-triggered failures of advanced high strength steels and aluminium alloys is a growing issue. This ductile damage can be predicted by incorporating continuum damage models (CDM) into forming simulations, if the available experimental tools are able to provide quantitative material-specific damage evolution parameters.

In the pioneering work of Lemaitre and Dufailly [84], it was reported that indentation is the most suited damage quantification methodology[2], which: (i) probes the mechanical response directly such that the influence of the full spectrum of damage mechanisms is captured, (ii) yields a "mechanical" damage parameter D instead of a geometrical damage parameter, (iii) provides enough spatial resolution to capture the high strain and damage gradients, and (iv) is practical and cost-effective. Consequently, the indentation approach has been used widely by researchers from academia and industry, where the D value was either determined from the degradation of the hardness (D_H = 1-H_D/H) or modulus (D_E = 1-E_D/E), see e.g. [84,90,117,120,123].

Unfortunately, in a recently published critical analysis of this methodology, the authors have shown that the experimental determination of the D values is not trivially possible using this methodology on the as-deformed material [105]. Numerical analysis of the indentation experiments confirmed the underlying problem: the damage-induced hardness and modulus degradation are masked by other deformation-induced microstructural changes including grain shape change, texture formation, residual stress build-up, etc.

In this article, we demonstrate that the intrinsic deficiencies of this methodology can be repaired upon removing these deformation-induced microstructural changes from the as-deformed material. This is achieved by partial homogenization of the deformed microstructure via an extensive deformation-history erasing heat treatment, yielding a spatially homogeneous polycrystalline matrix surrounding the geometrical damage (i.e. voids) which themselves remain unaffected. This partial homogenization allows the damage-induced hardness and modulus to be used as a reliable probe to obtain D (Fig.8.1).

[2]Note that, even though direct methods (e.g., electron microscopy, x-ray micro-tomography, or sensitive density measurements) are well suited for characterization of damage micro-mechanisms, they all have limited precision/resolution for damage quantification [70,90,138,139] and the geometrical damage parameter obtained does not necessarily account for possible "mechanical" damage effects, e.g. due to (volumeless) microcracks. Therefore, accurate prediction of damage-induced softening requires a proper methodology to quantify a "mechanical" D parameter.

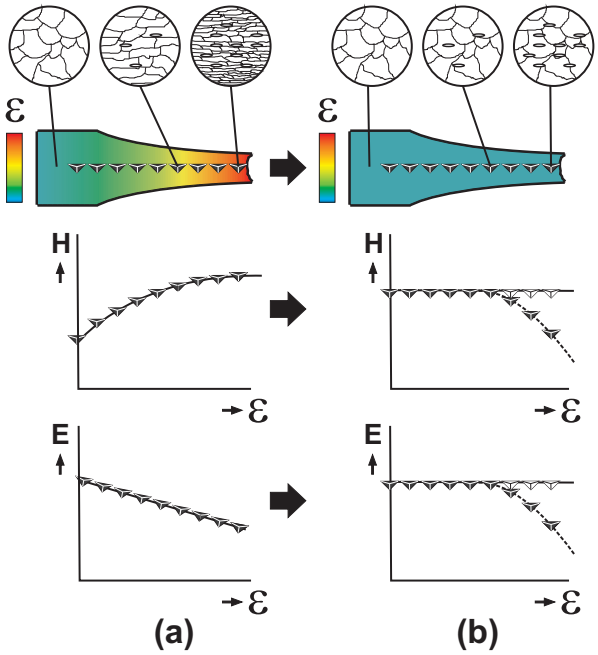

Figure 8.1: Schematic representation of the modified indentation-based damage quantification methodology: (a) Conventional indentations on as-deformed specimens show no drop in hardness and an early decrease of the modulus at strains far before microvoid nucleation, rendering the technique unreliable for damage quantification. (b) A carefully-designed follow-up heat treatment is used to generate newly recrystallized, strain-free, homogeneously-distributed grains, revealing constant indentation hardness and modulus before the onset of damage and the degradation of both afterwards. The damage parameter can then be calculated from the observed degradation.

8.2 Challenges in Partial Homogenization of the Deformed Microstructure

There are two challenges in developing a heat treatment for the concept shown in Fig.8.1. First, the heat treatment should restore a spatially homogeneous polycrystalline matrix surrounding the voids, such that the influence of damage can be captured unambiguously by follow-up indentation experiments. This requires the heat treatment to be designed carefully, taking into account the kinetics of recovery, recrystallization, grain growth and phase transformation processes. Second, the heat treatment should not have an influence on the prior deformation-induced damage existing in the material.

In the following, these challenges are addressed resulting in a heat treatment strategy that will subsequently be assessed and validated through indentation experiments and numerical simulations. For this assessment, an industrial dual-phase steel (DP600) was chosen as a representative test case, as it shows strong microstructural

changes and significant damage accumulation[3]. To this end, DP600 tensile samples are deformed to the point of fracture, yielding severe deformation of the ferritic-martensitic microstructure as measured with in-situ local strain field measurement with a $\sim 10\mu$m spatial resolution (using digital image correlation).

The first challenge is to homogenize the microstructure of the deformed matrix surrounding the voids. For many deformation modes, including the case of uniaxial tension considered here, severe deformation leads to a strong heterogeneity in the metal microstructure, as a result of diffuse and/or localized necking (Fig. 2a). The local strain level determines the grain elongation, grain rotation, stored strain energy, dislocation density, dislocation cell structure formation, etc., resulting in the observed heterogeneity in the microstructure. This heterogeneity significantly affects the recrystallization or phase transformation kinetics, e.g. through the nucleation rate, as severely deformed regions provide energetically more favorable nucleation sites. To overcome this significant obstacle for obtaining a homogeneous microstructure with a heat treatment, the following procedure is developed that is generally applicable for most metals: first, the heterogeneity in strain energy is reduced with a prolonged recovery step. The remaining strain energy, dislocation structures or differences in grain shape will still inevitably induce different nucleation rates in different regions of the specimen upon recrystallization, leading to a wide distribution of grain sizes. However, by extending the duration of the recrystallization step, sufficient time is allowed for grain boundary migration to minimize the grain size distribution via excessive grain growth. For severely heterogeneous microstructures, further microstructure homogenization can be achieved through repeated phase transformations at higher temperatures (e.g. eutectoid transformation for steels).

This strategy is applied to DP600 steel, for which the recovery and recrystallization temperatures are 500°C and 700°C, respectively. Following 24 hours at each of these temperatures, the samples are austenized (at 1000°C) for 24 hours and cooled below the eutectoid transformation temperature and held at 600°C for 24 hours[4]. After the heat treatments, cross sections of the samples are metallographically prepared[5]. Light microscopy (Zeiss Axioplan 2) is used for quantitative analysis of phase fractions, while orientation imaging microscopy (FEI Sirion scanning electron microscope) is used for grain orientation and grain size analysis.

Analyses of the heat treated samples confirm expectations that a pearlitic-ferritic microstructure is obtained from the heat treatment of deformed martensitic-ferritic DP600 steel specimens (Fig.8.2a). As shown by the optical images (Fig.8.2b), grain

[3]Damage accumulation in DP600 take places through martensite cracking and martensite-ferrite decohesion, although other mechanisms are also observed [34]

[4]All heating and cooling rates are controlled at 10 °C/min (Carbolite HVT 12/60/700 vacuum furnace) to avoid significant thermal stresses.

[5]For microstructural characterization and indentation experiments, sample cross sections are prepared using successive grinding and mechanical polishing, followed by electropolishing and (only for microscopy analysis) etching with 2 vol.% nital solution.

size distributions (Fig.8.2c), and grain orientation images (Fig.8.2d) at different specimen locations (and hence different strain levels) the severe heterogeneity of the as-deformed microstructure surrounding the voids (Fig.8.2a) is homogenized successfully using the adopted heat treatment strategy.

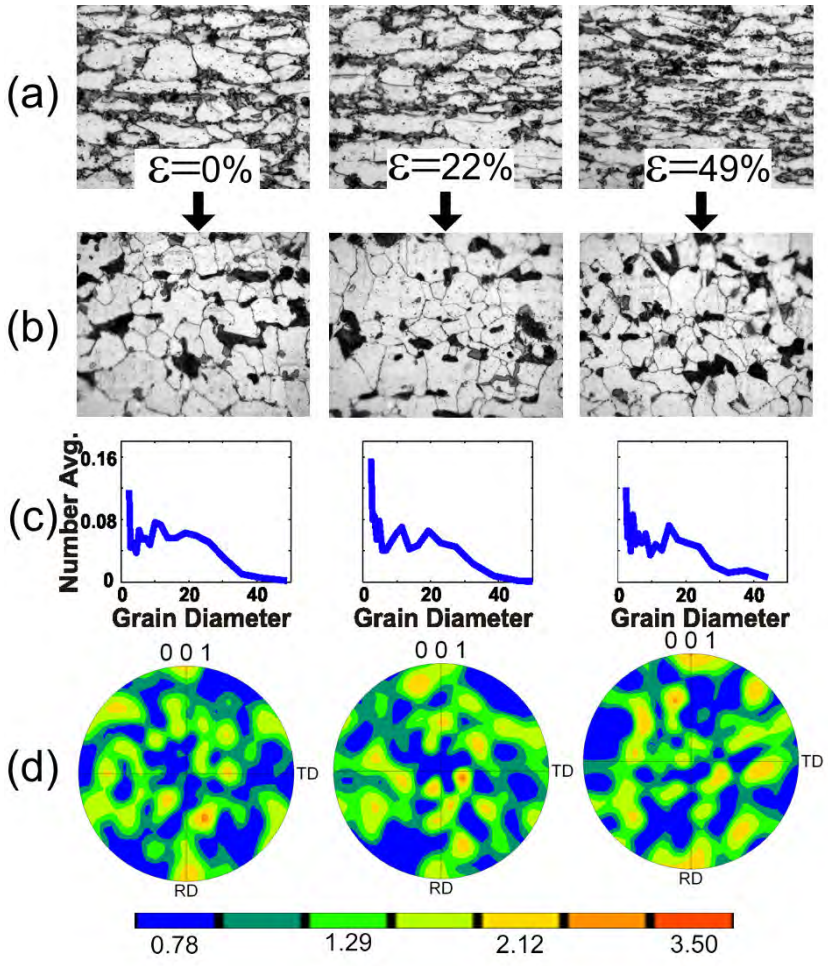

Figure 8.2: (a) As-received martensitic-ferritic microstructure deformed to strain levels of 0%, 22% and 49% before the heat treatment, and (b) the homogenized pearlitic-ferritic microstructure obtained after the heat treatment, as confirmed by (c) the grain size distributions and (d) grain orientation maps, both of which are constant over the complete specimen surface within statistical uncertainty.

Second, we consider possible changes to the deformation-induced damage in the material due to the adopted heat treatment. The implemented slow heating and cooling cycles rate of 10 °C/min. ensures a homogeneous temperature distribution within the specimen, thereby avoiding thermal stresses as a possible cause for damage alteration. Comparative microvoid area fraction measurements are carried out on as-deformed and heat treated samples to verify this assumption, which revealed

that the void area fraction in the heat treated microstructure is equal to that of the deformed microstructure within the statistical uncertainty of the measurement, being 0.01%. As further verification, in-situ SEM experiments are carried out, during which deformation-induced microvoids in DP600 steel are micrographically monitored during heating (FEI Quanta 600 SEM, equipped with a 1500°C heating stage). No significant changes in the morphology of individual voids are observed up to a temperature of 600°C, after which surface oxidation prohibited precise analysis (determination of void dimensions with an accuracy of ¡ 10nm.)[6] . All of these observations suggest that the influence of the heat treatment on damage is insignificant, i.e. the deformation-induced damage is preserved throughout the heat treatment.

8.3 Quantification of Damage through Indentation Experiments

With other deformation-induced microstructural mechanisms disabled in the microstructurally-homogenized material, the influence of the preserved damage on the indentation hardness and modulus can now be analyzed. For this purpose, load-controlled microindentation experiments are carried out using a CSM Instruments Micro-indenter with a Berkovich tip, up to a load of 4 N , and the local hardness and elastic modulus are obtained using the standard Oliver-Pharr methodology [103]. Hardness and modulus data are then coupled with the local strain data to investigate their coupled evolution with increasing deformation. All tests are repeated on six specimen parts to assess inter-specimen reproducibility. The obtained results are shown in Fig.8.3.

In Fig.8.3, the first striking observation is the constant hardness and modulus values at low levels of deformation. This is a clear indication of the effectiveness of the heat treatment, as earlier experiments on the as-deformed specimens (without heat treatment) for DP600 steel (as well as for three other metals) showed from the onset of deformation a clear increase in hardness and a clear decrease in modulus [105]. With further deformation, a sudden drop is observed in both hardness and modulus, starting at the same strain level of 0.2, which was identified by electron microscopy analysis as the starting point of martensite fracture. Such a drop at $\sim$0.2 strain was completely absent in the as-deformed state due to the masking influence of other microstructural changes on the indentation experiments. Finally, the D parameter is calculated from the relative drops in hardness and modulus, as shown in the lower part of Fig.8.3. Apart from the same onset of damage accumulation at $\sim$0.2 strain, it is also observed that the magnitude of the damage obtained from two substantially different physical properties (hardness degradation vs. modulus degradation)

[6]Preferably, one aims to verify this assumption by probing the morphology of internal microvoids before and after heat treatment. Unfortunately, the required spatial resolution cannot be attained, not even with the highest resolution micro-tomography technology (x-ray micro-tomography with a 0.5 μm voxel size).

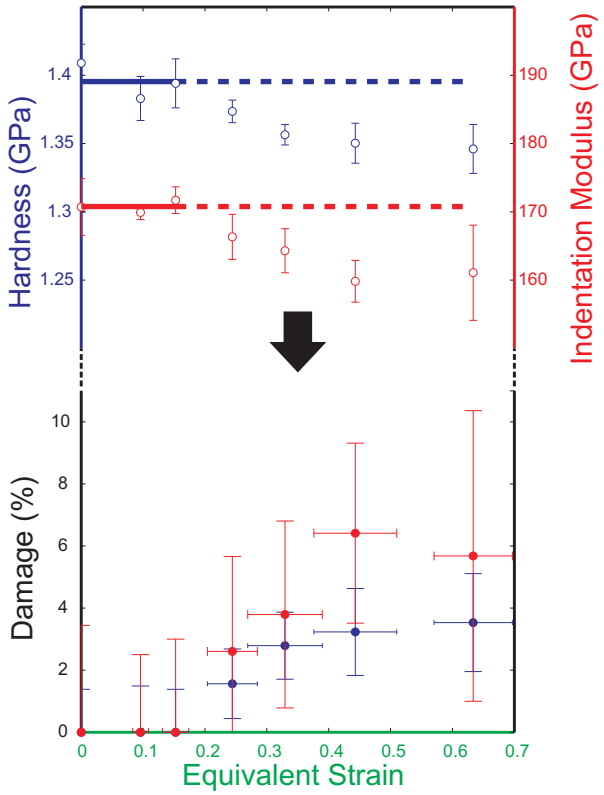

Figure 8.3: Results of the indentation measurements on the heat treated specimens showing an initial plateau in hardness (blue) and modulus (red) at low levels of deformation (no damage accumulation), and a clear decrease with further increasing deformation (onset of damage). Corresponding damage values are also plotted for the same strain levels and with the same color coding. The error bar represents the standard deviation of the mean.

are roughly equal within their statistical uncertainty. These trends, along with the microstructural characterization shown above, provide strong evidence that the deformation history is indeed successfully erased, while the damage is preserved, and that the observed drop in both hardness and modulus is only caused by the damage in the microstructure.

8.4 Reliability Assessment of the Measured Damage Parameter

A final concern may arise, because the D parameter is obtained from indentation experiments on a different matrix microstructure (but with the same preserved damage), which may not be representative for the damage evolution in the as-received

material[7]. Therefore, lastly, the reliability of the obtained D parameter is assessed. As explained above, alternative damage characterization methodologies (SEM, X-ray microtomography, etc.) lack the required precision to verify the results obtained here. Hence, finite element (FE) simulations of the indentation experiments are utilized to assess the influence of the matrix elasto-plastic response on the observed damage-induced degradation of hardness and modulus.

In these simulations, the actual Berkovich tip used in experiments (modeled as a rigid body) is indented into the metal (elasto-plastic material behavior with isotropic hardening) containing 2.0% porosity (see inset in Fig.8.4). Mechanical properties (i.e. yield strength, Young's modulus, strength coefficient and strain hardening exponent) of the DP600 steel, which serves as the base material in this comparative study, are obtained from the uniaxial tensile tests. The voids (i.e. 2% porosity) are modeled explicitly with a random spatial distribution and a realistic void size distribution, sampled from SEM analyses . The simulations yield force-displacement indentation curves, from which the hardness and elastic moduli are obtained using the Oliver and Pharr methodology, in the same way as done in the real indentation experiments.

To mimic possible changes in the mechanical response of the metal matrix due to the heat treatment, the simulations are repeated changing one property at a time exploring (reasonable) material limits , while keeping the other three properties and the FE mesh (i.e. void distribution and void volume fraction) fixed. Each simulation is repeated without porosity and the D parameter is calculated from the difference with and without porosity using D_H = 1-H_D/H and D_E = 1-E_D/E. Subsequent comparison of D_H and D_E with those of the DP600 control case yields the additional (relative) error in the D value due to changes of the matrix material.

The simulations reveal a maximum additional error in the experimentally-measured damage values due to changes of the matrix material of only 2% of the DH or DE value, and in most cases this additional error will even be much less (Fig.8.4). Apparently, the error introduced by possible changes in matrix microstructure due to the heat treatment is much smaller than the experimental uncertainties of the indentation results. In conclusion, the adopted heat treatment does not need to reproduce the original starting microstructure.

8.5 Conclusions

In summary, the proposed strategy to eliminate the influence of the microstructural heterogeneity to properly capture the damage-induced degradation of indentation hardness and modulus is verified by a thorough microstructural and mechanical analysis. The microscopy analysis reveals that a homogeneous microstructure

[7]Reproducing the starting matrix microstructure from a deformed state may be possible with more complex heat treatments, however, this would limit the application of the approach as a general methodology, especially for industrial case studies.

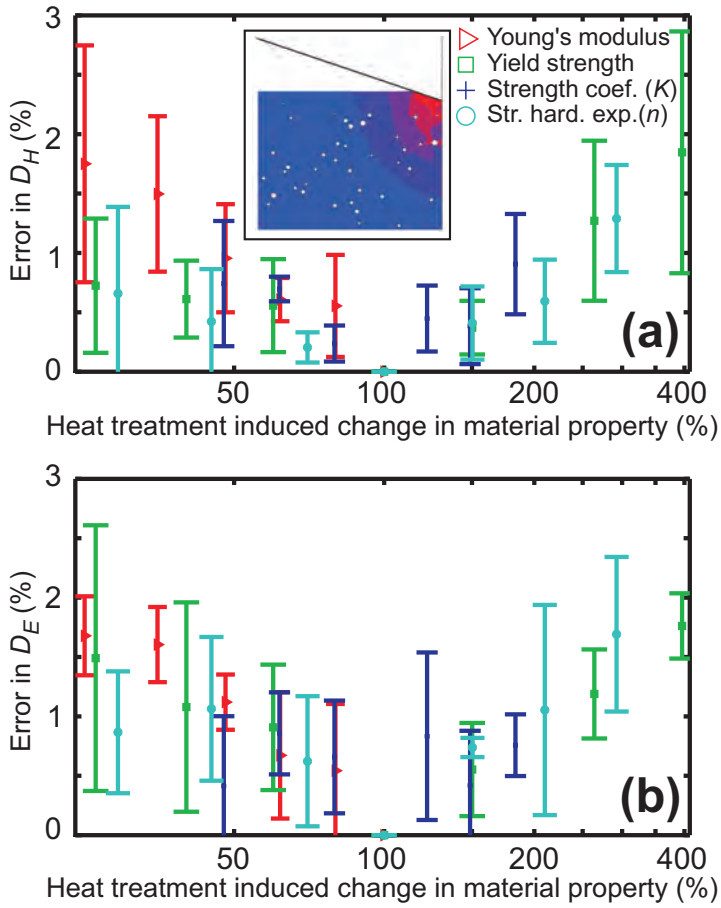

Figure 8.4: The sensitivity of the damage parameter, DH or DE, to heat treatment induced changes in material properties, as calculated from the change in D value due to a change in material input parameters compared to the DP600 control case (Young's modulus of 239 GPa, yield strength of 379 MPa, strength coefficient of 1009 MPa, and strain hardening exponent of 0.171), while keeping the (randomly-generated) void distribution constant. Each set of simulations is repeated for five different void distributions to probe the statistical uncertainty.

can be obtained with a dedicated heat treatment that preserves the deformation-induced damage. Subsequent indentation experiments show the expected hardness and modulus profiles (i.e. an initial plateau at low strain levels followed by a clear decrease with increasing deformation), consisted with microstructural observations made. Finally, accompanying finite element simulations of the indentation experiments show that the error in the measured damage due to possible heat treatment induced changes in the matrix microstructure is insignificant compared to experimental uncertainties.

Whereas indentation-based damage quantification, which is required for quantifying damage in continuum damage models, is intrinsically deficient in its original form, it can still be used to obtain the damage properly if a dedicated heat treatment is

applied prior to the indentation experiments. Therefore, the proposed method fills a critical gap in damage engineering, allowing mechanical damage parameter to be measured in a reliable manner.

8.6 Acknowledgements

This research was carried out under the project number MC2.05205 in the framework of the Research Program of the Materials innovation institute M2i (www.m2i.nl), the former Netherlands Institute for Metals Research. The authors acknowledge Paul van Beers and Mathijs Peters for their contributions.

CHAPTER NINE

Micropillar Compression Testing for Ductile Damage Quantification[1]

Abstract

Continuum damage models require experimentally obtained damage parameters to accurately predict material failure. However, existing experimental methodologies do not suffice the requirements. In this work, an original damage quantification methodology is presented which is based on elastic compression tests on electro-discharge machined micropillars. The damage parameter is obtained through the measured degradation of the modulus due to previous deformation. The capabilities of the methodology are demonstrated in a case study, where the damage evolution in a dual-phase steel due to a uniaxial tensile test is successfully quantified.

[1] *Reproduced from:* C.C. Tasan, J.P.M. Hoefnagels, M.G.D. Geers, A Micropillar Compression Methodology for Ductile Damage Quantification, *Submitted*, (2010).

9.1 Introduction

Continuum damage models (CDM) are attracting significant scientific and industrial interest in order to predict the complex mechanical behaviour and failure of new advanced metals (dual phase, transformation-induced plasticity and twinning-induced plasticity steels, advanced aluminium alloys, etc.). The application of CDM in real operations, on the other hand, is still limited due to the need for experimental identification of the adopted deformation-induced (and material specific) damage evolution laws. It was shown earlier that a quantification of damage-induced softening is not trivially possible using existing direct experimental techniques (e.g. electron micrography, x-ray micro-tomography, highly-sensitive mass and volume measurements), which effectively probe geometric damage (e.g. void area fraction, void volume fraction, and porosity density) [70,90,138]. This is essentially due to the insensitivity of a scalar geometric damage parameter to cover the full mechanical influence of deformation-induced damage. Moreover, experimental accuracy is generally also lacking[2]. These requirements (i.e. sensitivity to full damage spectrum, high accuracy) call for a mechanical testing method, with a high spatial resolution, capturing high strain and damage gradients. Consequently, Lemaitre et al. proposed an indentation based methodology [84], where deformation-induced hardness degradation is probed to quantify a mechanical damage parameter, D. This approach has received considerable attention [90, 120, 123] and was extended by Guelorget et al. [117] to probe the damage parameter from the degradation of the indentation-modulus (obtained via Oliver-Pharr methodology [103]), through:

$$D_E = 1 - \frac{E_d}{E} \tag{9.1}$$

where $E^D$is the modulus of the damaged material and E is the modulus in the undeformed state.

Recently, it was shown by the authors that the classical indentation based approach is intrinsically deficient due to plasticity-induced microstructural effects (indentation pile-up, strain hardening, grain shape change, texture formation, etc.), which mask the degradation of hardness and cause severe artifacts in the modulus [105].

Since these plasticity-induced microstructural effects render the conventional indentation-based methodology useless, an alternative mechanical method for damage quantification is required. Obviously such a new mechanical methodology should only probe the elastic response and avoid undesired plasticity effects to allow for the extraction of an accurate damage parameter.

In aiming to achieve this goal, we here present a novel methodology based on com-

[2]Nevertheless, these techniques allow qualitative (microscopic) analysis of damage mechanisms, which is required to optimize damage sensitive microstructures.

pression tests, which quantifies damage-induced softening through the degradation of the elastic modulus of compression. Afore-mentioned plasticity induced problems (e.g. indentation pile-up) are circumvent with the developed methodology, since the modulus of compression is measured on micropillars with a flat punch (instead of the sharp indenter in the original indentation methodology) and the load levels are kept well-below the point of yielding, thereby minimizing localized plasticity.

Results obtained demonstrate that this methodology overcomes the previously reported complications in damage quantification in a reliable and accurate manner.

9.2 Experimental Methodology

The developed methodology is demonstrated on a commonly-used industrial sheet metal grade: dual phase 600 (DP) steel, of 1mm thickness. Tensile specimens (Fig.9.1a) of DP steel are cut using electro-discharge machining (EDM), painted with a speckle-pattern and tested up to the point of fracture using a micro-tensile stage (Fig. 9.1b). To assess the reproducibility of the methodology, three samples are tested from each sheet. Following the tensile test, deformed samples are cut into four pieces each along their central axis using wire EDM (with a wire diameter of 0.1mm) (Fig. 9.1c). Pillars of square cross section (i.e. 0.2x0.2mm^2) are produced at the cross sections of the tensile specimens, with two perpendicular sets of 0.4mm-deep parallel wire EDM cuts (Fig. 9.1d)[3]. The size of the pillars (0.2x0.2x0.4mm3) are selected such that a representative material volume (covering hundreds of grains) is probed, while sufficient spatial resolution is maintained to capture high strain and damage gradients. Local equivalent strains are calculated from DIC measurements of the deformation during the initial tensile test to obtain the level of deformation at each pillar location. Finally, the EDM induced surface roughness of the pillars is removed with a short electro-polishing step.

Load controlled compression tests are carried out using a micro-indenter (CSM Instruments Micro-Indenter) with a flat punch of 0.35mm diameter. From each tested pillar, load vs. displacement data is obtained (Fig.9.2), used to extract the elastic compression modulus. The loading-unloading scheme is specially designed to minimize the influence of surface plasticity on the modulus measurement (Fig. 9.2): The pillars are first compressed up to 2N load level, which corresponds to approximately half of the material yield strength, subsequently unloaded to 0.4N, and then three times reloaded and unloaded between the 0.4N and 1N. The modulus is calculated upon the higher 60% portion of the unloading from the 1N. Obtained modulus data is used to calculate the damage parameter D^E, where the modulus in the undeformed state is measured on the pillars outside the specimen gauge section. Finally, D^E is coupled to the measured local strains to reveal its evolution with deformation.

[3]Recently, focus ion beam miled micro-pillars have received a lot fo attention in the literature to study the size dependency of plasticity phenomena [140,141]. For the present purpose, however, due to the total volume of material that needs to be removed, focus ion beam milling is not an option.

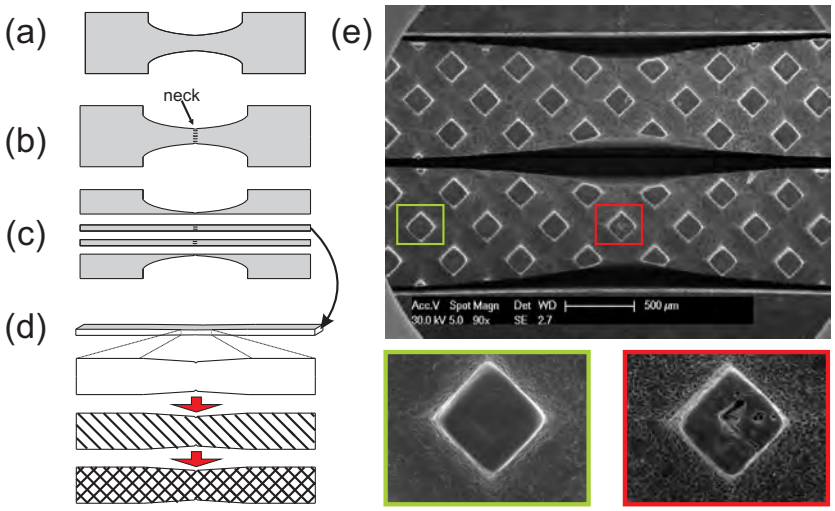

Figure 9.1: The adopted experimental methodology consists of tensile tests on dog-bone shaped specimens up to the point of fracture (b), cutting the deformed samples into two pieces along their central axis with 3 wire EDM cuts (c), followed by two perpendicular sets of 0.4mm-deep parallel wire EDM cuts on the cross section at 45° with the tensile direction (d) to produce the field of 0.2x0.2x0.4 mm^3pillars shown in (e). Note that the final electro-polishing step reveals microvoids at the top of pillars located at highly deformed regions around the neck.

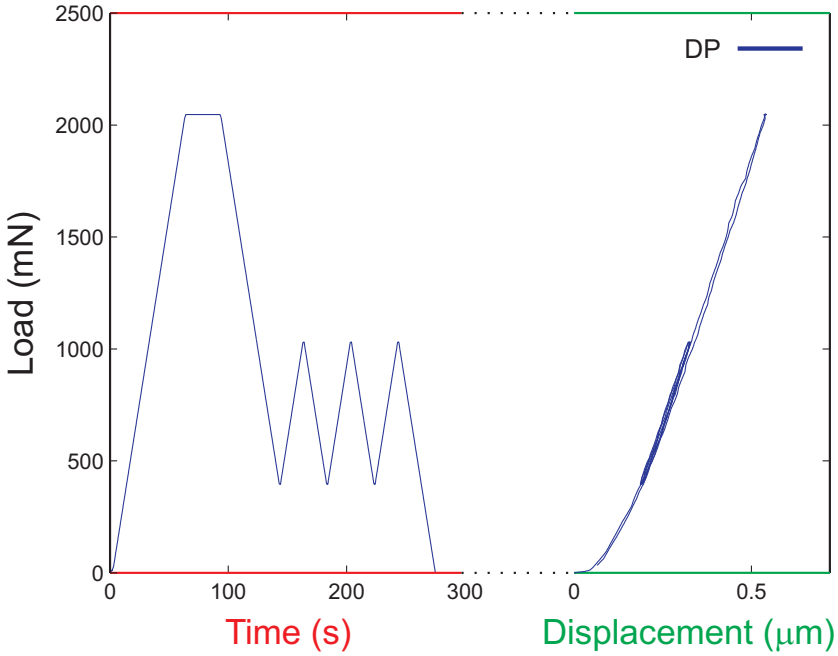

Figure 9.2: The loading sequence for the compression tests for the DP steel (left); Resulting load vs displacement curves (right)

9.3 Results

The deformation-induced evolution of the compressive modulus is shown in Fig.9.3. It is striking to observe that the modulus is constant at low strain levels and then begins to degrade at an increasing rate, and reaches a minimum at the onset of fracture. Note that this physically expected trend was not captured with the original indentation-based damage quantification methodology [105]. This overall trend and the total amount of decrease in modulus reveals a realistic damage evolution trend, with the damage value staying constant within experimental accuracy up to a strain level of $\sim$0.24, then increasing almost linearly to 5%, and finally growing rapidly to $\sim$20% at the onset of fracture. Note that these high levels of final damage values are in accordance with the microstructural observations obtained by the scanning electron microscope (see Fig. 9.1e).

While these results are highly promising, one should also consider other sources that might trigger a deformation-induced change in elastic modulus, such as texture evolution or residual stress built-up. Such effects may be very critical for the quantification of damage accurately, as shown earlier by the authors for the original indentation methodology. In order to reveal the influence of these microstructural effects for the case of DP steel, a dedicated heat treatment protocol is applied to deformed tensile specimens, details of which are provided elsewhere [142]. This heat treatment (which is originally developed and used for a new indentation-based damage quantification methodology [142]) aims at partially homogenizing the deformed microstructure such that the deformation-induced heterogeneity in grain size, grain shape, grain orientation etc. are removed, while the voids themselves are left unaffected. Micropillar compression tests on heat treated samples showed that the decrease in modulus and the overall trend is very similar before and after the heat treatment, revealing that the influence of other microstructural changes on the degradation of elastic modulus is within experimental uncertainty (Fig..9.3). As a final verification of the accuracy of the micropillar compression methodology, the damage evolution in the same dual phase steel is also quantified using the above-mentioned new indentation-based damage quantification methodology [142]. The obtained results verified the accuracy of the micropillar approach, revealing the same damage initiation point and the damage accumulation profile up to the onset of fracture, where strain measurement uncertainty obstructs the direct comparison between the two methodologies.

9.4 Conclusions

A promising damage quantification methodology is developed, whereby the elastic damage parameter is obtained through the deformation-induced degradation of the elastic compression modulus. Proof-of-principle experiments on dual-phase 600 steel demonstrated that a realistic mechanical damage parameter can be obtained in

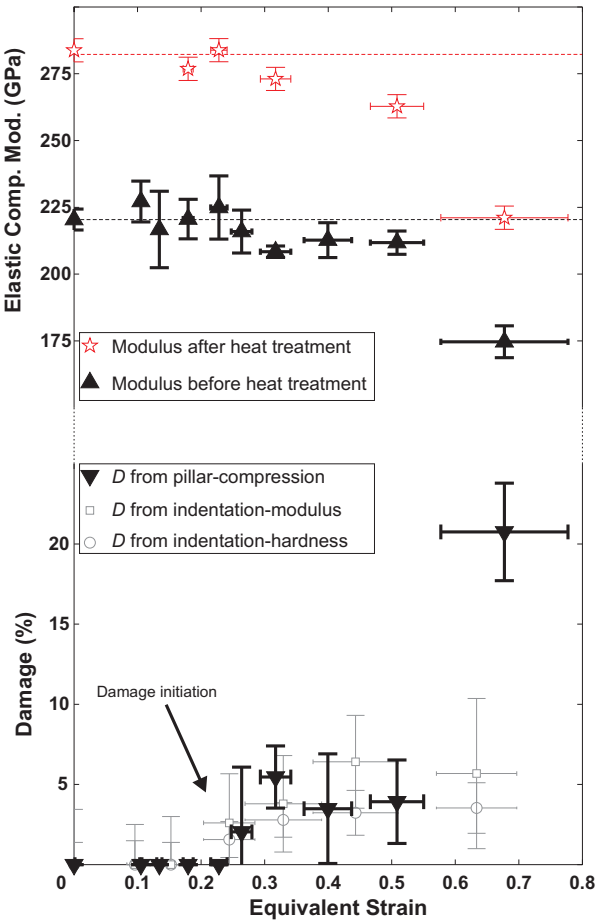

Figure 9.3: Compression modulus and damage evolution in DP steel (The reference modulus value at zero strain [measured at specimen pad, outside the clamp] is shown with a dashed line.) The error bars represents the standard deviation of the mean. Compression modulus measurements after microstructure partial-homogenization heat treatment are also shown, which reveal that deformation-induced microstructural effects (other than damage evolution) have no significant influence in the modulus trend. Obtained damage evolution is verified with an alternative (indentation-based) damage quantification methodology [142].

a reliable manner.

9.5 Acknowledgements

This research was carried out under the project number MC2.05205 in the framework of the Research Program of the Materials innovation institute M2i (www.m2i.nl), the former Netherlands Institute for Metals Research.

CHAPTER TEN

General Conclusions and Outlook

10.1 Conclusions

Acquiring an in depth understanding of damage evolution is a prerequisite to reach the objectives of the metals processing industry regarding weigh-reduction, miniaturization, multi-functionality, high durability, etc. While superior specific strength of metals may be achieved by processing complex microstructures (e.g. dual phase steels, transformation-induced plasticity steels, high strength aluminium alloys, etc.), formability remains at risk as a result of more prominent deformation-induced damage, the evolution of which is highly sensitive to the particular microstructural morphology. Reports of unexpected failure at low levels of deformation clearly indicate the difficulties encountered in optimizing complex microstructures for the deformation steps used in forming or in service. This sensitivity was also clearly demonstrated in this thesis (in chapter 2): the limits of stable deformation, i.e. localization (represented by the forming limit curve) and fracture (represented by the fracture limit curve) are lowered in microstructures with a significant number of potentially active damage mechanisms, underlining the need for an enhanced understanding.

10.1.1 Characterization of Ductile Damage Mechanisms

The detailed analysis of forming limits and damage mechanisms in chapter 2 also re-emphasize the first motivation of this PhD project, i.e. the need to provide new experimental techniques to enable characterization of damage evolution, since the experimental data in chapter 2 was obtained using conventional experimental tools (macro-scale tests) and methodologies (post-mortem fractography analysis). While the coupled use of existing tools can provide useful data of a relative nature (such as void area fraction), the analysis of physical nature of microstructural should be done with great care since the post-mortem fractography effectively requires back-tracking

the deformation history to interpret the findings. Accordingly, a full understanding of these damage mechanisms can only be achieved by enhancing the applied experimental methodologies such that: (i) more information on the spatial deformation field (e.g. real-time deformation image sequences, micro-level strain data, etc.) can be extracted, and (ii) the influence of the adopted methodology on the obtained experimental data itself is minimized. This point is demonstrated in the subsequent chapters (3, 4 and 5), where three original micro-mechanical methodologies are presented that enable the experimental characterization of damage mechanisms in considerable more detail.

First, a miniaturized Marciniak setup was designed (after discarding other possible setups such as hemi-sphere punch tests, cruciform tests, bulge tests, etc.), built and tested. This setup enables the analysis of sheet metal deformation in different strain paths up to the point of fracture, with parallel real-time in-situ electron microscopic examination (chapter 3). The amount of additional information on metal deformation that comes available by this setup is promising, as it allows tracking of specific microstructural features during deformation in strain paths ranging from uniaxial tension to biaxial tension.

A major benefit of such an in-situ analysis was shown in chapter 4, where electron microscopy image sequences of the deformation of the microstructure are post-processed to obtain the microstructural strain partitioning, revealing a detrimental influence of segregation-induced band morphology on damage evolution. On the basis of this detailed microstructural information, it has been concluded that microstructures with a hard, continuous band experience extensive damage nucleation due to shear bands developing through the narrowest section of the banded phase, forcing it to deform beyond its plastic limit.

However, while in-situ electron microscopy tests provide high quality information on the deformation micro-mechanisms at the metal surface, it is also required to carry out investigations beneath the metal surface. For this type of microstructural analysis, existing specimen preparation methodologies (e.g. mechanical polishing, electro-polishing) generally compromise the original microstructure, with changes that are mostly unacceptable. In chapter 5, an improved experimental methodology is presented, whereby samples previously deformed in a ductile manner are separated in a well-controlled brittle manner to open up the microstructure for analysis without any additional ductile deformation. Microscopic imaging of the two fracture surfaces permits to reconstruct the 3D characteristics from the ductile pre-deformation, providing a clean and effective way of visualizing grain deformations, microvoid nucleation sites and growth mechanisms, and other micro-events induced by ductile deformation.

10.1.2 Quantification of Damage Evolution

The proper characterization of damage micromechanisms typically allows for a *metallurgical* solution to avoid damage-induced failure. Accurate damage models (that

take microstructural damage evolution on board) would enable a precise prediction of deformation limits in different strain paths providing a mechanical solution of the problem. However, continuum damage models require material-specific damage evolution laws. Even though many damage quantification methods to measure the damage evolution laws have been proposed in literature, their predictive capabilities and engineering reliability have hardly been investigated. Therefore, the second goal of this PhD project was to investigate the reliability of existing techniques in an effort to assess ideal experimental probes for the quantification of the damage parameter.

The analysis presented in chapter 6 fills this gap by comparing the accuracy and resolution of existing "direct" damage quantification techniques (i.e. highly sensitive density measurements, X-ray microtomography, and SEM imaging) to "indirect" damage quantification techniques (i.e. indentation methodology, modified indentation methodology, micropillar compression methodology). Obtained results demonstrate that, even though the direct methods are well suited for *characterization* of damage micro-mechanisms, they all have limited precision/resolution for damage *quantification*, and the measured geometrical damage parameter does not account for all possible "mechanical" damage effects, e.g. due to the presence of (volumeless) microcracks. Therefore, accurate prediction of damage-induced softening with CDM requires a proper methodology that enables a reliable quantification of a mechanical damage parameter.

Chapter 7 proves that the existing methodologies that are commonly used (in the literature and the industry) to quantify a mechanical damage parameter may fall short. The most promising of such methodologies, i.e. the conventional indentation-based damage quantification methodology, was shown to be intrinsically deficient: by probing the indentation-based hardness or elastic modulus, not only the effect of damage is measured, but also surrounding plasticity effects of strain hardening, grain shape change, indentation pile-up, etc.

To overcome this problem two original mechanical methodologies have been developed in this project, whereby it is proven that a material representative mechanical damage parameter can be measured reliably. The first of these new methodologies is a modification of the above-mentioned (conventional) indentation-based damage quantification methodology: Following an innovative strategy to revise this methodology, it is shown in chapter 8 that the detrimental plasticity effects of deformation-induced microstructural changes can be resolved by employing a deformation-history erasing heat treatment that preserves the geometrical damage in the microstructure. Follow-up indentation experiments reveal a reliable damage-induced drop in hardness and modulus, enabling the quantitative extraction of a damage parameter.

The intrinsic problem of the conventional indentation-based damage quantification methodology can also be overcome by properly probing only the elastic response of the deformed material. In Chapter 9, a second technique to remedy the masking plasticity effects is presented. By applying micropillar-based local compression tests on electro-discharge machined pillars, the elastic compression modulus degradation

is captured in a purely elastic manner (due to the overall homogeneous deformation state that does not trigger localized plasticity) enabling a reliable measurement of the damage parameter.

In summary, the developed methodologies presented in this thesis allow for an improved analysis of damage micromechanisms and the precise quantification of damage accumulation. Using the developed methodologies, the challenges in the characterization of damage micro-mechanisms are effectively addressed, providing dedicated tools to enable a detailed investigation of damage-induced failure mechanisms.

10.2 Outlook

Current industrial trends of weight-reduction, miniaturization, multi-functionality, etc., are triggered by critical environmental and economical issues (energy conservation, material scarcity, global warming, etc.) and unlikely to lose momentum in the near future. From a materials and metallurgical engineering perspective, these trends steer the industry and the scientific community to explore the limits of metal performance through designing and producing new metals with complex microstructures. Nature allows limitless possibilities in terms of designing new microstructures, however, available research resources are too limited to investigate all possible routes. Moreover, every new microstructure inevitably introduces new problems, e.g. new failure modes. In overcoming these challenges in the metal microstructure optimization process, effective characterization of metal deformation, damage and failure plays (and will continue to play) a critical role. New experimental techniques that allow a mechanical-microscopic approach, such as in-situ mechanical testing with real-time electron microscopy imaging, offer an effective strategy for in-depth analysis of the metal failures, and the underlying physical mechanisms. However, these tools are relatively new, and hence, have not so far been used to their limit. From an industrial perspective, such methodologies can be effectively employed in the near future to set general guidelines for the development of new metals, in order to meet the requirements arising from the critical environmental and economical issues. From a scientific perspective, current understanding of the microstructural deformation mechanisms can be largely expanded by the immense amount of data that can be produced with this approach (e.g. sequential high-resolution images of microstructure deformation, microstructure-level strain fields, grain orientation maps, etc.), especially if effective means of producing model materials can be developed.

While the mechanical-microscopic approach addresses the fundamental issues in microstructure-performance relationship, there is also a strong need in metals industry for new experimental techniques to address arising engineering problems. Determination of safe forming limits and fracture points for the newly developed metals is among those problems, and addressed extensively in this thesis. The most economic approach to optimize forming operations is through computational sim-

ulations. Commonly observed damage-induced failures can be predicted through the implementation of continuum damage models in forming simulations, hence taking deformation-induced damage evolution into account. However these models require experimentally obtained damage parameters, and existing experimental methodologies do not suffice the requirements to provide these parameters. The in-depth analysis in this thesis provides deepened insight to explore ideal experimental approaches to measure the damage parameters, while also demonstrating the future challenges in this field. The damage spectrum of the conventional damage quantification techniques is significantly enlarged with the techniques developed in this thesis, which also capture mechanical damage effects, allowing damage evolution to be successfully quantified up to a level of 10-20%. Yet, continuum damage models still require the full evolution of damage to the point of fracture (D=100%). This is a difficult task for the case of uniaxial tension considered here, since the accurate quantification of the high damage gradients in the post-strain localization regime is extremely challenging. A promising strategy for future work could be modifying the developed methodologies to probe damage evolution in other deformation modes (such as bending) where deformation is more constrained, and high strain gradients due to localization are avoided.

Bibliography

[1] W.M.F. Petrie. *Tools and Weapons*. British School of Archaeology, London, 1974.

[2] International Iron and Steel Institute Committee on Automotive Applications. *Advanced High Strength Steel (AHSS) Application Guidelines*. World Steel Association, Brussels, 2006.

[3] J. Mediavilla, R.H.J. Peerlings, and M.G.D. Geers. An integrated continuous-discontinuous approach towards damage engineering in sheet metal forming processes. *Engineering Fracture Mechanics*, 73:895–916, 2006.

[4] S. Sadagopan and D. Urban. *Formability characterization of a new generation of high strength steels*. American Iron and Steel Institute, 2003.

[5] S.F. Golovashchenko. Sharp flanging and flat hemming of aluminum exterior body panels. *Journal of Materials Engineering and Performance*, 14(4):508–515, 2005.

[6] D.R. Metzger, X. Duan, M. Jain, D.S. Wilkinson, R. Mishra, S. Kim, and A.K. Sachdev. The influence of particle distribution and volume fraction on the post-necking behaviour of aluminium alloys. *Mechanics of Materials*, 38(11):1026–1038, 2006.

[7] Z. Marciniak and J.L. Duncan. *Mechanics of Sheet Metal Forming*. Edward Arnold, London, 1992.

[8] M. Jain, J. Allin, and D.J. Lloyd. Fracture limit prediction using ductile fracture criteria for forming of an automotive aluminum sheet. *International Journal of Mechanical Sciences*, 41(10):1273–1288, 1999.

[9] A.L. Gurson. Continuum theory of ductile rupture by void nucleation and growth .1. yield criteria and flow rules for porous ductile media. *Journal of Engineering Materials and Technology-Transactions of the Asme*, 99(1):2–15, 1977.

[10] C.C. Chu and A. Needleman. Void nucleation effects in biaxially stretched sheets. *Journal of Engineering Materials and Technology-Transactions of the Asme*, 102(3):249–256, 1980.

[11] V. Tvergaard and A. Needleman. Analysis of the cup-cone fracture in a round tensile bar. *Acta Metallurgica*, 32(1):157–169, 1984.

[12] V. Tvergaard. Influence of voids on shear band instabilities under plane-strain conditions. *International Journal of Fracture*, 17(4):389–407, 1981.

[13] S.P. Keeler. *Plastic instability and fracture in sheet stretched over rigid punches*. PhD thesis, Massachusetts Institute of Technology, 1961.

[14] D. Banabic, H.-J. Bunge, K. Pohlandt, and A.E. Tekkaya. *Formability of Metallic Materials.* Springer-Verlag, Berlin, 1993.

[15] A.K. Ghosh. Criterion for ductile fracture in sheets under biaxial loading. *Metallurgical Transactions A-Physical Metallurgy and Materials Science*, 7(4):523–533, 1976.

[16] R.J. Bourcier and D.A. Koss. A fracture limit diagram for determining hydrogen embrittlement of sheet under multiaxial loading conditions. *Scripta Metallurgica*, 16(5):515–518, 1982.

[17] H. Takuda, K. Mori, N. Takakura, and K. Yamaguchi. Finite element analysis of limit strains in biaxial stretching of sheet metals allowing for ductile fracture. *International Journal of Mechanical Sciences*, 42(4):785–798, 2000.

[18] H.N. Han and K.H. Kim. A ductile fracture criterion in sheet metal forming process. *Journal of Materials Processing Technology*, 142(1):231–238, 2003.

[19] Y.W. Lee, J.C. Woertz, and T. Wierzbicki. Fracture prediction of thin plates under hemi-spherical punch with calibration and experimental verification. *International Journal of Mechanical Sciences*, 46(5):751–781, 2004.

[20] R. Narayanasamy and C.S.A. Narayanan. Some aspects on fracture limit diagram developed for different steel sheets. *Materials Science and Engineering A-Structural Materials Properties Microstructure and Processing*, 417(1-2):197–224, 2006.

[21] Z. Yu, Z. Lin, and Y. Zhao. Evaluation of fracture limit in automotive aluminium alloy sheet forming. *Materials & Design*, 28(1):203–207, 2007.

[22] K.E. Puttick. Ductile fracture in metals. *Philosophical Magazine*, 4(44):964–969, 1959.

[23] M.J. Tan, X.J. Zhu, and S. Thiruvarudchelvan. Cavitation phenomenon of commercially pure titanium. *Journal of Materials Processing Technology*, 191(1-3, Sp. Iss. SI):202–205, 2007.

[24] M.A. Greenfield and H. Margolin. Mechanism of void formation, void growth, and tensile fracture in an alloy consisting of 2 ductile phases. *Metallurgical Transactions*, 3(10):2649–&, 1972.

[25] A. Gysler, G. Lutjerin, and V. Gerold. Deformation behavior of age-hardened Ti-Mo alloys. *Acta Metallurgica*, 22(7):901–909, 1974.

[26] R.N. Gardner, T.C. Pollock, and H.G.F. Wilsdorf. Crack initiation at dislocation cell boundaries in ductile fracture of metals. *Materials Science and Engineering*, 29(2):169–174, 1977.

[27] A.A. Benzerga, J. Besson, and A. Pineau. Anisotropic ductile fracture Part I: experiments. *Acta Materialia*, 52(15):4623–4638, 2004.

[28] H.P. Ganser, E.A. Werner, and F.D. Fischer. Plasticity and ductile fracture of IF steels: Experiments and micromechanical modeling. *International Journal of Plasticity*, 14(8):789–803, 1998.

[29] M. Sarwar, E. Ahmad, K. A. Qureshi, and T. Manzoor. Influence of epitaxial ferrite on tensile properties of dual phase steel. *Materials & Design*, 28(1):335–340, 2007.

[30] R.W.K. Honeycombe and H.K.D.H. Bhadeshia. *Steels: Microstructure and Properties.* Elsevier, London, 1995.

[31] E. Ahmad, T. Manzoor, K.L. Ali, and J.I. Akhter. Effect of microvoid formation on the tensile properties of dual-phase steel. *Journal of Materials Engineering and Performance*, 9(3):306–310, JUN 2000.

[32] Z. Marciniak and K. Kuczynski. Limit strains in the processes of strecht-forming sheet metal. *International Journal of Mechanical Sciences*, 9:609–620, 1967.

[33] F. Bron, J. Besson, and A. Pineau. Ductile rupture in thin sheets of two grades of 2024 aluminum alloy. *Materials Science and Engineering A-Structural Materials Properties Microstructure and Processing*, 380(1-2):356–364, 2004.

[34] C.C. Tasan, J.P.M. Hoefnagels, C.H.L.J. ten Horn, and M.G.D. Geers. Experimental analysis of strain path dependent ductile damage mechanics and forming limits. *Mechanics of Materials*, 41(11):1264–1276, 2009.

[35] P.J. Jacques, Q. Furnemont, F. Lani, T. Pardoen, and F. Delannay. Multiscale mechanics of TRIP-assisted multiphase steels: I. Characterization and mechanical testing. *Acta Materialia*, 55(11):3681–3693, 2007.

[36] J. Kang, Y. Ososkov, J. Embury, and D. Wilkinson. Digital image correlation studies for microscopic strain distribution and damage in dual phase steels. *Scripta Materialia*, 56(11):999–1002, 2007.

[37] Hoefnagels J.P.M. Geers M.G.D. Tasan, C.C. Microstructural Banding Effects Clarified Through Micrographic Digital Image Correlation. *Scripta Materialia (Accepted)*, 2010.

[38] A.J. Rantaeskola. Use of the hydraulic bulge test in biaxial tensile testing. *International Journal of Mechanical Sciences*, 21(8):457–465, 1979.

[39] D.W.A. Rees. Plastic-flow in the elliptic bulge test. *International Journal of Mechanical Sciences*, 37(4):373–389, 1995.

[40] C.C. Tasan, J.P.M. Hoefnagels, G. Quaak, and M.G.D. Geers. In-plane biaxial loading of sheet metal until fracture. *in proceedings of the 2008 SEM XI international congress and exposition on experimental and applied mechanics*, 2008.

[41] S. Demmerle and J.P. Boehler. Optimal-design of biaxial tensile cruciform specimens. *Journal of the Mechanics and Physics of Solids*, 41(1):143–181, 1993.

[42] J. Gozzi, A. Olsson, and O. Lagerqvist. Experimental investigation of the behavior of extra high strength steel. *Experimental Mechanics*, 45(6):533–540, 2005.

[43] K.S. Raghavan. A simple technique to generate inplane forming limit curves and selected applications. *Metallurgical and Materials Transactions A-Physical Metallurgy And Materials Science*, 26(8):2075–2084, 1995.

[44] F. Barlat, R.C. Becker, Y. Hayashida, Y. Maeda, M. Yanagawa, K. Chung, J.C. Brem, D.J. Lege, K. Matsui, S.J. Murtha, and S. Hattori. Yielding description for solution strengthened aluminum alloys. *International Journal of Plasticity*, 13(4):385–401, 1997.

[45] H. Vegter, C.H.L.J. ten Horn, Y. An, E.H. Atzema, H.H. Pijlman, T.H. van den Boogaard, and H. Hutink. Characterization and modelling of the plastic material behaviour and its application in sheet metal forming simulation. *Proceedings of the VII International Conference on Computational Plasticity*, 2003.

[46] P. Jimbert, A. Arroyo, I. Eguia, J.I. Fernandez, E. Silveria, I. Garuz, and G.S. Daehn. Efficiency improvement and analysis of changes in microstructure associated to a uniform pressure actuator. *Proceedings of the 2nd International Conference on High Speed Forming*, 2006.

[47] P. Jimbert, I. Eguia, E. Iriondo, J.I. Fernandez, E. Silveria, and I. Garuz. On the influence of high speed forming technologies in the forming of conical specimens: fluid-specimen interaction against magnetically induced repulsion. *Proceedings of the International Deep Drawing Research Group Conference*, 2006.

[48] C.M. Wichein, B.C. De Cooman, and C.J. Van Tyne. Surface roughness of a hot-dipped galvanized sheet steel as a function of deformation mode. *Journal of Materials Processing Technology*, 160(3):278–288, 2005.

[49] S.W. Banovic and T. Foecke. Evolution of strain-induced microstructure and texture in commercial aluminum sheet under balanced biaxial stretching. *Metallurgical and Materials Transactions A-Physical Metallurgy and Materials Science*, 34(3):657–671, 2003.

[50] T. Foecke, M. A. Iadicola, A. Lin, and S. W. Banovic. A method for direct measurement of multiaxial stress-strain curves in sheet metal. *Metallurgical and Materials Transactions A-Physical Metallurgy and Materials science*, 38A(2):306–313, 2007.

[51] E. Hsu, J.E. Carsley, and R. Verma. Development of forming limit diagrams of aluminum and magnesium sheet alloys at elevated temperatures. *Journal of Materials Engineering and Performance*, 17(3):288–296, 2008.

[52] H.M. Howe. *The Metallography of Steel and Cast Iron*. McGraw-Hill, New York, 1916.

[53] J.H. Whitely. *Journal of Iron and Steel Institute*, 113:213, 1926.

[54] L.E. Samuels. *Optical Microscopy of Carbon Steels*. ASM, Metals Park, Ohio, 1980.

[55] R.A. Grange. Effect of microstructural banding in steel. *Metallurgical and Materials Transactions B*, 2:417, 1971.

[56] J.D. Verhoeven. A review of microsegregation induced banding phenomena in steels. *Journal of Materials Engineering and Performance*, 9:286, 2000.

[57] F.G. Caballero, A. Garcia-Junceda, C. Capdevila, and C. Garcia de Andres. Evolution of microstructural banding during the manufacturing process of dual phase steels. *Materials Transactions*, 47(9):2269–2276, 2006.

[58] P.E.J. Rivera-Diaz-del Castillo and S. van der Zwaag. Assuring microstructural homegeniety in dual phase and trip steels. *Steel Research International*, 75(11):711–715, 2004.

[59] Rivera-Diaz-del-Castillo P.E.J. Xu, W. and S. van der Zwaag. Ferrite/pearlite band prevention in dual phase and TRIP steels: Model development . *ISIJ International*, 45:380, 2005.

[60] A.R. Marder. Deformation characteristics of dual-phase steels. *Metallurgical Transactions A-Physical Metallurgy and Materials Science*, 13(1):85–92, 1982.

[61] X.L. Cai, A.J. Garrattreed, and W.S. Owen. The development of some dual-phase steel structures from different starting microstructures. *Metallurgical Transactions A-Physical Metallurgy and Materials Science*, 16(4):543–557, 1985.

[62] C.F. Jatczak, D.J. Girardi, and E.S. Rowland. On banding in steel. *Transactions of American Society of Metals*, 48:279–303, 1956.

[63] W.A. Spitzig. Effect of sulfide inclusion morphology and pearlite banding on anisotropy of mechanical-properties in normalized C-Mn steels . *Metallurgical Transactions A*, 14:271, 1983.

[64] A.S. Bor. Effect of pearlite banding on mechanical-properties of hot-rolled steel plates . *ISIJ International*, 31:1445, 1991.

[65] X.L. Cai, J. Feng, and W.S. Owen. The dependence of some tensile and fatigue properties of a dual-phase steel on its microstructure. *Metallurgical Transactions A*, 16:1405–1415, 1985.

[66] A.A. Korda, Y. Mutoh, Y. Miyashita, T. Sadasue, and S.L. Mannan. In situ observation of fatigue crack retardation in banded ferrite-pearlite microstructure due to crack branching. *Scripta Materialia*, 54(11):1835–1840, 2006.

[67] M. Mazinani and W. J. Poole. Effect of martensite plasticity on the deformation behavior of a low-carbon dual-phase steel. *Metallurgical and Materials Transactions A-Physical Metallurgy and Materials Science*, 38A(2):328–339, 2007.

[68] S. Kim, S.Y. Kang, S.J. Oh, S.J. Kwon, S. Lee, J.H. Kim, and J.H. Hong. Correlation of the microstructure and fracture toughness of the heat-affected zones of an SA 508 steel. *Metallurgical and Materials Transactions A-Physical Metallurgy and Materials Science*, 31(4):1107–1119, 2000.

[69] J.A. Ewing and W. Rosenhain. Bakerian lecture. The crystalline structure of metals. *Philosophical Transactions of the Royal Society of London Series A-Containing Papers of a Mathematical or Physical Character*, 193:353–U101, 1900.

[70] E. Maire, O. Bouaziz, M. Di Michiel, and C. Verdu. Initiation and growth of damage in a dual-phase steel observed by X-ray microtomography. *Acta Materialia*, 56(18):4954–4964, 2008.

[71] L.E. Samuels. The nature of mechanically polished metal surfaces - the surface deformation produced by the abrasion and polishing of 70-30 brass. *Journal of the Institute of Metals*, 85:51, 1956.

[72] Y.B. Guo and A.W. Warren. Microscale mechanical behavior of the subsurface by finishing processes. *Journal of Manufacturing Science And Engineering-Transactions of The Asme*, 127(2):333–338, 2005.

[73] P.J.M. Janssen, J.P.M. Hoefnagels, T.H. de Keijser, and M.G.D. Geers. Processing induced size effects in plastic yielding upon miniaturisation. *Journal of the Mechanics and Physics of Solids*, 56:2687, 2008.

[74] Z.W. Zhong and N.P. Hung. Grinding of alumina/aluminum composites. *Journal of Materials Processing Technology*, 123(1):13–17, 2002.

[75] Y.W. Shi and J.T. Barnby. Void nucleation during tensile deformation of a c-mn structural-steel. *International Journal of Fracture*, 25(2):143–151, 1984.

[76] J.P.M. Hoefnagels, C.C. Tasan, M. Pradelle, and M.G.D. Geers. Brittle Fracture-Based Experimental Methodology for Microstructure Analysis. In Dulieu-Barton, J.M. and Lord, J.D. and Greene, R.J., editor, *Advances in Experimental Mechanics Vi*, volume 13-14 of *Applied Mechanics and Materials*, pages 133–139, 2008.

[77] S. Govindjee and J. Simo. A micro-mechanically based continuum damage model for carbon black-filled rubbers incorporating mullins effect. *Journal of the Mechanics and Physics of Solids*, 39(1):87–112, 1991.

[78] G.Z. Voyiadjis and P.I. Kattan. A plasticity-damage theory for large deformation of solids .1. theoretical formulation. *International Journal of Engineering Science*, 30(9):1089–1108, 1992.

[79] C.L. Chow and J. Wang. An anisotropic theory of elasticity for continuum damage mechanics. *International Journal of Fracture*, 33(1):3–16, 1987.

[80] R.H.J. Peerlings, R. de Borst, W.A.M. Brekelmans, and J.H.P. de Vree. Gradient enhanced damage for quasi-brittle materials. *International Journal for Numerical Methods in Engineering*, 39(19):3391–3403, 1996.

[81] A.F. Johnson, A.K. Pickett, and P. Rozycki. Computational methods for predicting impact damage in composite structures. *Composites Science and Technology*, 61(15, Sp. Iss. SI):2183–2192, 2001.

[82] C. Ruggieri, T.L. Panontin, and R.H. Dodds. Numerical modeling of ductile crack growth in 3-D using computational cell elements. *International Journal of Fracture*, 82(1):67–95, 1996.

[83] L.M. Kachanov. On the time to rupture under creep conditions. *Akad Nauk SSR Otd Tekh*, 8:26, 1958.

[84] J. Lemaitre and J. Dufailly. Damage measurements. *Engineering Fracture Mechanics*, 28(5-6):643–&, 1987.

[85] T.F. Morgeneyer, M.J. Starink, and I. Sinclair. Evolution of voids during ductile crack propagation in an aluminium alloy sheet toughness test studied by synchrotron radiation computed tomography. *Acta Materialia*, 56(8):1671–1679, 2008.

[86] O. Bouaziz, E. Maire, M. Giton, J. Lamarre, Y. Salingue, and M. Dimichiele. A model for initiation and growth of damage in dual-phase steels identified by X-ray micro-tomography. *Revue De Metallurgie-Cahiers D Informations Techniques*, 105(2):102–107, 2008.

[87] L. Babout, E. Maire, and R. Fougeres. Damage initiation in model metallic materials: X-ray tomography and modelling. *Acta Materialia*, 52(8):2475–2487, 2004.

[88] R.K. Everett, K.E. Simmonds, and A.B. Geltmacher. Spatial distribution of voids in Hy-100 steel by X-ray tomography. *Scripta Materialia*, 44(1):165–169, 2001.

[89] E. Maire, C Bordreuil., L Babout., and JC Boyer. Damage initiation and growth in metals. Comparison between modelling and tomography experiments. *Journal of The Mechanics And Physics of Solids*, 53(11):2411–2434, 2005.

[90] Alves M. Measurement of ductile material damage. *Mechanics Based Design of Structures and Machines*, 29:451, 2001.

[91] D. Chae and D.A. Koss. Damage accumulation and failure of HSLA-100 steel. *Materials Science and Engineering A-Structural Materials Properties Microstructure and Processing*, 366(2):299–309, 2004.

[92] M.F. Horstemeyer, K. Gall, K.W. Dolan, A Waters, JJ Haskins, DE Perkins, AM Gokhale, and MD Dighe. Numerical, experimental, nondestructive, and image analyses of damage progression in cast A356 aluminum notch tensile bars. *Theoretical and Applied Fracture Mechanics*, 39(1):23–45, 2003.

[93] T. Pardoen, I. Doghri, and F. Delannay. Experimental and numerical comparison of void growth models and void coalescence criteria for the prediction of ductile fracture in copper bars. *Acta Materialia*, 46(2):541–552, 1998.

[94] A Ochsner, J Gegner, W Winter, and G Kuhn. Experimental and numerical investigations of ductile damage in aluminium alloys. *Materials Science and Engineering A-Structural Materials Properties Microstructure and Processing*, 318(1-2):328–333, 2001.

[95] R. Lapovok. Damage evolution under severe plastic deformation. *International Journal of Fracture*, 115(2):159–172, 2002.

[96] D.R. Mahapatra. Wave propagation in elastic solids undergoing damage and growth process. *Acta Mechanica*, 203(3-4):163–181, 2009.

[97] J.H. Liu, G.L. Li, X.Y. Hao, D.B. Zeng, and Z.H. Sun. Ultrasonic measurement of fatigue damage of nodular cast iron. *Materials Letters*, 50(4):194–198, 2001.

[98] J.M. Ferreira, J.T.B. Pires, J.D. Costa, Z.Y. Zhang, O.A. Errajhi, and A. Richardson. Fatigue damage analysis of aluminized glass fiber composites. *Materials Science and Engineering A-Structural Materials Properties Microstructure and Processing*, 407(1-2):1–6, 2005.

[99] B.X. Sun and Y.M. Guo. High-cycle fatigue damage measurement based on electrical resistance change considering variable electrical resistivity and uneven damage. *International Journal of Fatigue*, 26(5):457–462, 2004.

[100] J.H. Liu, G.L. Li, G.S. Liu, and X.Y. Hao. Damaged evaluation of ferrite ductile iron with electric resistance. *Materials Letters*, 58(6):1051–1055, 2004.

[101] G. Straffelini and A. Molinari. Evolution of tensile damage in porous iron. *Materials Science and Engineering A-Structural Materials Properties Microstructure and Processing*, 334(1-2):96–103, 2002.

[102] C.Y. Tang and W.B. Lee. Effects of damage on the shear modulus of aluminum-alloy 2024t3. *Scripta Metallurgica Et Materialia*, 32(12):1993–1999, 1995.

[103] W.C. Oliver and G.M. Pharr. An improved technique for determining hardness and elastic-modulus using load and displacement sensing indentation experiments. *Journal of Materials Research*, 7(6):1564–1583, 1992.

[104] C.C. Tasan, J.P.M. Hoefnagels, and M.G.D. Geers. A Micropillar Compression Methodology for Ductile Damage Quantification. *Submitted*, 2010.

[105] C.C. Tasan, J.P.M. Hoefnagels, and M.G.D. Geers. A critical assessment of indentation-based ductile damage quantification. *Acta Materialia*, 57(17):4957–4966, 2009.

[106] Z.-H. Xu and X. Li. Effect of sample tilt on nanoindentation behaviour of materials. *Philosophical Magazine*, 87(16-17):2299–2312, 2007.

[107] X. Chen and J.J. Vlassak. Numerical study on the measurement of thin film mechanical properties by means of nanoindentation. *Journal of Materials Research*, 16(10):2974–2982, 2001.

[108] Meuleman D.J. Rupp M. Fekete J.R., Hall J.N. *Iron& Steel Technology*, 5:55, 2008.

[109] M.S. Rashid. Dual phase steels. *Annual Review of Materials Science*, 11:245–266, 1981.

[110] N. Bonora. Identification and measurement of ductile damage parameters. *Journal of Strain Analysis for Engineering Design*, 34(6):463–478, 1999.

[111] W.J. Poole and E.J. Dowdle. Experimental measurements of damage evolution in Al-Si eutectic alloys. *Scripta Materialia*, 39(9):1281–1287, 1998.

[112] J.P.M. Hoefnagels, C.C. Tasan, L.C.N. Louws, and M.G.D. Geers. Comparison of quantitative damage characterization methodologies. In *Proceedings of 12th International Conference on Fracture (ICF 2009).*, 2009.

[113] F.H. Moussy and P. Lefebure. Critical damage and ductile fracture: quantitative experimental determination. *Computational Methods for Predicting Material Processing Defects : Proceedings (Studies in Applied Mechanics*, 15:275, 1987.

[114] C.C. Tasan, Hoefnagels J.P.M., and Geers M.G.D. A brittle-fracture methodology for three-dimensional visualization of ductile deformation micromechanisms. *Scripta Mater*, 61(1):20–23, 2009.

[115] U. Stigh. Effects of interacting cavities on damage parameter. *Journal of Applied Mechanics-Transactions of The Asme*, 53(3):485–490, 1986.

[116] S. Jansson, , and U. Stigh. Influence of cavity shape on damage parameter. *Journal of Applied Mechanics-Transactions Of The Asme*, 52(3):609–614, 1985.

[117] B. Guelorget, M. Francois, and J. Lu. Microindentation as a local damage measurement technique. *Materials Letters*, 61(1):34–36, 2007.

[118] J. Lemaitre, J. Dufailly, and R. Billardon. Damage evaluation through microhardness measurements. *Comptes Rendus De L Academie Des Sciences Serie Ii*, 304(12):601–604, 1987.

[119] D. Ye and Z. Wang. An approach to investigate pre-nucleation fatigue damage of cyclically loaded metals using vickers microhardness tests. *International Journal of Fatigue*, 23(85), 2001.

[120] G. Arnold, O. Hubert, M. Dutko, and Billardon R. Identification of a continuum damage model from micro-hardness measurements: Application to a backward extrusion process. *International Journal of Forming Processes*, 5:163, 2002.

[121] M. Cotterell, J. Schambergerova, J. Ziegelheim, and J. Janovec. Dependence of micro-hardness on deformation of deep-drawing steel sheets. *Journal of Materials Processing Technology*, 124(3):293–296, 2002.

[122] A.A. Lebedev, I.V. Makovetskii, N.R. Muzyka, and V.P. Shvets. A study of deformation and damage accumulation processes in 10gn2mfa steel under low-cycle loading. *Strength of Materials*, 40(2):163–167, 2008.

[123] A. Mkaddem, F. Gassara, and R. Hambli. A new procedure using the microhardness technique for sheet material damage characterisation. *Journal of Materials Processing Technology*, 178(1-3):111–118, 2006.

[124] J. Luo and R. Stevens. Porosity-dependence of elastic moduli and hardness of 3Y-TZP ceramics. *Ceramics International*, 25(3):281–286, 1999.

[125] J. Adachi, K. Kurosaki, M. Uno, and S. Yamanaka. Porosity influence on the mechanical properties of polycrystalline zirconium nitride ceramics. *Journal of Nuclear Materials*, 358(2-3):106–110, 2006.

[126] A. Portinha, V. Teixeira, J. Carneiro, J. Martins, M.F. Costa, R. Vassen, and D. Stoever. Characterization of thermal barrier coatings with a gradient in porosity. *Surface & Coatings Technology*, 195(2-3):245–251, 2005.

[127] S.P. Duttagupta, X.L. Chen, S.A. Jenekhe, and P.M. Fauchet. Microhardness of porous silicon films and composites. *Solid State Communications*, 101(1):33–37, 1997.

[128] H.K. Oh and H. Son. A basic study of the hardness measurement of sintered porous metals. *Journal of Mechanical Working Technology*, 13(2):175–187, 1986.

[129] C.A. Brookes, J.B. Oneill, and B.A.W. Redfern. Anisotropy in hardness of single crystals. *Proceedings of the Royal Society of London Series A-Mathematical and Physical Sciences*, 322(1548):73–&, 1971.

[130] J.J. Vlassak and W.D. Nix. Measuring the elastic properties of anisotropic materials by means of indentation experiments. *Journal of The Mechanics And Physics of Solids*, 42(8):1223–1245, 1994.

[131] P.W. Bridgman. The effect of pressure on the tensile properties of several metals and other materials. *Journal of Applied Physics*, 24(5):560–570, 1953.

[132] J. Tirosh and O. Abraham. On enhancing ductility of brittle-like materials by high confining hydro-pressure. *Mechanics of Materials*, 39(8):760–772, 2007.

[133] J.L. Chaboche. Continuum damage mechanics i and ii. *ASME Transactions*, 55:59, 1988.

[134] J. Lemaitre. *A Course on Damage Mechanics*. Springer, Berlin, 1985.

[135] R.H.J. Peerlings, M.G.D. Geers, R. de Borst, and W.A.M. Brekelmans. A critical comparison of nonlocal and gradient-enhanced softening continua. *International Journal of Solids and Structures*, 38(44-45):7723–7746, 2001.

[136] J. Lemaitre. A continuous damage mechanics model for ductile fracture. *Journal of Engineering Materials and Technology-Transactions of The Asme*, 107(1):83–89, 1985.

[137] R. Taljera. A continuum mechanics characterization of damage in composite materials. *Proceedings of the Royal Society A: Mathematical, Physical & Engineering Sciences*, 399:195, 1985.

[138] J.P.M. Hoefnagels, C.C. Tasan, and M.G.D. Geers. Comparison of quantitative damage characterization methodologies. *Proceedings of the 7th Euromech Solid Mechanics Conference*, 2009.

[139] J.P.M. Hoefnagels, C.C. Tasan, L.C.N. Louws, and M.G.D. Geers. Comparison of quantitative damage characterization methodologies. *Proceedings of the 12th International Conference on Fracture*, 2009.

[140] M.D. Uchic, D.M. Dimiduk, J.N. Florando, and W.D. Nix. Sample dimensions influence strength and crystal plasticity. *Science*, 305(5686):986–989, 2004.

[141] J.R. Greer, W.C. Oliver, and W.D. Nix. Size dependence of mechanical properties of gold at the micron scale in the absence of strain gradients. *Acta Materialia*, 53(6):1821–1830, 2005.

[142] C.C. Tasan, J.P.M. Hoefnagels, and M.G.D. Geers. Indentation Based Damage Quantification Revisited. *submitted*, 2010.

[143] R. Andersson. *Deformation Characteristics of Stainless Steels*. PhD thesis, Lulea University of Technology, 2005.

[144] A.G. Atkins. Fracture in forming. *Journal of Materials Processing Technology*, 56(1-4):609–618, 1996.

[145] B. Gardey, S. Bouvier, and B. Bacroix. Correlation between the macroscopic behavior and the microstructural evolutions during large plastic deformation of a dual-phase steel. *Metallurgical and Materials Transactions A-Physical Metallurgy and Materials Science*, 36A(11):2937–2945, 2005.

[146] G. Leroy, J.D. Embury, G. Edward, and M.F. Ashby. A model of ductile fracture based on the nucleation and growth of voids. *Acta Metallurgica*, 29(8):1509–1522, 1981.

[147] C.Y. Tang, C.L. Chow, W. Shen, and W.H. Tai. Development of a damage-based criterion for ductile fracture prediction in sheet metal forming. *Journal of Materials Processing Technology*, 91(1-3):270–277, 1999.

[148] J.S. Yu, J.L. Liu, J.X. Zhang, and J.S. Wu. TEM investigation of FIB induced damages in preparation of metal material TEM specimens by FIB. *Materials Letters*, 60(2):206–209, 2006.

[149] A. Pineau. Modeling ductile to brittle fracture transition in steels-micromechanical and physical challenges. *International Journal of Fracture*, 150(1-2):129–156, 2008.

[150] G.E. Dieter. *Mechanics of Materials*. McGraw-Hill, Tokyo, 1961.

Samenvatting

De opkomst van zogenaamde 'advanced high strength steels' (AHSS) and aluminium legeringen voor gewichtsbesparing van auto-onderdelen heeft de interesse vanuit de industrie naar deformatie-gerelateerde ductiele schade in bladmetaal de laatste decennia, sterk doen toenemen. Grote deformaties tijdens productie of onderhoud zorgen voor verschillende micromechanismen voor schadeontwikkeling in de multifase microstructuren van deze materialen die dikwijls leiden tot onverwacht faalgedrag op macroniveau. Dit kan worden voorkomen door a) microstructuren van metalen zodanig te optimaliseren dat deze minder gevoelig zijn voor schadegerelateerd falen, waarvoor een experimentele karakterisering van die micromechanismen voor schadeontwikkeling nodig is of b) de incorporatie van continumschademodellen van vormingssimulaties om vormingsprocessen te ontwerpen binnen de grenzen van toegestane deformaties (waarvoor op experimentele wijze de opstapeling van schade moet worden gekwantificeerd). Hoe dan ook, beide strategien worden belemmerd door de beperkingen van de nu beschikbare experimentele diagnostieken. Daarom is het doel van dit onderzoek het ontwikkelen van nieuwe experimentele methodologien voor (i) karakterisering van micromechanismen voor schadeontwikkeling en (ii) nauwkeurige kwantificering van accumulatie van schade met het oog op voor industrieel relevant bladmetaal.

Als eerste wordt de invloed van het schadeverloop op lokalisatie en breuk onderzocht door twee typen staal met verschillende microstructuren te vervormen volgens verschillende rekpaden. De resultaten laten zien dat bij microstructuren met veel schademechanismen, zoals AHSS, accumulatie van schade zowel het moment van insnoering als de breukrek significant benvloedt. Dit bevestigt het belang van een grondige karakterisatie van micromechanismen voor schadeontwikkeling bij verschillende rekpaden. Voor de analyse van deze mechanismen moet een testopstelling van miniatuurformaat ontwikkeld worden die in een scanning elektronenmicroscoop (SEM) past om de deformatie-geinduceerde microstructurele evolutie in real-time te kunnen monitoren. Hiervoor is een mini-Marciniak opstelling ontworpen, gebouwd en getest die real-time multi-axiale tests van industrieel bladmetaal tot aan het punt van breken mogelijk maakt in een SEM. Een groot voordeel van in-situ analyse met behulp van een dergelijk kleine uitrusting is de mogelijkheid om het verloop van de lokale rekverdeling op microstructuur niveau te volgen, zoals is

gedemonstreerd in een case studie naar de mechanische invloeden van de morfologie en eigenschappen van microstructurele bandvorming in metaal. Het effect van bandcontinuteit en hardheid is verklaard, wat met name voor harde banden met een continue morfologie resulteert in een duidelijke invloed van schade. Ten slotte is er een verbeterde experimentele methodologie ontwikkeld om 3D kenmerken van ductiele schademechanismen te analyseren onder minimale beinvloeding door de prepatie van het monster. Er zijn reeds vele experimentele methodologien voor het kwantificeren van schade verschenen in de literatuur, maar deze zijn niet grondig getoetst op meetnauwkeurigheid, precisie, toepasbaarheid, etc. Om de meest geschikte schade kwantificeringsstrategie voor continum-schademodellen te bepalen, zijn methodes die de schademorphologie bemonsteren (de volume-fractiemethode, oppervlakte-fractie methode en dichtheids methode) en methodes die de verandering van materiaal eigenschappen bemonsteren (de standaard en gemodifeerde indentatiemethodes en de micropillaarcompressie methode) op een vergelijkende wijze geanalyseerd. De verkregen resultaten laten duidelijk zien dat methodologien die ductile schade kwantificeren via de morfologie, een beperkte nauwkeurigheid hebben en een beperkt schade-spectrum bemonsteren. Dit geeft dus aan dat nauwkeurige kwantificeringstechnieken op basis van de materiaaleigenschappen nodig zijn. De standaard indentatie methode is een veel gebruikt voorbeeld hiervan echter hoewel een numeriek-experimentele analyse heeft aangetoond dat deze techniek niet voor dit doeleinde kan worden gebruikt, omdat de degradatie van de schade van zowel de hardheid als de modulus wordt gemaskeerd door andere deformatiegedreven microstructurele mechanismen, zoals veranderingen van de korrelvorm of de textuur. Daarom zijn er in dit onderzoek twee originele schade kwantificeringsmethodologien voorgesteld die op een andere manier de degradatie de mechanische eigenschappen bemonsteren. Een nieuwe methodologie op basis van indentatie is ontwikkeld en gevalueerd welke de invloed van de microstructurele heterogeniteit elimineert om op een juiste wijze de door schade veroorzaakte verlaging van indentatie-hardheid en modulus te verkrijgen. Ten slotte is er een micropillaar compressie methode ontwikkeld, waarbij de elastische schadeparameter wordt verkregen via deformatie-gedreven degradatie van de compressibiliteitsmodulus van gedraadvonkte micropillaren. De resultaten van deze twee methodologien tonen duidelijk aan dat methodologien die ductile schade kwantificeren door diens invloed op een mechanische eigenschap (bijv. de hardheid of de modulus) te meten een significant hogere nauwkeurigheid hebben en daarom meer geschikt zijn voor het identificeren van schadeparameters in continum-schademodellen.

List of Related Publications

Journal Publications

- C.C. Tasan, J.P.M. Hoefnagels, M.G.D. Geers, A brittle-fracture methodology for three-dimensional visualization of ductile deformation micromechanisms, Scripta Materialia, 61(1), 20-23, (2009)
- C.C. Tasan, J.P.M. Hoefnagels, M.G.D. Geers, A critical assessment of indentation-based ductile damage quantification, Acta Materialia, 57(15), 4957-4966, (2009)
- C.C. Tasan, J.P.M. Hoefnagels, C.H.L.J. ten Horn, M.G.D. Geers, Experimental analysis of strain path dependent ductile damage mechanics and forming limits, Mechanics of Materials, 41(11), 1264-1276, (2009)
- C.C. Tasan, J.P.M. Hoefnagels, M.G.D. Geers, Microstructural banding effects clarified through micrographic digital image correlation, Scripta Materialia, *accepted*, (2010)
- C.C. Tasan, J.P.M. Hoefnagels, E.C.A. Dekkers, M.G.D. Geers, Multi-axial deformation setup for microscopic testing of sheet metal to fracture, *submitted*, (2010)
- C.C. Tasan, J.P.M. Hoefnagels, L.C.N. Louws, M.G.D. Geers, Comparative analysis of damage quantification methodologies, *submitted*, (2010)
- C.C. Tasan, J.P.M. Hoefnagels, M.G.D. Geers, Indentation based damage quantification revisited, *submitted*, (2010)
- C.C. Tasan, J.P.M. Hoefnagels, M.G.D. Geers, A micropillar compression methodology for ductile damage quantification, *submitted*, (2010)

Proceedings of International Conferences

- J.P.M. Hoefnagels, C.C. Tasan, M.G.D. Geers, Comparison of quantitative damage characterization methodologies, in Proceedings of the 7th Euromech Solid Mechanics Conference; Editors: J.A.C. Ambrsio, M.P.T. Silva, Lissabon, Portugal, on cd-rom, (2009)
- C.C. Tasan, J.P.M. Hoefnagels, M.G.D. Geers, Indentation based damge quantification methodology revisited, in Proceedings of the 7th Euromech Solid Mechancis Conference; Editors: J.A.C. Ambrsio, M.P.T. Silva, Lissabon, Portugal, on cd-rom, (2009)
- J.P.M. Hoefnagels, C.C. Tasan, L.C.N. Louws, M.G.D. Geers, Comparison of quantitative damge characterization methodologies, in Proceedings of the 12th International Conference on Fracture; Editors: x, Ottawa, Canada, on cd-rom, (2009)
- J.P.M. Hoefnagels, C.C. Tasan, M.G.D. Geers, Direct damage quantification techniques - comparative study, in Proceedings of the SEM Annual Conference; Editors: x, Albuquerque, United States, on cd-rom, (2009)
- C.C. Tasan, J.P.M. Hoefnagels, M. Pradelle, M.G.D. Geers, 3D Damage analysis of sheet metal, in Proceedings of the WCCM8, ECCOMAS 2008; Editors: B.A. Schrefler, U. Perego, Venice, Italy, on cd, (2008)
- J.P.M. Hoefnagels, C.C. Tasan, M. Pradelle, M.G.D. Geers, Brittle fracture-based experimental methodology for microstructure analysis, in Applied Mechanics and Materials ; Editors: J.M. Dulieu-Barton, J.D. Lord, R.J. Greene, London, United Kingdom, 133-139, (2008)
- C.C. Tasan, J.P.M. Hoefnagels, L.C.N. Louws, M.G.D. Geers, Experimental-numerical analysis of the indentation-based damage characterization methodology, in Applied Mechanics and Materials; Editors: J.M. Dulieu-Barton, J.D. Lord, R.J. Greene, London, United Kingdom, 151-160, (2008)
- C.C. Tasan, J.P.M. Hoefnagels, L.C.N. Louws, M.G.D. Geers, Experimental-numerical analysis of the indentation-based damage characterization methodology, in Proceedings of the 2008 SEM XI International Congress and Exposition on Experimental and Applied Mechanics; Editors: Thomas Proulx, Orlando, United States, on cd rom, (2008)
- C.C. Tasan, J.P.M. Hoefnagels, G. Quaak, M.G.D. Geers, In-plane biaxial loading of sheet metal until fracture, in Proceedings of the 2008 SEM XI international congress and exposition on experimental and applied mechanics; Editors: Thomas Proulx, Orlando, United States, on cd rom, (2008)

- C.C. Tasan, J.P.M. Hoefnagels, R.H.J. Peerlings, M.G.D. Geers, Experimental characterization of ductile damage using nanoindentation, in Proceedings of the 13th international conference on experimental mechanics; Editors: E.E. Gdoutos, Alexandroupolis, Greece, on CD, (2007)
- C.C. Tasan, J.P.M. Hoefnagels, R.H.J. Peerlings, M.G.D. Geers, C.H.L.J. ten Horn, H. Vegter, Ductile damage evolution and strain path dependency, in AIP Conference Proceedings; Editors: Elias Cueto, Francisco Chinesta, Zaragoza, Spain, 187-192, (2007)

Acknowledgements

There are many people who have contributed to the work presented in this thesis directly, as well as others contributing indirectly. Without their help, this would have been hardly possible.

Above all, I would like to thank prof. Marc Geers for giving me the opportunity to do my PhD in his group. His critical comments throughout the project kept me on the right track and increased the productivity tremendously. Just as crucial was his guidance in non-PhD related issues, and his continuous support in the stressful final run. Marc, thanks for all!

I find myself very lucky for having Johan Hoefnagels as my copromotor during this project. We've had many meetings, numerous discussions, we've gone to conferences (and to follow-up road-trips!), have written papers which finally ended up in this thesis as chapters. During this long process of collaborative research, which inevitably had its downs as much as ups, Johan's ever-existing optimism and energy has fueled my personal motivation, and his scientific creativity has solved many of the faced challenges. Apart from all this, it was always fun for me to drop by his room even when there was nothing scientific to discuss about. Future collaborations are already being planned (and I didn't forget about the promised tour of eastern Turkey), but for all of this up to now, thanks Johan!

As well as my promotors, I would like to thank staff members of Mechanics of Materials, and especially Ron Peerlings and Varya Kouznetsova for their input during the joint damage meetings. Ron, I also appreciate very much the guidance during Johan's absence in my first year, when it was needed the most. (And I still think the voice-recording idea was not that bad!).

I am also grateful to the committee members, prof. Vikram Deshpande, prof. Thomas Pardoen, prof. Dierk Raabe, prof. Erman Tekkaya and prof. Sybrand van der Zwaag for their critical comments to this thesis and their attendance to my defense.

The motivation for this research project was triggered from the challenges faced in the industry. I was lucky enough to have in-depth input and readily available help

from all industrial partners and contacts involved, especially Carel ten Horn and Henk Vegter from Corus, Gerrit Klaseboer and Harmen Altena from Philips DAP, Mark de Vries from DAF Trucks, and Joep Broekhuijsen from Schelde. Obviously, Materials Innovation Institute was the ”bridge”that made all these communications possible, as well as the funding for the whole research. This strong support is gratefully acknowledged. I would also like to thank all the attendants of the M2i Project and Cluster Meetings for their valuable comments.

A large number of experiments were carried out for this thesis, using many different equipments, materials and samples. I’ve had help from Marc van Maris in almost all of these experiments, either directly or indirectly. Thanks Marc (and sorry for the occasional mess I caused in the lab). Also, contributions of Sjef Garenfeld and especially of Erwin Dekkers, Samu Ooesterink, Rob de Kluijver from GTD were critical to wrap-up Chapter 3 under great time pressure. Many thanks!

Even with these contributions, the total required amount of time for all these experiments is clearly more than the elapsed time span of the project. What made it all possible were the contributions from students who did their internship, open space or graduation projects under my supervision. Such contributions of Roel Vos, Cyriel Verberne, Mark Heeren, Mathijs Peters, Michael Dogge, Michiel Schellekens, Mickael Pradelle, Paul van Beers, Ruud Hawinkels, Bart Vossen, Gerard Quaak and Nard Louws are gratefully acknowledged. I hope you had as much fun as I did working with you...

Without the assistance of Alice van Litsenburg in Mate, and Monika Hoekstra, Oscar Ruigrok and others in the M2i office, it would have been very difficult to solve many of the practical issues faced during my stay in the Netherlands. Monika: additional thanks for your efforts in the complicated post-PhD arrangements. Without your help, it would have been a nightmare to deal with all these while trying to finalize my thesis. Leo, thanks for your help with computer-related problems. Sjoerd, thanks for designing the cover in such short notice.

A PhD degree was only a part of what I have been looking for in this journey which took me to the Netherlands. The rest I found in all the shared moments with you: Frederico (a white sheep walking in the snow), İzzet (*küçük idris*), Tuncay (”so you ate my fish?”), Gabriel (a Paraguayan with Dutch passport), Mohammad (flying *vaporetto* ticket), Ana (go for the he-man haircut), Kanat (best vocals of all times), Rudy (”I have a theory...”), Müge (ultimate dinner organizer), Britta (”What!!!”), Erica (the latex master), Gwen (let’s have some fresh air), Graham (we are men of extremely strict cultures), Pina (spiritual sister), Caroline & Christophe (lovely yearly dinners), and Murthy, Hamid, Bhairav, Lars, Bart, Roy, Juan Carlos, Peter, Francesco, Kurtuluş, Arash, Sebastian, Atike, Koray, Tanır, Barış, Tarkan, Sandra, Vinayak, İsa, William, Ulaş, Mustafa, Daniel, Yang, Lambert, Jan, Alexei, Selim, Sinan, Ceylan, Carole, Roberto, Cem and all others... Thanks for making this journey a pleasant ride!

Can, Özlem and Peynir: I cannot imagine how boring it would be if we hadn’t started this journey together. Where are we heading next? (Peynir: please record some footage in your next plane crash.)

And then my family... My mother Asuman Taşan, my father Mevlüt Taşan, my brother Caner Taşan, my sister Tuna Taşan-Kok, Herman Kok, Bahar Durna-Taşan, Meral Özdamar and all others: You are my source of warmth, quietness, laughter, and energy. I am lucky to have your love and support at every step along the way.

And finally, Seçkin'im... It always feels too far, whether 3000 kilometers or 3 meters apart, as it is your presence that makes all the rain tolerable, and with your smile was all this at all possible...

Cem Taşan
Maastricht, March 2010.

Curriculum Vitae

Cem Tasan was born on 22 January 1980 in Ankara, Turkey. After elementary school education in Bor and Aydin, and high school education in Izmir American Collegiate Institute and METU College in Ankara, he completed his BS in Metallurgical and Materials Engineering Department of Middle East Technical University in 2002. Between 2002 and 2005 he worked as a teaching assistant in the same department, where he got his MSc degree with his thesis on polymer/clay nanocomposites, under the supervision of prof.Cevdet Kaynak. In November 2005 he moved to the Netherlands to work as a M2i PhD researcher in the group of prof.Marc Geers in Mechanical Engineering Department of Eindhoven University of Technology. His PhD research was on developing new experimental methodologies for characterization and quantification of ductile damage in sheet metal. Since March 2010, he is working as a M2i post-doc researcher in Max-Planck Institute for Iron Research in Düsseldorf, Germany, under the supervision of prof.Dierk Raabe, investigating micro-plasticity at phase boundaries of dual-phase steels.